AWARD NUMBER: **W81XWH-14-1-0358 (BC134025)**

TITLE: **Musculoskeletal Complications and Bone Metastases in Breast Cancer Patients Undergoing Estrogen Deprivation Therapy**

PRINCIPAL INVESTIGATOR: **Laura E. Wright, Ph.D.**

CONTRACTING ORGANIZATION: **Indiana University School of Medicine Indianapolis, IN 46202**

REPORT DATE: **December 2018**

TYPE OF REPORT: **Final Report**

PREPARED FOR: **U.S. Army Medical Research and Materiel Command Fort Detrick, Maryland 21702-5012**

REPORT DOCUMENTATION PAGE

Form Approved
OMB No. 0704-0188

1. REPORT DATE	**2. REPORT TYPE**	**3. DATES COVERED**
DEC 2018	Final Report	30SEP2014 - 29SEP2018

4. TITLE AND SUBTITLE

Musculoskeletal Complications and Bone Metastases in Breast Cancer Patients Undergoing Estrogen Deprivation Therapy

5a. CONTRACT NUMBER

5b. GRANT NUMBER
W81XWH-14-1-0358

5c. PROGRAM ELEMENT NUMBER

6. AUTHOR(S)

Laura E. Wright, Ph.D.

E-Mail: laewrig@iu.edu

5d. PROJECT NUMBER

5e. TASK NUMBER

5f. WORK UNIT NUMBER

7. PERFORMING ORGANIZATION NAME(S) AND ADDRESS(ES)

Indiana University School of Medicine
980 West Walnut Street R3 Room C132
Indianapolis, IN 46202

8. PERFORMING ORGANIZATION REPORT NUMBER

9. SPONSORING / MONITORING AGENCY NAME(S) AND ADDRESS(ES)

U.S. Army Medical Research and Materiel Command
Fort Detrick, Maryland 21702-5012

10. SPONSOR/MONITOR'S ACRONYM(S)

11. SPONSOR/MONITOR'S REPORT NUMBER(S)

12. DISTRIBUTION / AVAILABILITY STATEMENT

Approved for Public Release; Distribution Unlimited

13. SUPPLEMENTARY NOTES

14. ABSTRACT

Between 25-50% of women treated with endocrine therapies develop musculoskeletal toxicities that result in treatment discontinuation. In previous reporting periods, I demonstrated that aromatase inhibitor (AI) treatment caused bone loss and skeletal muscle weakness in mice and that prevention of AI-induced osteoclastic bone resorption using a bisphosphonate attenuated ER-negative breast cancer bone metastases and improved muscle function. These preclinical findings highlight the bone microenvironment as a modulator of tumor growth locally and muscle function systemically. Because muscle weakness is also commonly reported in women treated with selective estrogen receptor modulators (SERMs), during this reporting period I compared musculoskeletal effects of AI with a bone-sparing SERM endoxifen in a non-tumor model. Endoxifen (Endx), an active metabolite of tamoxifen, is currently in phase I trials for ER+ advanced breast cancer and little is known of its effects on the musculoskeletal system. Mature female C57BL/6 mice underwent sham surgery or ovariectomy (OVX) and were treated daily with vehicle, the AI letrozole (Let), or Endx. After eight weeks, changes in cancellous and cortical bone indices were assessed by μCT and muscle contractility of the extensor digitalis longus (EDL) was measured *ex vivo*. Bone volume fraction (BV/TV) decreased by 50% in OVX-vehicle and OVX-AI mice ($p<0.05$), whereas BV/TV increased threefold in Endx mice relative to sham-vehicle. Periosteal expansion of cortical bone was inhibited by Endx evidenced by a decrease in medullary area, total cortical cross-sectional area, and polar moment of inertia relative to sham- and OVX-vehicle. Despite changes in cortical bone deposition, the biomechanical properties of bone in Endx-treated mice were significantly improved relative to OVX-vehicle and OVX-AI mice. Muscle-specific force was lower in OVX-Endx mice relative to OVX-vehicle and OVX-AI mice, indicating that SERM-induced muscle weakness is independent of bone resorption.

15. SUBJECT TERMS

Breast cancer; bone metastases; estrogen; endocrine therapy; aromatase inhibitors; letrozole; selective estrogen receptor modulators; tamoxifen; endoxifen; bone loss; skeletal muscle; myocyte; bone marrow adipose tissue.

16. SECURITY CLASSIFICATION OF:			**17. LIMITATION OF ABSTRACT**	**18. NUMBER OF PAGES**	**19a. NAME OF RESPONSIBLE PERSON**
a. REPORT	**b. ABSTRACT**	**c. THIS PAGE**			USAMRMC
Unclassified	Unclassified	Unclassified	Unclassified	55	**19b. TELEPHONE NUMBER** *(include area code)*

TABLE OF CONTENTS

1. INTRODUCTION

Adjuvant endocrine therapy using an aromatase inhibitor (AI), which drastically depletes peripheral 17β-estradiol (E2) concentrations, is a standard treatment for postmenopausal women with estrogen receptor (ER)-positive breast cancer. Unlike selective estrogen receptor modulators (SERMs), which spare bone, AI treatment leads to severe bone loss and musculoskeletal complications that result in low patient compliance for life-prolonging AI therapy. The mechanism(s) of AI-induced muscular dysfunction have not been identified, however, E2-deprivation is characterized by inflammation and release of systemic factors during bone resorption, which together have been demonstrated in other disease models to cause skeletal muscle weakness through oxidation and nitrosylation of RyR1 and SERCA1, critical calcium channels required for skeletal muscle contraction. What is more, a state of high bone turnover resulting from AI-induced E2 depletion could alter the bone microenvironment by releasing matrix-derived growth factors (e.g., TGF-β) that prime the pre-metastatic niche and increase breast cancer progression in bone. This project was therefore designed to evaluate the effects of AI therapy on the musculoskeletal system in the context of breast cancer by determining 1) how AI-induced E2 depletion impairs muscle function, 2) whether AI-induced E2 depletion increases breast cancer bone metastases and 3) the relative contribution of bone loss in each case. Data obtained during course of the project further our understanding of the mechanism of AI-induced muscle weakness through the identification of genes that contribute to muscle wasting during estrogen deprivation therapy. Furthermore, we compare and contrast the musculoskeletal side effects of AI with the novel SERM endoxifen.

2. KEYWORDS

Breast cancer; bone metastases; estrogen; endocrine therapy; aromatase inhibitors; letrozole; selective estrogen receptor modulators; tamoxifen; endoxifen; bone loss; skeletal muscle; ryanodine receptor; myocyte; bone marrow adipose tissue.

3. ACCOMPLISHMENTS

A. Major scientific goals

Task 1. Determine effects of the aromatase inhibitor (AI) letrozole and the selective estrogen receptor modulator (SERM) endoxifen on skeletal muscle function in vivo.

Figure 1. Muscle function was impaired and uterine hypertrophy was stimulated by endoxifen

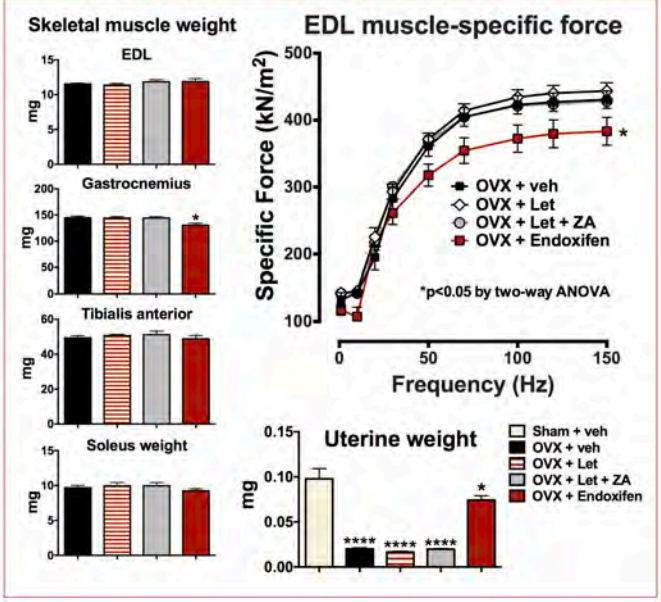

- A non-tumor *in vivo* study was carried out to determine the relative effects of letrozole and endoxifen on skeletal muscle function in mature (20-week) female C57Bl/6 mice. Animals were ovariectomized and treated daily with letrozole (10μg/day), endoxifen (1mg/kg/day), bisphosphonate (5μg/kg 3x/week), or sterile PBS (vehicle, 50μL/day). After eight weeks of dosing, the extensor digitalis longus (EDL) muscle was removed by microdissection and tested *ex vivo* for contractile force. Despite no change in muscle mass in the EDL, gastrocnemius, tibialis anterior, or soleus, EDL muscle-specific force was reduced in mice treated with endoxifen relative to all other treatment groups (**Figure 1**). To our surprise, letrozole had no effect on muscle-specific force in this non-tumor model of estrogen deficiency. We also observed significant uterine hypertrophy in endoxifen treated mice.

- These data indicate that endoxifen may have negative effects on calcium handling, and/or sarcomeric proteins in skeletal muscle via actions on the estrogen receptor (ER)-alpha. Uterine hypertrophy is also likely occurring via agonistic effects on the ER, similar to what is observed in humans.

Figure 2. Gene expression changes in skeletal muscle following endoxifen treatment

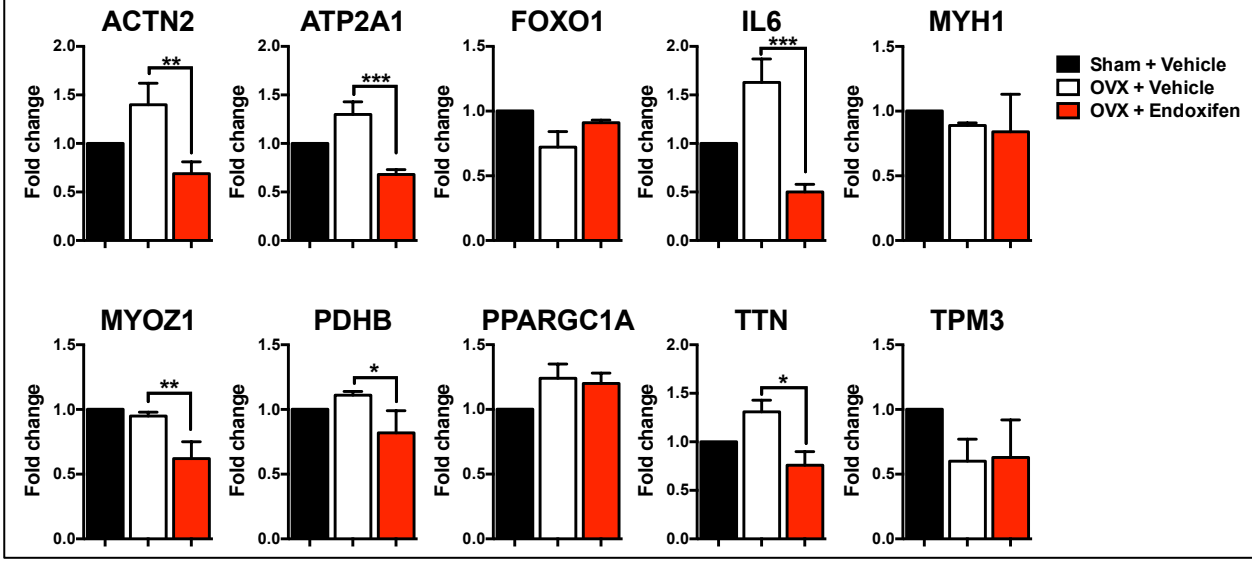

- Following *ex vivo* muscle-specific force measurement, the EDL muscle was flash frozen and RNA was later isolated in order to determine changes in gene expression resulting from endoxifen treatment. These studies revealed that expression levels of the sarcomeric proteins alpha-activin-2 (ACTN2), myozenin-1 (MYOZ1), and titin (TTN) were significantly reduced in muscle following endoxifen treatment (**Figure 2**). Furthermore, expression levels of the metabolic enzyme pyruvate dehydrogenase E1 beta subunit (PDHB) and the inflammatory factor interleukin-6 (IL-6) were reduced in skeletal muscle isolated from mice treated with endoxifen (**Figure 2**). These RT-PCR results provide a mechanistic basis for muscle weakness following endoxifen treatment.
- Endoxifen, the predominant CYP2D6 metabolite of the selective estrogen receptor modulator (SERM) tamoxifen, is currently being developed as a novel anti-estrogen therapy for the treatment of estrogen receptor (ER)+ breast cancer [clinicaltrials.gov: NCT02311933, NCT01327781, NCT01273168]. Based on our results in Task 1, we conclude that clinicians may need to consider muscle weakness as a side effect of the SERM endoxifen in postmenopausal women. These data therefore contribute to our relatively new understanding of the muscoloskeletal effects of endoxifen treatment.

Task 2. Evaluate biochemical changes in skeletal muscle resulting from estrogen (E2) deprivation therapy.

- In order to assess changes in skeletal muscle at the genomic level in mice treated with the aromatase inhibitor letrozole, RNA was isolated from frozen muscle samples collected from tumor-bearing mice treated with letrozole ± the anti-resorptive drug zoledronic acid. In order to gain a holistic picture of drug-induced changes to muscle, genetic markers were selected in the following categories: 1) functional/sarcomeric markers (**Figure 3**), 2) atrophy/hypertrophy markers (**Figure 4**), 3) inflammatory markers (**Figure 5**), 4) and uncoupling protein markers (**Figure 5**).

Figure 3 **Functional/sarcomeric muscle markers**

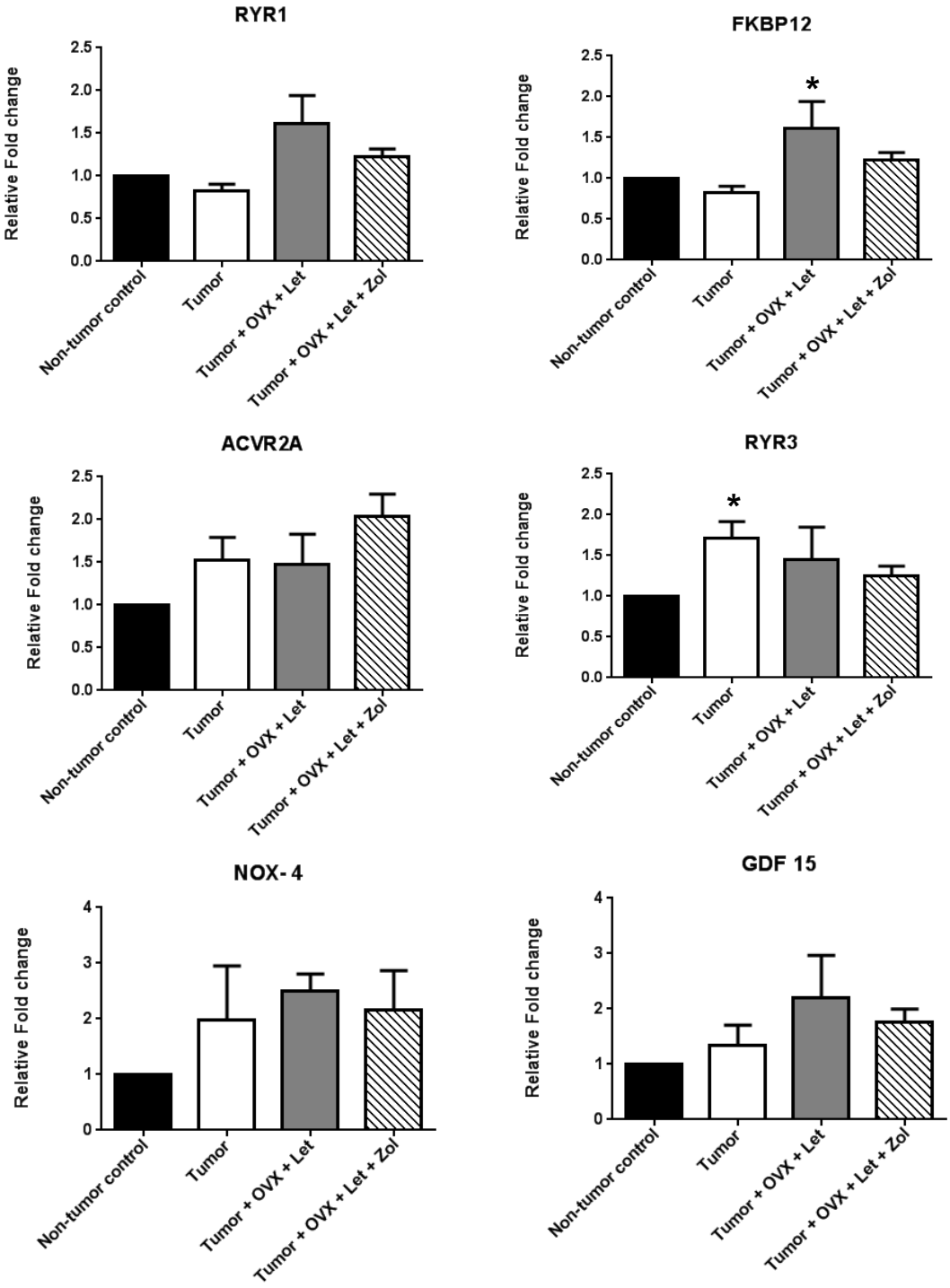

Figure 4 Atrophy/hypertrophy muscle markers

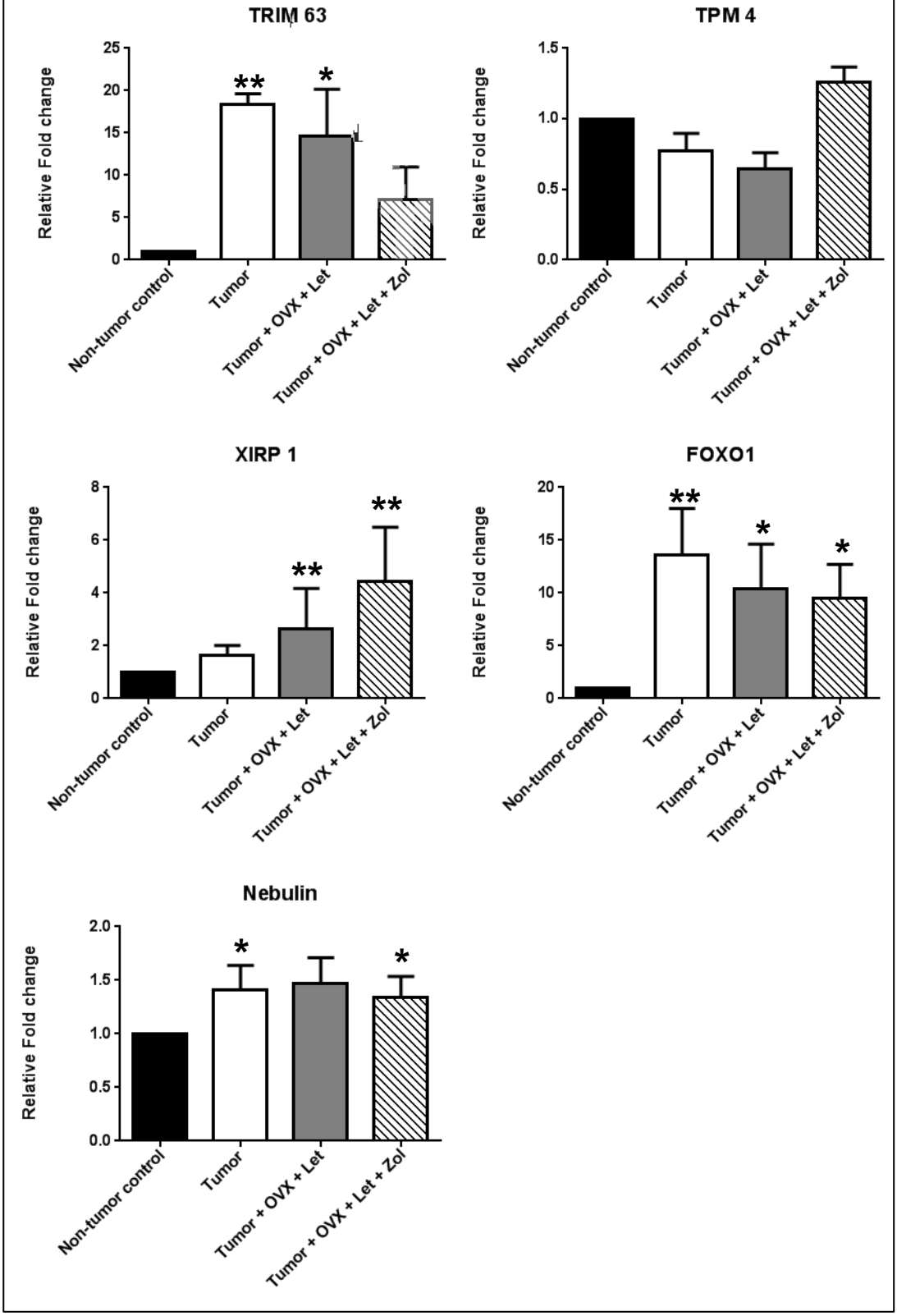

Figure 5 Inflammatory muscle marker Uncoupling muscle marker

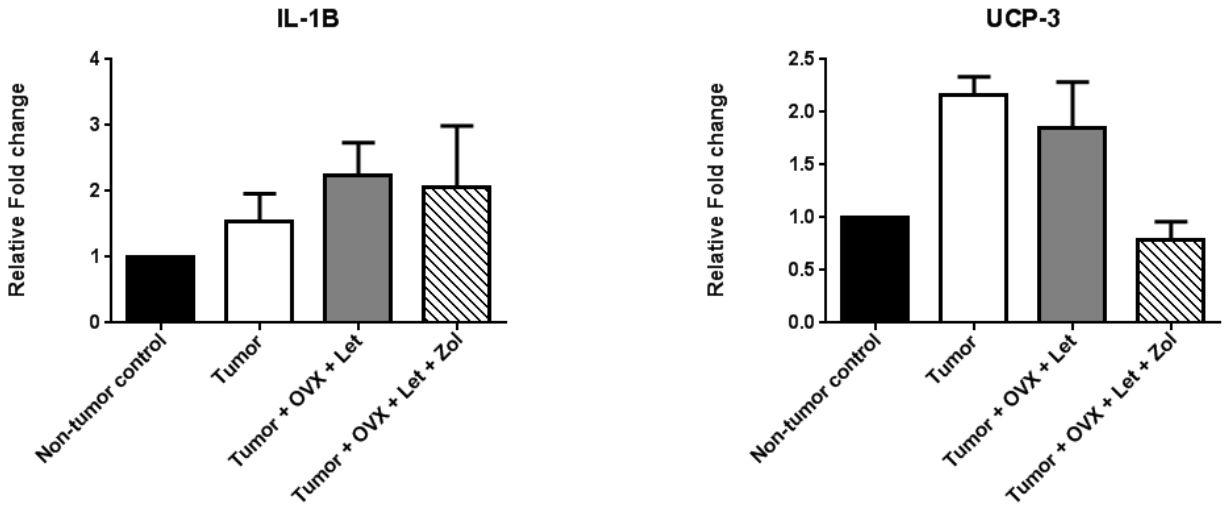

- RT-PCR results indicated that tumor- and letrozole-induced muscle weakness can largely be attributed to muscle wasting or atrophy (**Figure 3**) rather than changes to functional proteins in muscle (**Figure 4**) that lead to calcium mishandling. Additionally, inflammatory or uncoupling markers were largely unaffected (**Figure 5**), although UCP3 tended to be higher in tumor-bearing and letrozole treated mice. While not statistically significant, these data support clinical findings that exercise capacity is reduced in women with breast cancer undergoing letrozole treatment.
- Interestingly, zoledronic acid tended to have positive effects on muscle at the genomic level, supporting the functional data presented in last year's annual report and published in the resulting *Oncotarget* manuscript (see appendices) wherein muscle-specific force was improved in zoledronic acid treated mice.
- Muscle lysates were also evaluated for changes in the calcium receptor complex RyR1-Calstabin1 by co-immunoprecipitation and western blot (**Figure 6**). These proteomic data confirmed our RT-PCR data and demonstrated that letrozole treatment was not associated with dissociation or destabilization of the RyR1-complex.

Figure 6. Protein lysates were evaluated for association of RyR1 with its stabilizing subunit Calstabin 1 and for total levels of each protein in the whole muscle lysates.

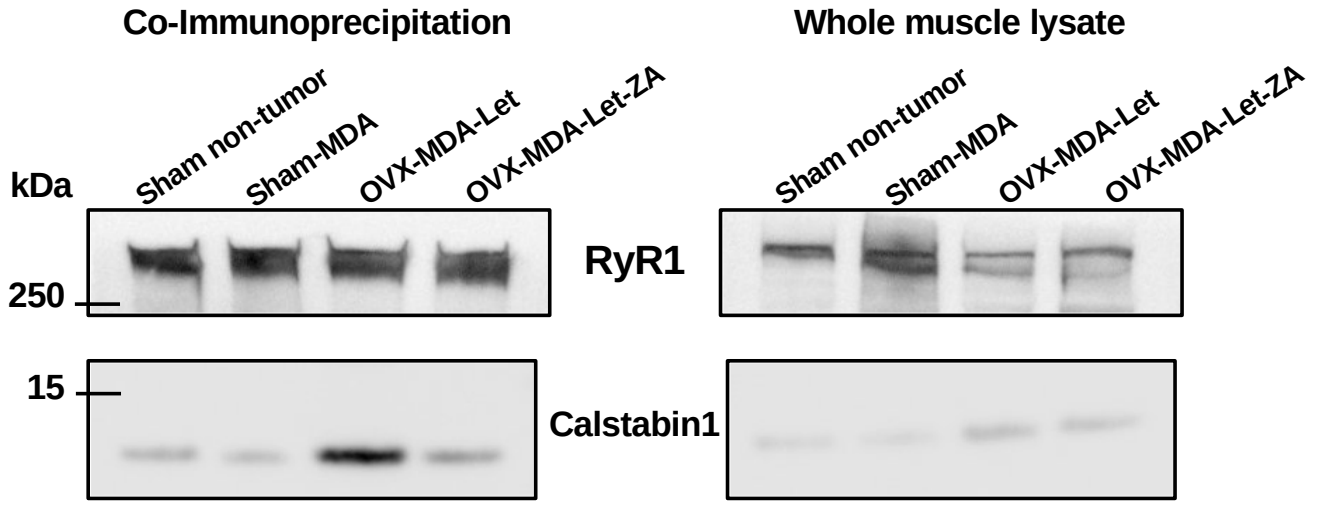

Task 3. Evaluate whether the degree of AI- and SERM-induced muscle weakness correlates with treatment-induced bone loss.

- As demonstrated in the absence of tumor, endoxifen treatment results in reduced muscle specific force in mice (**Figure 1**). In order to determine whether changes in muscle function correlate with bone loss in our model, we used bone micro-computed tomography (μCT) to measure both trabecular (cancellous) and cortical bone volume and morphology.
- Trabecular bone volume was drastically increased in endoxifen treated mice relative to ovariectomized (OVX) mice treated with or without letrozole (**Figure 7**). Moreover, microarchitectural parameters including trabecular number, trabecular separation, trabecular thickness, structure model index (SMI), and connectivity density (Conn.D) were also greatly improved. Surprisingly, these effects were more pronounced in endoxifen treated mice than in mice treated with the powerful anti-resorptive agent zoledronic acid.
- Representative images of trabecular bone at the proximal tibia are presented for comparison.

Figure 7. Cancellous bone volume and microarchitecture were improved by the SERM endoxifen in OVX mice

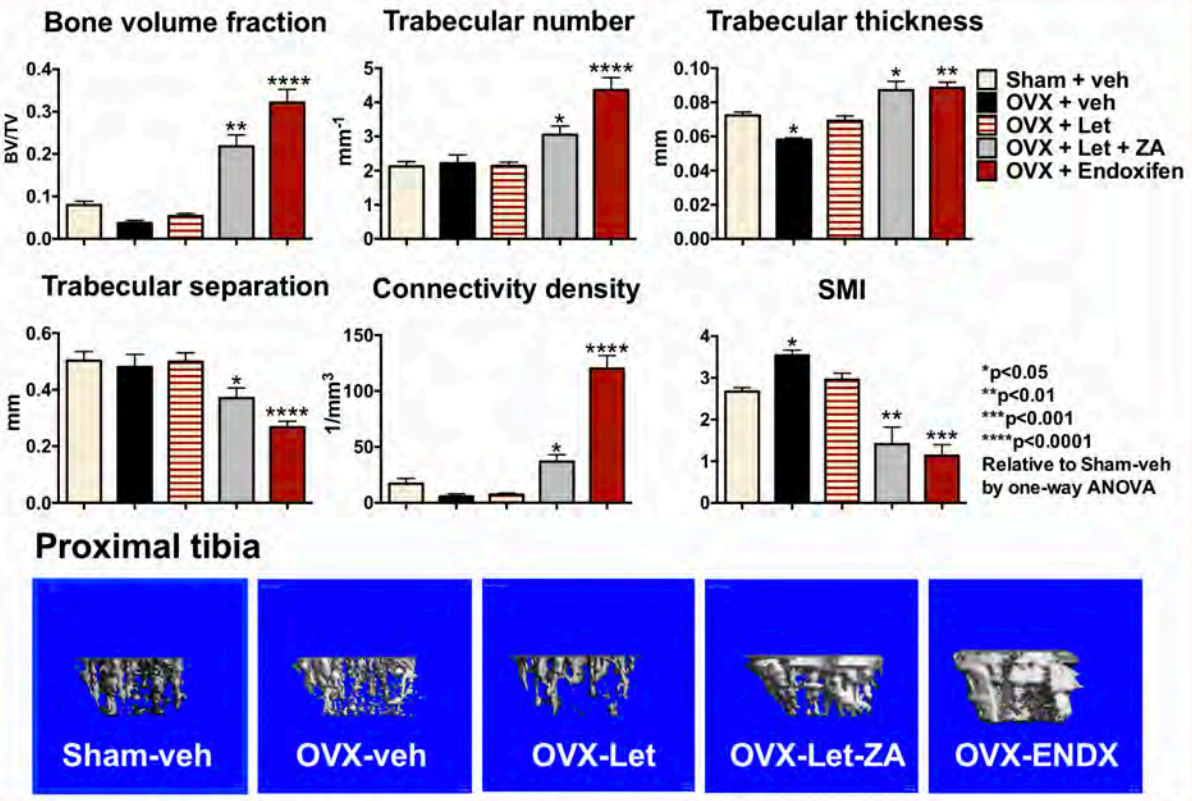

- Despite the presence of more bone overall, cortical bone analyses revealed that endoxifen treatment impaired periosteal expansion of bone, resulting in significantly reduced total cross-sectional area and medullary area (**Figure 8**). These morphological changes in cortical bone ultimately led to reduced polar moment of inertia in endoxifen bones, which indicates that resistance to torsional strain in these bones may be impaired. We postulated that while trabecular/cancellous bone volume and morphology is improved, that changes in cortical bone geometry would likely result in reduced mechanical strength of the bones.

Figure 8. Periosteal and endosteal expansion of cortical bone and polar moment of inertia were reduced by endoxifen

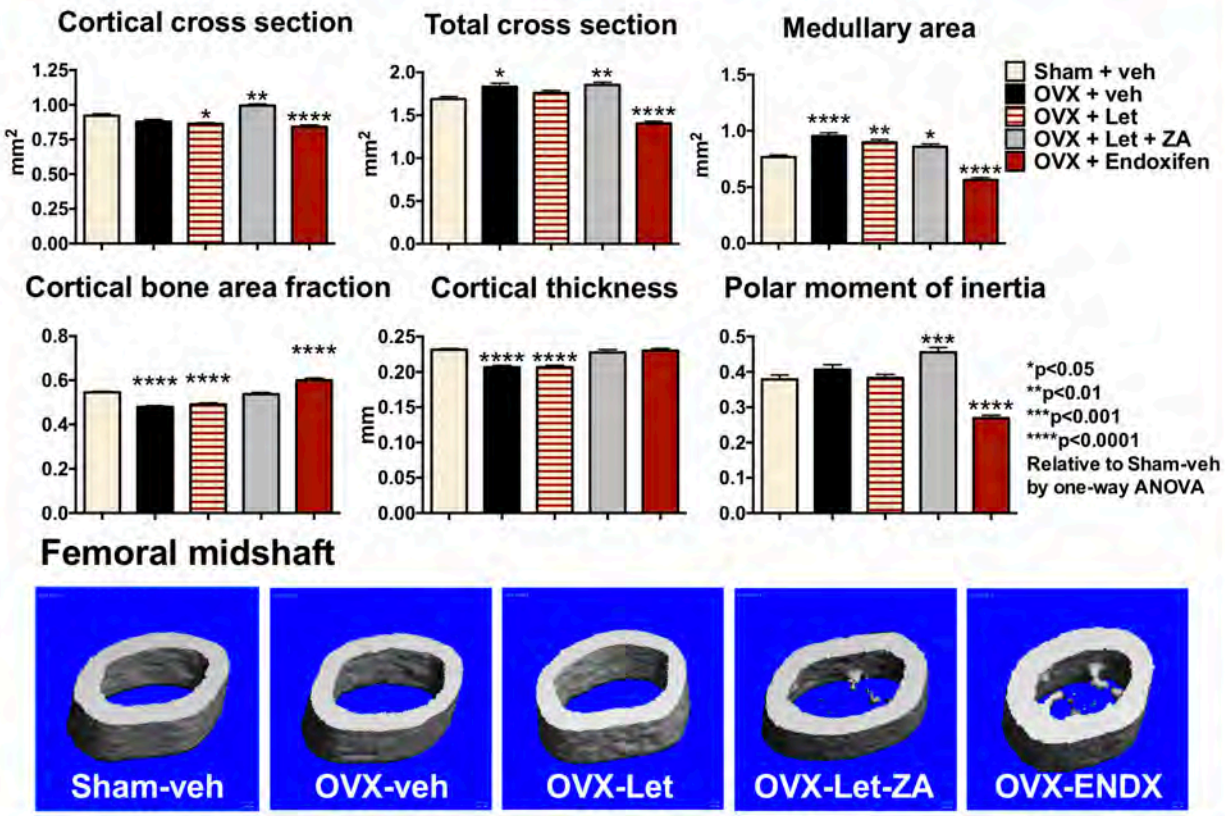

- In the final project period, we tested this postulate by analyzing the biomechanical properties of bone using a three-point bending test wherein resistance to fracture can be measured directly and quantitated. These final bone analyses will reveal whether changes observed in the bone μCT parameters translate to biomechanical changes and increase risk of fracture following endoxifen treatment.

Figure 9. Biomechanical properties of bone are improved with endoxifen treatment

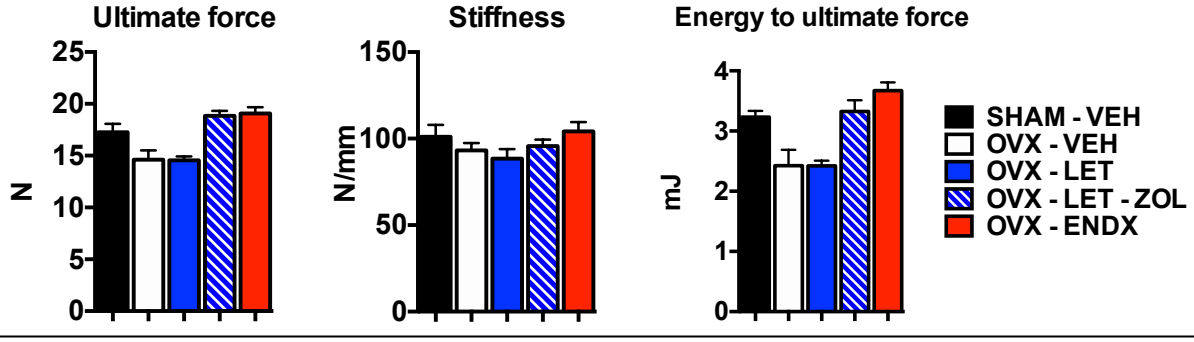

- Using a three-point bend test, we found that despite a predicted reduced resistance to fracture by bone microCT, the ultimate force, stiffness, and energy to ultimate force were increased in

femurs of endoxifen treated mice relative to OVX mice dosed with vehicle or letrozole (**Figure 9**). As expected, letrozole treatment had deleterious effects on the biomechanical properties of bone. The improvement in resistance to fracture in endoxifen treated mice was similar with observed improvements in zoledronic treated mice, the standard of care for postmenopausal osteoporotic women. These surprising results indicate that endoxifen may improve the biomechanics of bone and prevent fracture in postmenopausal breast cancer patients.

Task 4. Determine whether prevention of osteoclastic bone resorption can ameliorate muscle weakness associated with E2 deprivation *in vivo*.

- In order to determine whether inhibition of bone resorption can improve muscle function in E2 deprived mice, non-tumor bearing C57Bl mice were ovariectomized and dosed for eight weeks with vehicle, letrozole, letrozole + zoledronic acid, or endoxifen. *Ex vivo* muscle-specific force was measured at the termination of the study. Prevention of bone resorption with the anti-resorptive zoledronic acid did not improve muscle-specific force in letrozole treated mice (**Figure 10**).

Figure 10. Prevention of bone loss did not improve muscle-specific force in non-tumor bearing OVX mice

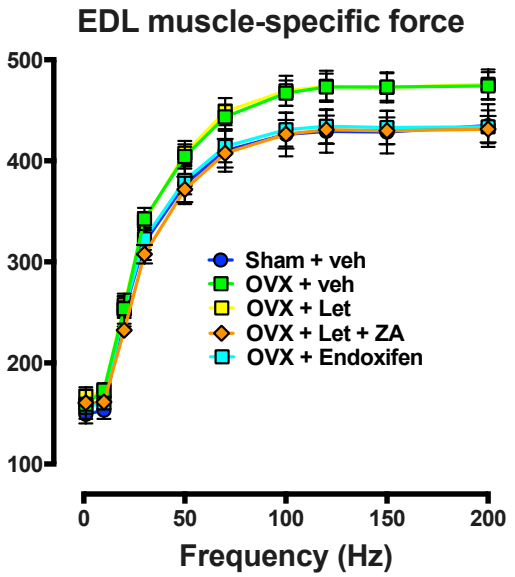

- We found no evidence for bone-loss induced muscle weakness in endoxifen treated mice. As demonstrated in Task 3, endoxifen did not result in an elevated state of bone resorption but rather inhibits bone resorption and increases new bone formation through estrogen receptor signaling (**Figure 7**). Despite this fact, muscle weakness was observed (**Figure 10**). These findings lead us to postulate that endoxifen-induced muscle weakness is likely due to direct toxic effects on skeletal muscle.

- Furthermore, from a functional standpoint forelimb grip strength was not improved with either zoledronic acid or endoxifen treatment (**Figure 11**).

Figure 11. Forelimb grip strength

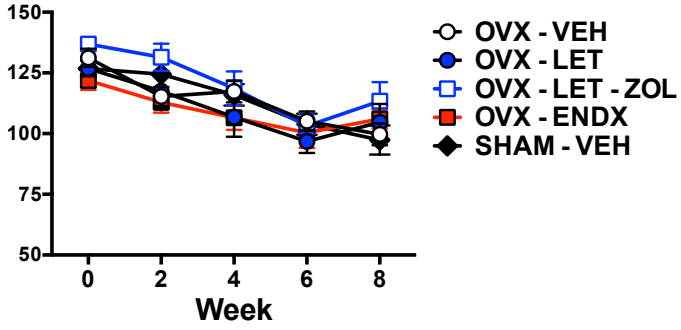

- In summary, results from Task 4 indicate that SERMs may induce muscle weakness and that this skeletal muscle side effect is independent of bone loss.

Task 5. Test the direct effects of E2 deprivation therapies letrozole (AI), endoxifen (SERM), and the anti-resorptive therapy bisphosphonate (zoledronic acid) on skeletal muscle *in vitro*.

- We evaluated drug treatments *in vitro* on myocyte differentiation and morphology using murine derived C2C12 myocytes, which when stimulated by differentiation medium containing 2% horse serum, differentiate into myotubes, as pictured:

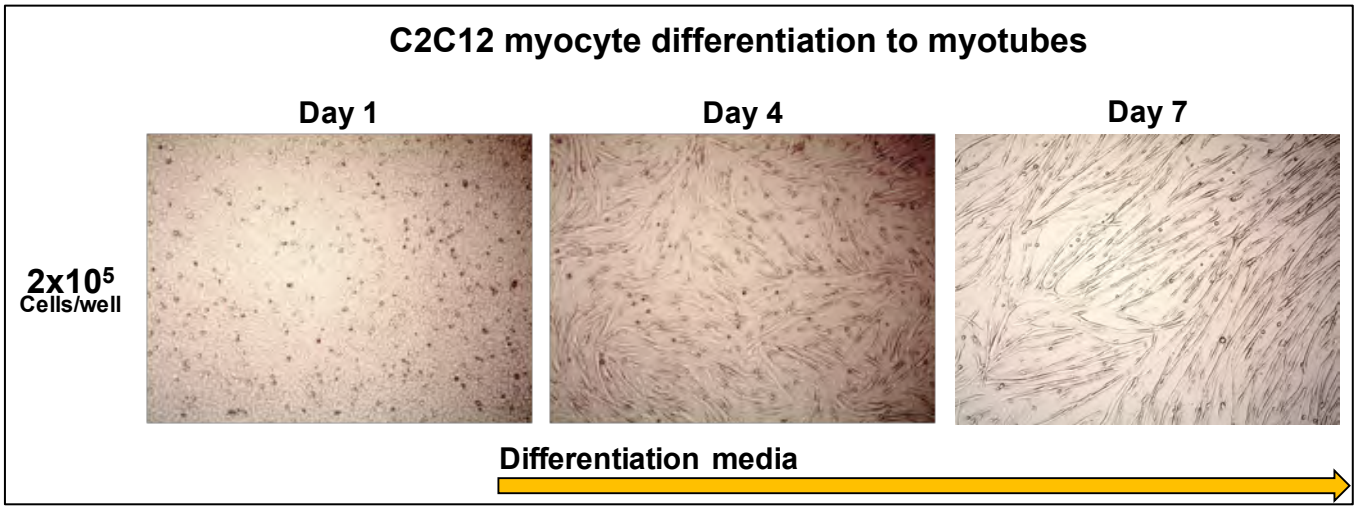

- Results from these studies did not reveal direct effects of zoledronic acid (**Figure 12**), letrozole, or endoxifen on C2C12 differentiation (fusion index) or morphology (fiber diameter).

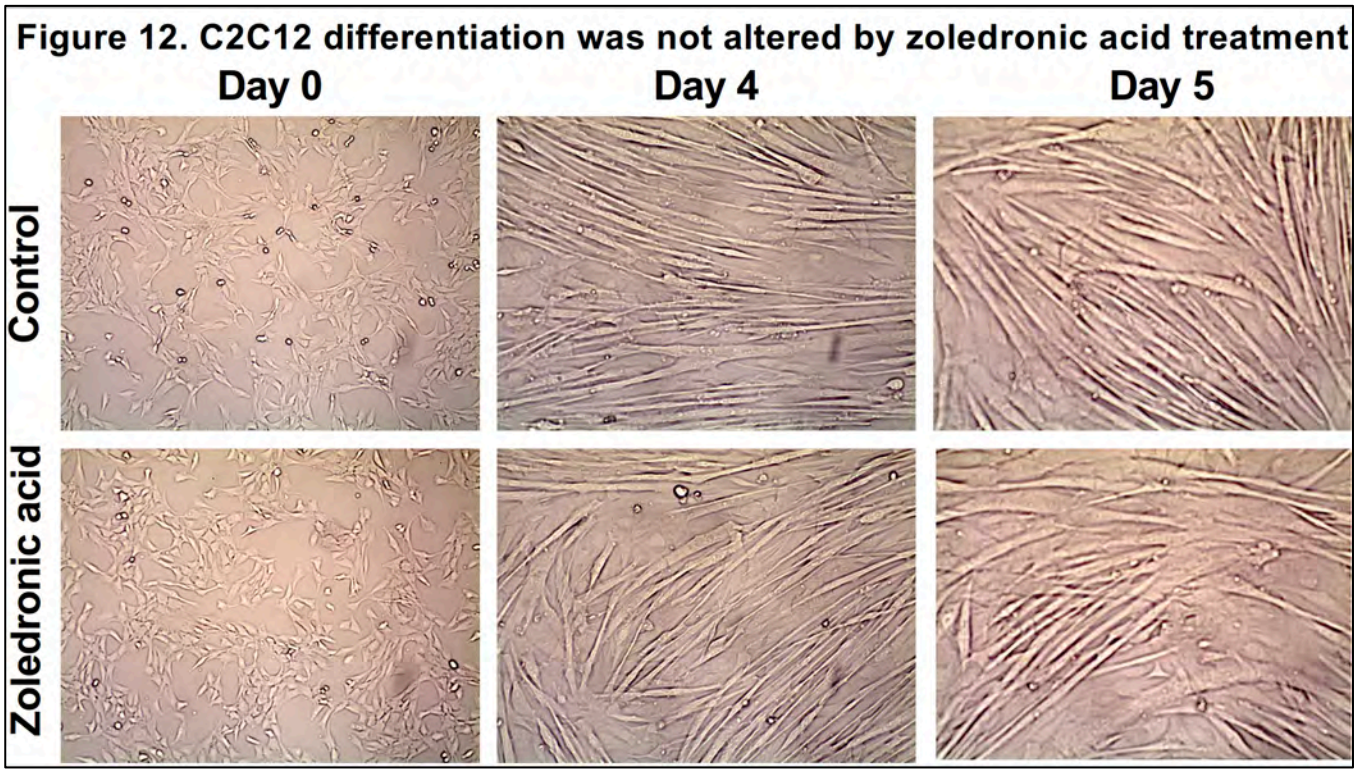

Task 6. Determine the impact of estrogen deprivation therapy (AI and SERM) on the accumulation of bone marrow adipose tissue (MAT), and whether bisphosphonate treatment (zoledronic acid) can prevent MAT accumulation in vivo.

- The right tibia was collected from OVX non-tumor bearing mice treated with letrozole, endoxifen, and zoledronic acid. In order to determine the impact of these drug treatments on bone marrow adipose tissue accumulation, bones were scanned by µCT in order to measure total bone marrow volume. After scanning the calcified tissue, bones were decalcified, and stained with osmium tetroxide, a lipid-specific radio-dense compound. Tibiae were then re-scanned by µCT and volumetric quantitation of osmium stained tissue (adipose) was assessed and expressed as a percentage of the total marrow compartment in the proximal tibia region.

- OVX-induced infiltration of bone with marrow adipose tissue was blocked by both endoxifen and zoledronic acid treatment, and peripheral adipose tissue assessed by DXA was also reduced in endoxifen treated mice (**Figure 13**). These data indicate that endoxifen may act on fat directly via the ER.

Figure 13. OVX-induced accrual of peripheral and bone marrow adipose tissue was blocked by the SERM endoxifen

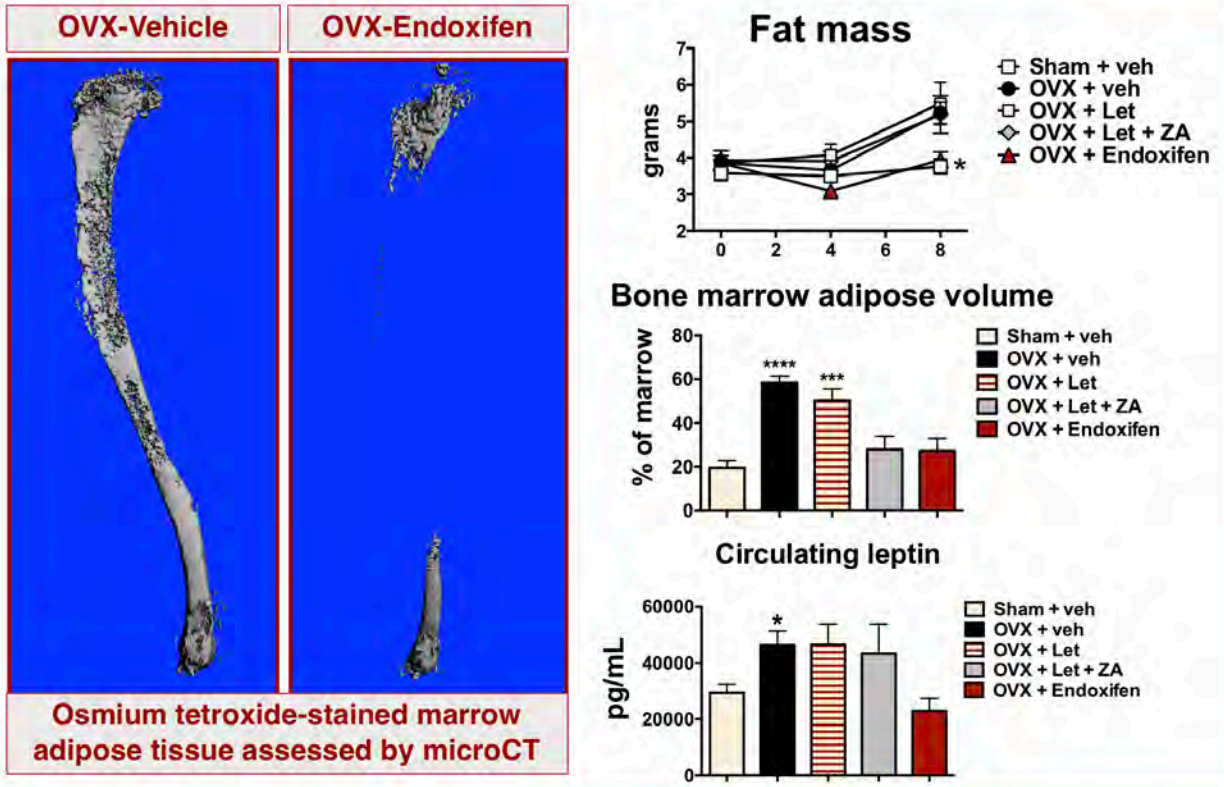

- In line with the marrow and peripheral adipose tissue findings, circulating levels of the adipokine leptin were reduced in endoxifen treated mice (**Figure 13**).
- Results obtained from Task 6 indicate that endoxifen may elicit positive effects on metabolism and adipose depots in the context of estrogen deficiency (OVX).

Task 7. Prepare manuscript containing novel findings from Tasks 1-6.

- A manuscript detailing our findings with regard to the effects of letrozole ±zoledronic acid or endoxifen on muscle, bone, and adipose tissue is being prepared for publication in the *Journal of Bone Oncology*.

Task 8. Determine whether the E2 deprivation therapy accelerates the progression of breast cancer bone metastases *in vivo*.

- As planned, four-week female athymic nude mice underwent OVX or sham surgery and were treated daily with vehicle or AI (10µg/day; n=20/group). Three weeks after surgery and onset of treatment, serum levels of 17beta-estradiol in OVX-AI mice were reduced by 56% (**Figure 14**, p<0.01; Calbiotech ELISA) and bone mineral density assessed by DXA was also significantly reduced (**Figure 14**, p<0.01). Furthermore, trabecular bone volume fraction at the proximal tibia was reduced by 67% (**Figure 15**, p<0.001; SCANCO viva40CT) relative to vehicle-sham and representative images are presented.
- After confirming estrogen deficiency and bone loss, the same animals were inoculated with ER-negative MDA-MB-231 human breast cancer cells into the left cardiac ventricle and followed for cancer progression in bone. Since MDA-MB-231 cells are ER-negative, effects of estrogen deprivation on the tumor should be indirect and attributed to the microenvironment.

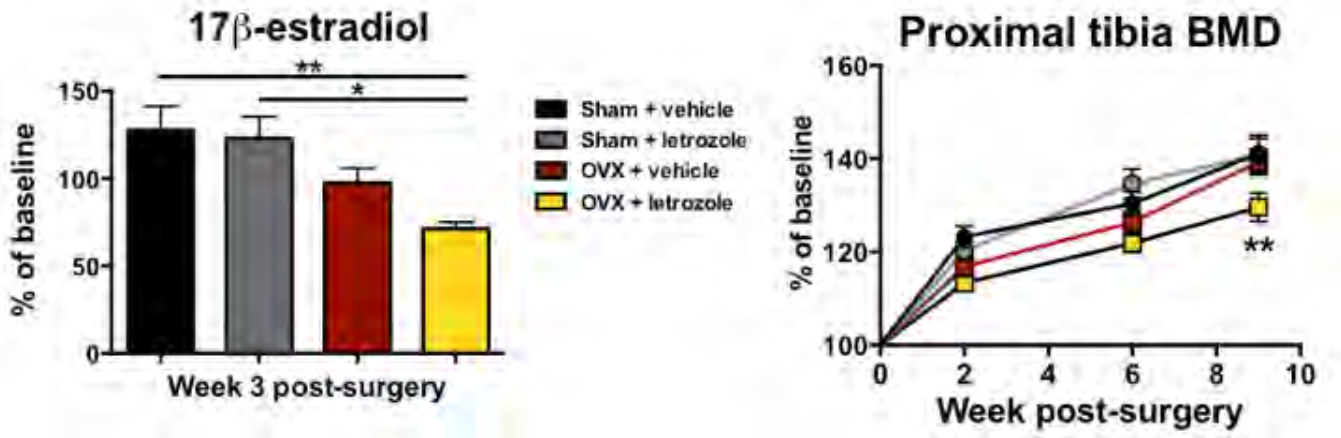

Figure 14. Three weeks post-surgery, serum 17β-estradiol levels were reduced as assessed by ELISA and bone mineral density (BMD) was reduced over time in OVX + letrozole-treated mice.

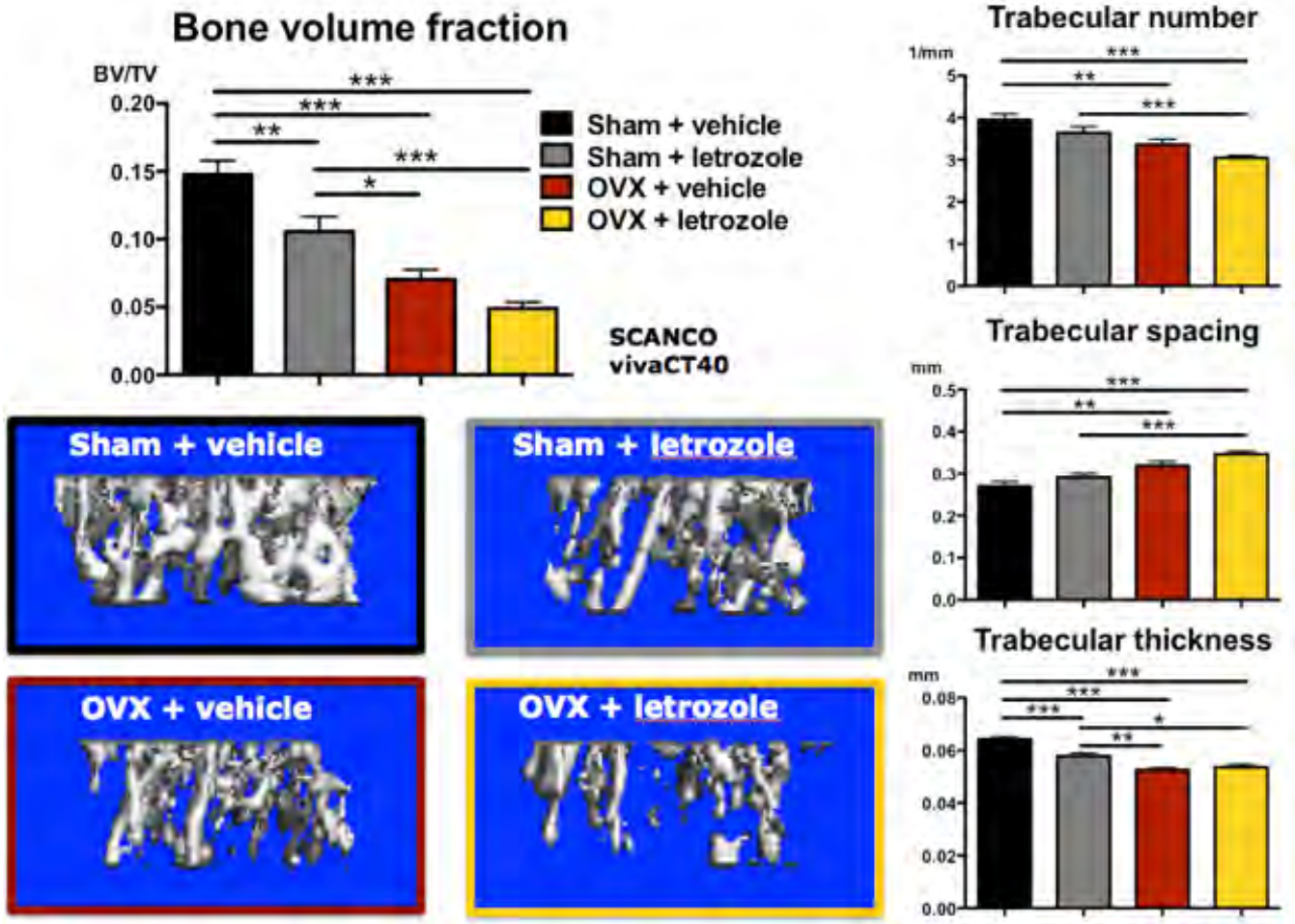

Figure 15. Three weeks post-surgery, bone volume fraction and bone microarchitectural parameters were compromised in OVX + letrozole-treated mice.

- Five weeks after inoculation of MD-MB-231 human breast cancer cells, osteolytic lesion area in bone increased by 110% (**Figure 16**, $p<0.01$, X-Ray) and tumor burden in bone assessed histologically was increased by 87% (**Figure 17**, $p<0.01$) in OVX-AI mice relative to sham-vehicle.

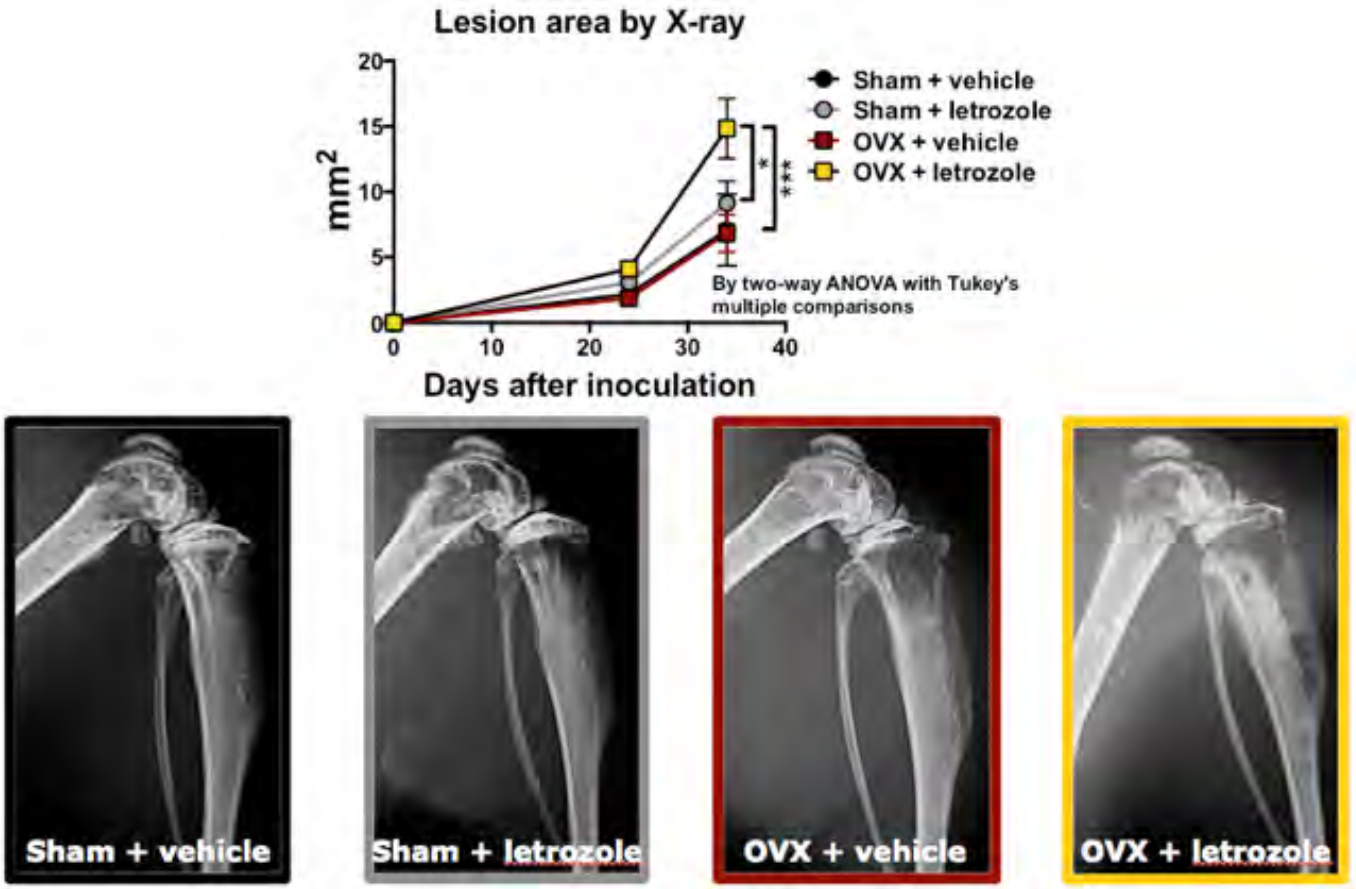

Figure 16. Five weeks after MDA-MB-231 cell inoculation, osteolytic lesion area was increased in OVX + letrozole-treated mice relative to all groups, as assessed by X-ray.

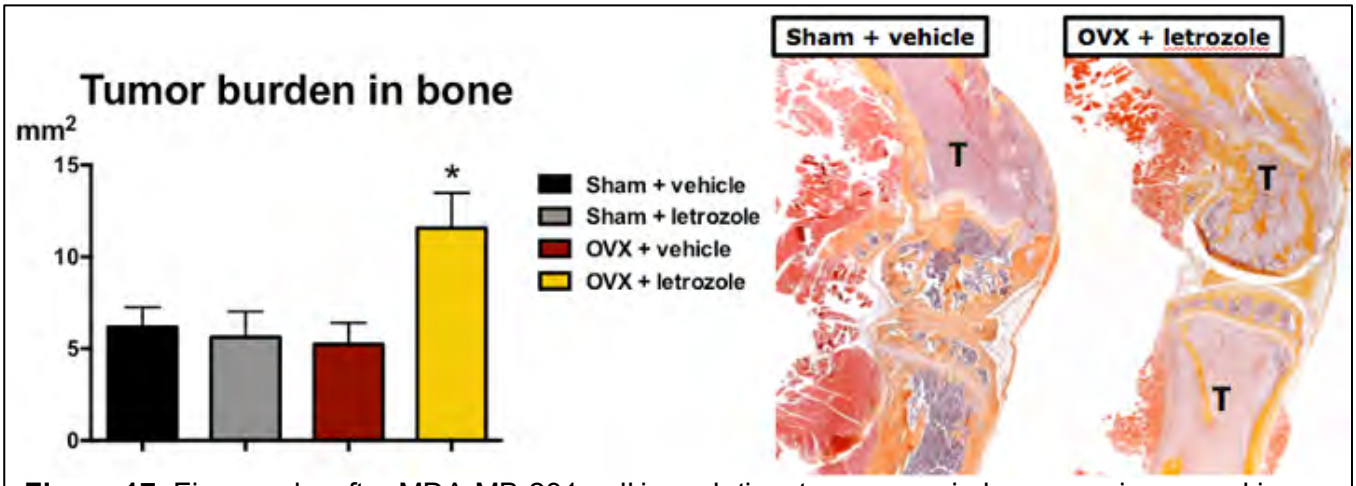

Figure 17. Five weeks after MDA-MB-231 cell inoculation, tumor area in bone was increased in OVX + letrozole-treated mice relative to all groups.

- Furthermore, we found that *ex vivo* maximal contractile force of the extensor digitorum longus muscle was significantly reduced in OVX-AI mice (**Figure 18**, -12%, $p<0.001$) relative to sham-vehicle.
- Studies in Task 8 confirmed that AI treatment induced bone loss and skeletal muscle weakness, recapitulating effects in cancer patients. As hypothesized, the severe bone loss resulting from AI-induced estrogen depletion may prime the bone microenvironment for the development of breast cancer metastases to bone and potentiate muscle weakness. This model serves as an excellent tool to

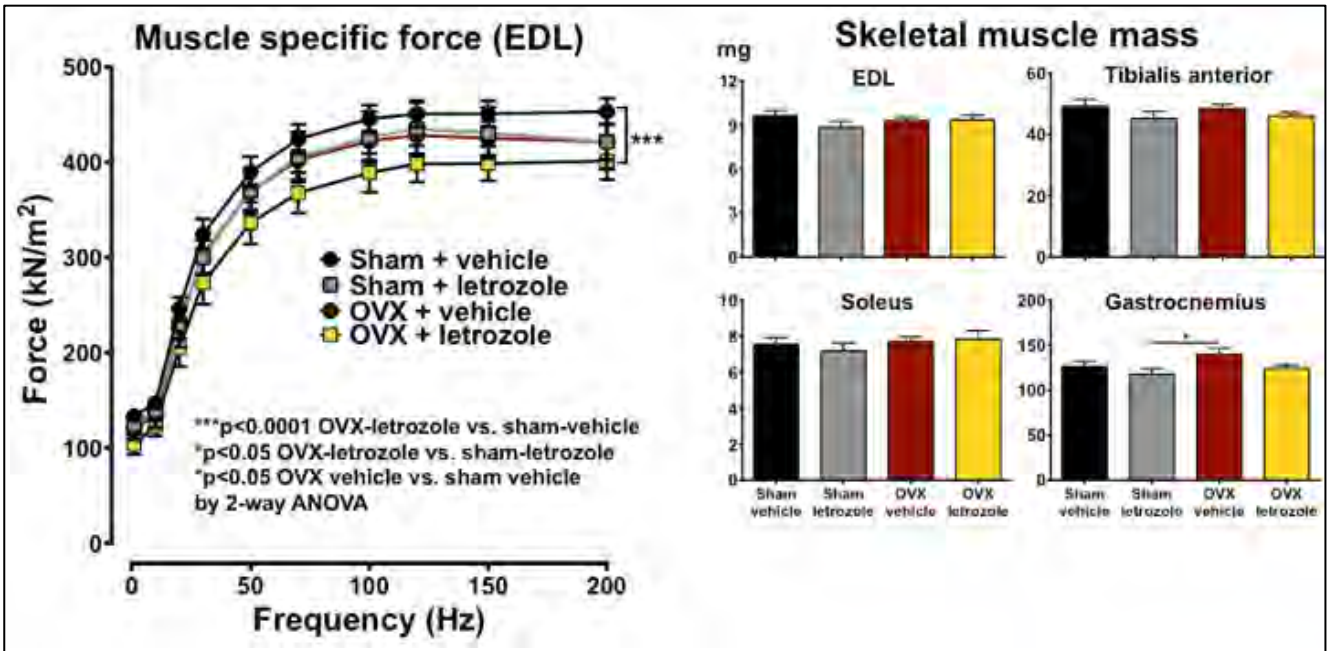

Figure 18. Five weeks after MDA-MB-231 cell inoculation, isolated whole muscle contractility was reduced in OVX mice treated with letrozole despite no change in muscle mass.

study the mechanisms of underlying musculoskeletal defects in cancer patients and to assess potential therapeutics. Studies in Task 9 will evaluate whether protection of bone with bisphosphonates can prevent AI-induced musculoskeletal complications in this model of breast cancer bone metastases.

Task 9. Determine whether prevention of E2 deprivation-induced bone loss can reduce the progression of breast cancer bone metastases *in vivo*.

OVX mice treated with AI (letrozole; 5mg/kg/d; i.p.) were also treated with the bisphosphonate zoledronic acid (ZA; 0.5 mg/kg/d) and monitored for changes in bone. As anticipated, AI-treated OVX mice lost bone relative to sham-controls, however, bisphosphonate treatment drastically reversed these deleterious effects in bone (**Figure 19**).

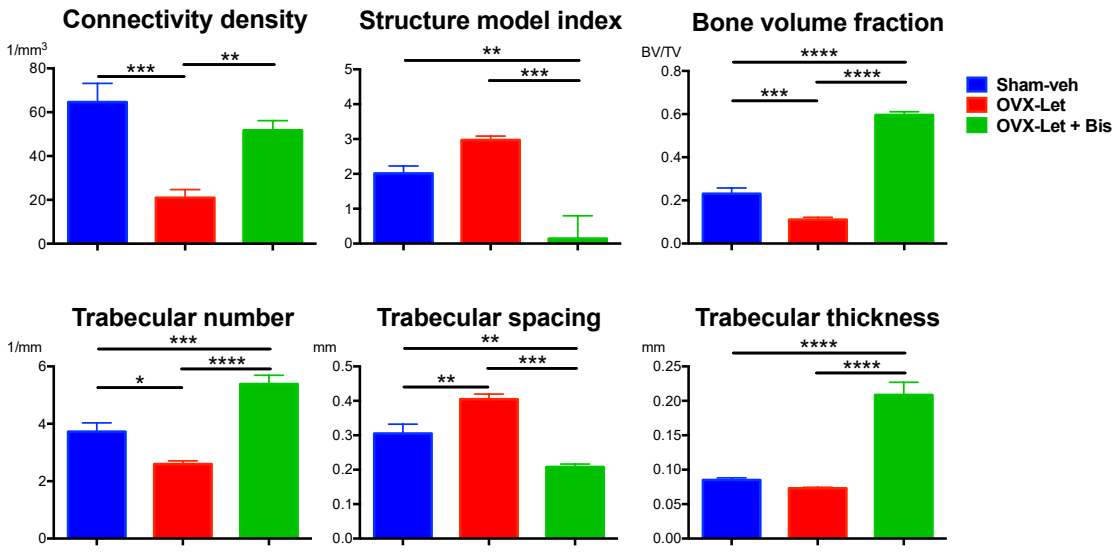

Figure 19. Three weeks post-surgery, bone volume fraction and bone microarchitectural parameters were compromised in OVX + letrozole-treated mice, and these effects were reversed by bisphosphonates.

After bone loss was confirmed in OVX-letrozole treated mice, MDA-MB-231 cells were inoculated into the left cardiac ventricle and mice were followed prospectively for changes in body weight and grip

strength (**Figure 20**).

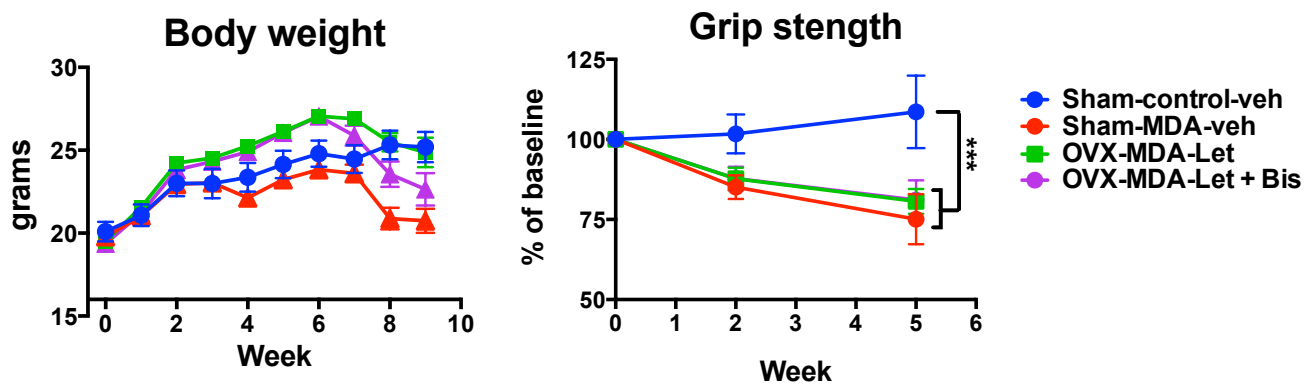

Figure 20. Following inoculation with breast cancer cells, weight and grip strength declined in cancer-bearing mice and these effects were not reversed by bisphosphonate treatment.

Despite no change in body weight or grip strength in bisphosphonate-treated mice, osteolytic lesion area was reduced relative to OVX-letrozole-treated mice and sham-vehicle-treated mice (**Figure 21**).

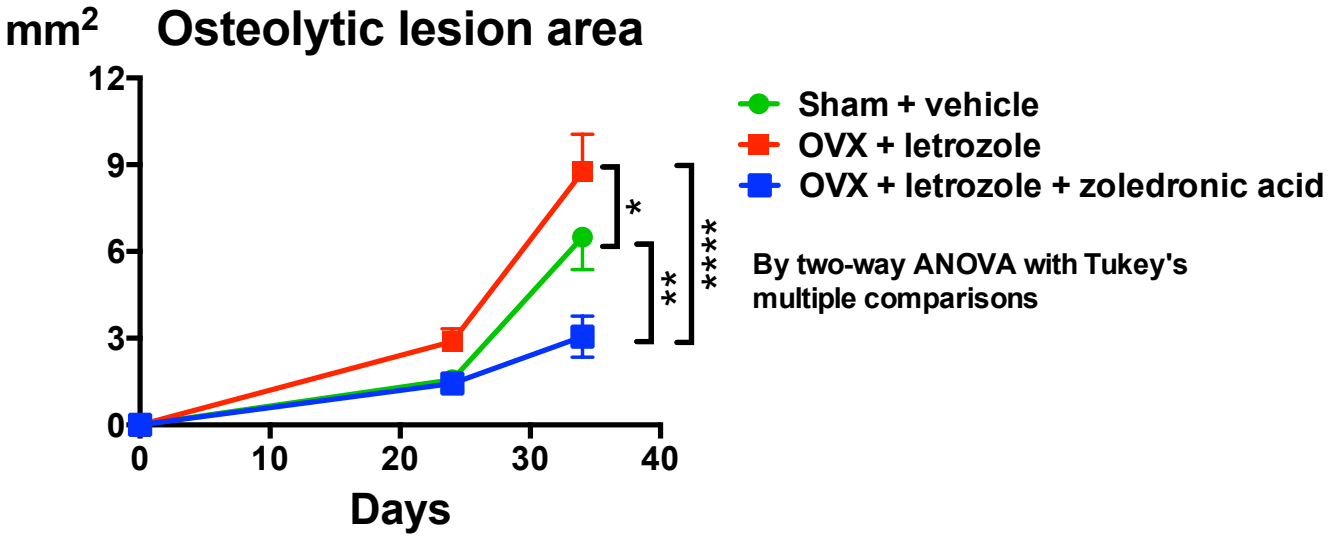

Figure 21. Osteolytic lesion area was increased in estrogen-deprived mice (OVX + letrozole) relative to sham + vehicle treated mice and this effect was reversed by the addition of bisphosphonates.

At the time of sacrifice, *ex vivo* whole muscle contractility of the EDL was recorded in all treatment groups and cancer-bearing mice with bone metastases had reduced muscle specific force relative to non-tumor control (**Figure 21**). Bisphosphonates improved muscle contractility.

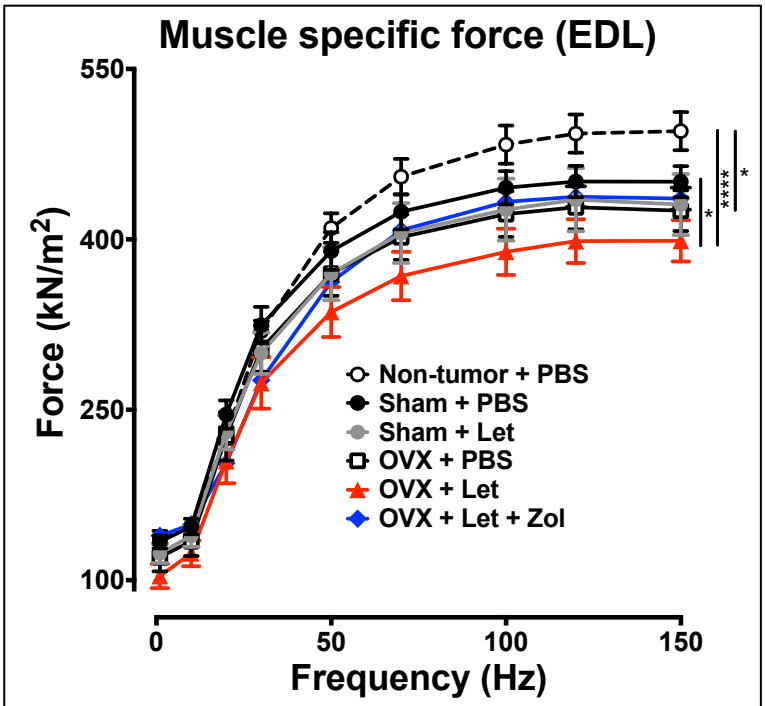

Figure 22. Five weeks after MDA-MB-231 cell inoculation, isolated whole muscle contractility was reduced in all cancer-bearing mice relative to non-tumor bearing control mice. Bisphosphonate-treated mice had increased muscle specific force relative to other cancer-bearing groups.

Task 10. Prepare manuscript containing novel findings from Tasks 8-9.

- The work described in Tasks 8-10 was submitted and accepted for publication in the peer-reviewed cancer research journal *Oncotarget* (see appendices).

B. Training & professional development accomplishments

A major component to this postdoctoral grant involves scientific and professional training in order for me to reach my primary career objective of becoming an independent cancer investigator.

- During the course of the award, I learned the following laboratory techniques, which were required for the successful completion of the aims of this grant:
    1) micro-dissection of skeletal whole muscles from the hindlimbs of mice
    2) isolated whole muscle contractility measurement of the EDL and soleus muscles
    3) hormone and cytokine assays by ELISA
    4) grip strength measurement in mice
    5) subcutaneous injection of drugs in mice
    6) immunoprecipitation of proteins from muscle lysates
- In addition to technical training, I attended career development workshops at both the American Society for Bone and Mineral Research (ASBMR) conference in September 2014 and the Orthopedic Research Society (ORS) conference in August 2015.
- In the summer of 2015, I was selected as a scientific mentor for an undergraduate student through the National Institutes of Health (NIH) Bridges to Baccalaureate Program here at Indiana University. This opportunity was my first chance to serve as a scientific mentor to an up-and-coming scientist. The Bridges to the Baccalaureate program is a collaborative project between Indiana University-Purdue University Indianapolis (IUPUI) and Ivy Tech Community

College of Central Indiana. This NIH-sponsored research program provides underrepresented minority students with experience in sciences within a research community and opens doors for those considering a career in research-related fields. During the eight-week program (June – August 2015), I trained the student in laboratory research techniques, aided in scientific writing, taught the student basic statistical concepts, and provided general college and career guidance.

- The head of the Endocrinology Section in the Department of Medicine nominated me for a promotion to junior faculty at Indiana University in the fall of 2015. The nomination and promotion was awarded in January of 2016, and contributed to my career development in terms of access to faculty resources and privileges (e.g., human tissue bank, seminars, conferences, eligibility for faculty awards, etc.,). These resources had an overall positive impact on this DoD project, and certainly on my progression toward becoming an independent cancer researcher.
- In March of 2016, I received the John G. Haddad Young Investigator Award from the American Society for Bone and Mineral Research (ASBMR) for outstanding research in the field of bone.
- As part of my development as primary investigator, I mentored a second-year medical student named Michael Campbell through the Indiana University Student Research Program in Academic Medicine (SRPinAM). During his three months under my wing, I developed a project for him related to his interests in radiation therapy, trained him in the necessary laboratory techniques, and monitored his progress throughout the study. Upon successful completion of the project, he presented his work to peers and researchers associated with the SRPinAM program at Indiana University.
- In March of 2016, I became a member of the Indiana University Simon Cancer Center (IUSCC) where I will be able to make meaningful contributions to research and outreach activities in collaboration with other members. Through the IUSCC, I now have access to its research programs and resources that will support and augment the aims of this grant proposal.
- As part of my development as primary investigator, I mentored a second-year medical student named Gabrielle Duprat through the Indiana University Student Research Program in Academic Medicine (SRPinAM). During her three months under my wing this summer, I developed a project for her related to her interests in diet-induced changes to bone marrow adipose tissue. During the course of the project I trained her in the necessary laboratory techniques and monitored her progress throughout the study. Upon successful completion of the project, she presented his work to peers and researchers associated with the SRPinAM program at Indiana University and won first place in the program's research competition.
- In June of 2017, I was awarded an American Cancer Society Internal Research Grant ($40,000) for the pursuit of a pilot project focused on how bone marrow adipose tissue affects the tumor microenvironment.
- In September of 2017, I was accepted as a member of the American Association of Cancer Research (AACR).

C. Dissemination of results to communities of interest

Results for these studies were presented by invitation to peers and thought-leaders in the fields of oncology and bone biology at the following national and international research conferences:

1. **Wright LE**, Regan JN, Robling AG, Mohammad KS, Guise TA. The anti-estrogen endoxifen altered bone morphology and reduced muscle function in mice. American Association for Cancer Research (AACR) Annual Meeting, Chicago, IL, April 2018.
2. **Wright LE**, Regan JN, Marks AR, Mohammad KS, Guise TA. Effects of the anti-estrogen endoxifen on the musculoskeletal system and implications for the tumor microenvironment. American Society for Bone and Mineral Research Annual Meeting, Denver, CO, September 2017.
3. Yi X, **Wright LE**, Pagnotti GM, Regan JN, Uzer G, Rubin CT, Mohammad KS, Guise TA, Thompson WR. Low magnitude signals decrease invasion and expression of osteolytic factors in MDA-MB-231 breast cancer cells, with subsequent suppression of osteoclastogenesis. American Society for Bone and Mineral Research Annual Meeting, Denver, CO, September 2017.
4. **Wright LE**, Harhash AA, Waning DL, Mohammad KS, Marks AR, Guise TA. Bisphosphonates prevent osteolysis and muscle weakness in aromatase inhibitor-treated mice with breast cancer bone metastases. Cancer and Bone Society (CABS) Annual Meeting, Rome, Italy, May 2016.

5. **Wright LE**, Waning DL, Harhash AA, Mohammad KS, Marks AR, Guise TA. Aromatase inhibitor-induced bone loss causes muscle weakness and increased progression of ER-negative breast cancer in bone in a murine model. American Society for Bone and Mineral Research Annual Meeting, Seattle, WA, October 2015.
6. **Wright LE**, Harhash AA, Waning DL, Chiechi A, Mohammad KS, Marks AR, Guise TA. Letrozole and ovariectomy cause bone loss, muscle weakness and increased breast cancer bone metastases in mice. American Society for Bone and Mineral Research Annual Meeting, Houston, TX, September 2014.
7. **Wright LE**, Harhash AA, Waning DL, Chiechi A, Mohammad KS, Marks AR, Guise TA. Ovariectomy combined with aromatase inhibitor treatment cause bone loss, muscle weakness and increased breast cancer metastases in mice. International Bone & Mineral Society's 13th International Conference on Cancer-Induced Bone Disease, Miami, FL, November 2013.
8. **Wright LE**, Joseph D, Harhash A, Waning D, John S, Mohammad KS, Marks AR, Guise TA. Effects of sex steroid deprivation on skeletal muscle function and ryanodine receptor (RyR1) modulation. American Society for Bone and Mineral Research Annual Meeting, Baltimore, MD, October 2013.

Invited seminars:

08/08/16	Indiana University Simon Cancer Center (IUSCC) Tumor Microenvironment and Metastasis annual retreat, invited seminar, Indianapolis, IN
05/15/16	European Calcified Tissue Society (ECTS)/Cancer and Bone Society (CABS), Cancer and Bone Pre-Clinical Day, invited seminar, Rome, Italy
03/29/16	Advance in Mineral Metabolism (AIMM) John Haddad Young Investigators Meeting, invited seminar, Snowmass, CO
08/03/15	Orthopedic Research Society (ORS) Sun Valley Workshop on Musculoskeletal Biology, Featured Young Investigator, Sun Valley, ID

Accepted peer-reviewed publications:

Investigators rely on mouse models to better understand the pathogenesis of skeletal complications of malignancy in order to identify therapeutic targets that may ultimately prevent and treat tumor metastasis to bone. In the process of working on this project, I have learned about the many experimental models of breast cancer bone metastases in use today, each with its own caveats. In collaboration with cancer researchers from around the world, I spearheaded the publication of a methods review article (see appendix) where we described and reported methods for optimizing tumor-take in murine models of bone metastasis. We then provided working protocols for four of the most common xenograft and syngeneic inoculation routes for modeling breast cancer metastasis to the skeleton in mice, including the intra-cardiac method of tumor cell injection utilized in my studies. Recommendations for *in vivo* and *ex vivo* assessment of tumor progression and bone destruction were also provided, followed by discussion of the strengths and limitations of the available tools and translational models that aid investigators in the study of breast cancer metastasis to bone.

1. **Wright LE**, Ottewell PD, Rucci N, Peyruchaud O, Pagnotti GM, Chiechi A, Buijs JT, Sterling JA. Murine models of breast cancer bone metastases. *Bonekey Rep*. 2016, doi:10.1038/bonekey.2016.31.
2. **Wright LE**, Harhash AA, Kozlow WM, Waning DL, Regan JN, She Y, John SK, Murthy S, Niewolna M, Marks AR, Mohammad KS, Guise TA. Aromatase inhibitor-induced bone loss increases the progression of estrogen receptor-negative breast cancer in bone and exacerbates muscle weakness in vivo. *Oncotarget.* 2017, Jan 31;8(5):8406-8419.

D. Anticipated activities for the next reporting period
Not applicable

4. IMPACT

Impact of accomplishments on breast cancer field

Results obtained during the granting period were significant for the field of breast cancer metastasis in that they supported the concept that a state of high bone turnover can alter the bone microenvironment to increase the progression of tumor growth at this site. The greater implications for the field are that any treatment or environmental factor that leads to bone loss (e.g., glucocorticoids, GnRH inhibitors, radiation, fracture, osteoporosis, etc.) could increase the homing of dormant disseminated cancer cells to the skeleton. Clinicians thus need to be mindful of bone health in breast cancer patients and survivors.

Additionally, we tested the musculoskeletal side effects of the novel selective estrogen receptor modulator (SERM) endoxifen, which is currently being tested in NCI sponsored trials as an alternative to tamoxifen in the adjuvant setting [clinicaltrials.gov: NCT02311933, NCT01327781, NCT01273168]. Relatively little is known about its impact on the musculoskeletal system. Our data obtained during this reporting period indicate that while endoxifen treatment leads to the accrual of high bone volume, the geometrical arrangement of bone may not be in a biomechanically optimal conformation. Testing of the mechanical properties of bone will be important for determining how endoxifen-induced changes in skeletal morphology and/or bone quality may impact strength and resistance to fracture. Our work is important because it is the first of its kind to demonstrate musculoskeletal side effects of endoxifen. While endoxifen shows promise as a potent anti-estrogen therapy for the treatment of ER+ breast cancer, our studies show that it may be important for clinicians to monitor patients for musculoskeletal side effects that could reduce drug compliance, and/or for morphological changes in bone that increase fracture risk.

Impact on society and public health

Next to nothing is known about the impact that hormone therapies have on muscle function at the cellular and molecular level, despite clinical reports of muscle weakness in patients undergoing AI treatment. Work from this second reporting period investigating this common yet understudied complication of breast cancer treatment revealed that oxidation and nitrosylation of calcium channels in skeletal muscle are likely not the mechanistic basis for AI-induced muscle weakness. If this can be confirmed in future reporting periods, antioxidants may be a viable therapeutic in the prevention or treatment of muscle weakness with AI therapy.

Finally, cancer mortality is typically not caused by growth of the primary tumor, but rather is the result of complications associated with tumor cell metastasis to secondary organ sites including bone. Information obtained from my studies could help guide the selection of therapeutics for breast cancer patients and survivors, with emphasis on the importance of maintaining bone health in order to reduce patient risk of deadly breast cancer bone metastases. The studies presented here address important unanswered clinical questions that have the potential to improve the quality and longevity of life for breast cancer patients.

5. CHANGES/PROBLEMS

Changes in approach and reasoning

Nothing to report

Anticipated problems or delays

Nothing to report

Changes that had a significant impact on expenditures

Nothing to report

Changes in use or care of vertebrate animals

Nothing to report

6. PRODUCTS

Published abstracts:

1. **Wright LE**, Regan JN, Robling AG, Mohammad KS, Guise TA. The anti-estrogen endoxifen altered bone morphology and reduced muscle function in mice. American Association for Cancer Research (AACR) Annual Meeting, Chicago, IL, April 2018.
2. **Wright LE**, Regan JN, Marks AR, Mohammad KS, Guise TA. Effects of the anti-estrogen endoxifen on the musculoskeletal system and implications for the tumor microenvironment. American Society for Bone and Mineral Research Annual Meeting, Denver, CO, September 2017.
3. Yi X, **Wright LE**, Pagnotti GM, Regan JN, Uzer G, Rubin CT, Mohammad KS, Guise TA, Thompson WR. Low magnitude signals decrease invasion and expression of osteolytic factors in MDA-MB-231 breast cancer cells, with subsequent suppression of osteoclastogenesis. American Society for Bone and Mineral Research Annual Meeting, Denver, CO, September 2017.
4. **Wright LE**, Harhash AA, Waning DL, Mohammad KS, Marks AR, Guise TA. Bisphosphonates prevent osteolysis and muscle weakness in aromatase inhibitor-treated mice with breast cancer bone metastases. Cancer and Bone Society (CABS) Annual Meeting, Rome, Italy, May 2016.
5. **Wright LE**, Waning DL, Harhash AA, Mohammad KS, Marks AR, Guise TA. Aromatase inhibitor-induced bone loss causes muscle weakness and increased progression of ER-negative breast cancer in bone in a murine model. American Society for Bone and Mineral Research Annual Meeting, Seattle, WA, October 2015.
6. **Wright LE**, Harhash AA, Waning DL, Chiechi A, Mohammad KS, Marks AR, Guise TA. Letrozole and ovariectomy cause bone loss, muscle weakness and increased breast cancer bone metastases in mice. American Society for Bone and Mineral Research Annual Meeting, Houston, TX, September 2014.
7. **Wright LE**, Harhash AA, Waning DL, Chiechi A, Mohammad KS, Marks AR, Guise TA. Ovariectomy combined with aromatase inhibitor treatment cause bone loss, muscle weakness and increased breast cancer metastases in mice. International Bone & Mineral Society's 13th International Conference on Cancer-Induced Bone Disease, Miami, FL, November 2013.
8. **Wright LE**, Joseph D, Harhash A, Waning D, John S, Mohammad KS, Marks AR, Guise TA. Effects of sex steroid deprivation on skeletal muscle function and ryanodine receptor (RyR1) modulation. American Society for Bone and Mineral Research Annual Meeting, Baltimore, MD, October 2013.

Peer-reviewed publications:

1. **Wright LE**, Ottewell PD, Rucci N, Peyruchaud O, Pagnotti GM, Chiechi A, Buijs JT, Sterling JA. Murine models of breast cancer bone metastases. *Bonekey Rep*. 2016, doi:10.1038/bonekey.2016.31.
2. **Wright LE**, Harhash AA, Kozlow WM, Waning DL, Regan JN, She Y, John SK, Murthy S, Niewolna M, Marks AR, Mohammad KS, Guise TA. Aromatase inhibitor-induced bone loss increases the progression of estrogen receptor-negative breast cancer in bone and exacerbates muscle weakness in vivo. *Oncotarget.* 2017, Jan 31;8(5):8406-8419.
3. **Wright LE,** Regan JN, Pagnotti GM, Trivedi T, Narasimhan A, She Y, John S, Murthy S, Suresh S, Mohammad KS, Robling AG, Guise TA. Comparison of the musculoskeletal effects of the aromatase inhibitor letrozole and the novel selective estrogen receptor modulator endoxifen. *J Bone Oncology* (submitted).

Book chapter:

Wright LE. (2018). Radiation Therapy-Induced Osteoporosis. In CJ Rosen, R Bouillon, JE Compston & V Rosen (Eds.) *Primer on the Metabolic Bone Diseases and Disorders of Mineral Metabolism, 9th Edition (pp. 788-92)*. Ames, IA: Wiley-Blackwell.

7. PARTICIPANTS & OTHER COLLABORATING ORGANIZATIONS

Primary investigator (PI): Laura E. Wright, Ph.D. – *no change*.

8. SPECIAL REPORTING REQUIREMENTS

Nothing to report

9. APPENDICES

See attached documents

LAURA E. WRIGHT

Curriculum Vitae

Assistant Research Professor of Medicine
Indiana University School of Medicine
Department of Medicine, Division of Endocrinology
980 West Walnut Street
Walther Hall R3, Room #C132
Indianapolis, IN 46202

Laboratory: 317.278.6017
Office: 317-278-6014
FAX: 317.278.2912
Laewrig@iu.edu

OBJECTIVE

My long-term objective is to work as a physician scientist at a top-tier academic research institution where I can positively impact treatment outcomes for cancer patients and make meaningful contributions in oncology research, mentorship, and administrative roles.

EDUCATION

- M.D., Indiana University School of Medicine, Indianapolis, IN – 2022 *(anticipated)*
- Executive Certificate in the Business of Life Sciences, Kelley School of Business, Indiana University, Bloomington IN – 2015
- Ph.D., Physiological Sciences, University of Arizona, Tucson, AZ – 2012
- M.S., Physiological Sciences, University of Arizona, Tucson, AZ – 2007
- B.S., Human Biology, Biola University, La Mirada, CA – 2005

POSITIONS

2016 – 2018	Assistant Research Professor of Medicine, Department of Medicine, Division of Endocrinology, Indiana University School of Medicine, Indianapolis, IN
2012 – 2015	Postdoctoral Research Fellow, Department of Medicine, Division of Endocrinology, Indiana University School of Medicine, Indianapolis, IN
2006 – 2012	Graduate Research Associate, Department of Medicine, Endocrinology Section, University of Arizona, Tucson, AZ
2005 – 2006	Graduate Research Assistant, McKnight Brain Institute, Neural Systems, Memory and Aging (NSMA), Department of Psychology, University of Arizona, Tucson, AZ
2005 – 2011	Graduate Teaching Assistant, Department of Physiology, University of Arizona, Tucson, AZ

EXPERIENCE AND PROFESSIONAL MEMBERSHIPS

2018	Member, Review Committee for Clinical and Translational Sciences Institute (CTSI), Collaboration in Translational Research (CTR) Pilot Grant Program, Indiana
2017 – present	Member, American Association for Cancer Research (AACR)
2016 – 2018	Member, Indiana University Simon Cancer Center (IUSCC)
2016 – present	Member, Cancer and Bone Society (CABS)
2015 – present	Mentor, National Institutes of Health (NIH) Bridges to Baccalaureate Program, IUPUI, Indianapolis, IN
2007 – present	Member, The American Society for Bone and Mineral Research
2009 – 2010	Member, Graduate Student Library Advisory Council Committee, University of Arizona
2008 – 2009	Member, Recruitment & Admission Committee, University of Arizona, Graduate Interdisciplinary Program in Physiological Sciences

INVITED SEMINARS

08/08/16	Indiana University Simon Cancer Center (IUSCC) Tumor Microenvironment and Metastasis annual retreat, invited seminar, Indianapolis, IN
05/15/16	European Calcified Tissue Society (ECTS)/Cancer and Bone Society (CABS), Cancer and Bone Pre-Clinical Day, invited seminar, Rome, Italy
03/29/16	Advance in Mineral Metabolism (AIMM) John Haddad Young Investigators Meeting, invited seminar, Snowmass, CO

08/03/15	Orthopedic Research Society (ORS) Sun Valley Workshop on Musculoskeletal Biology, Featured Young Investigator, Sun Valley, ID
11/1/13	Indiana University, Tumor Biology Microenvironment Program Seminar Series, Indianapolis, IN
08/14/12	The National Institutes of Allergy and Infectious Diseases (NIAID) Medical Countermeasures Against Radiological Threats (MCART) site visit to Indiana University, invited seminar, Indianapolis, IN
12/12/11	Indiana University, Tumor Biology Microenvironment Program Seminar Series, Indianapolis, IN
12/07/11	Veterans Affairs Medical Center/University of California-San Francisco, Bone Imaging Core, Endocrine Research Unit, San Francisco, CA
07/31/11	The American Society of Pharmacognosy Annual Meeting, Mechanism of Action Series, San Diego, CA
03/07, 11/08, 11/10	Physiological Sciences Student Forum Series Speaker, Arizona Health Sciences Center, University of Arizona, Tucson, AZ
11/04/10	Arizona Physiological Society, Featured Graduate Student Free Communication Lecturer, Midwestern University, Glendale, AZ

TEACHING EXPERIENCE

2009	University of Arizona Undergraduate Department of Physiology, Graduate Teaching Assistant, PSIO 480 “Human Physiology,” Discussion Section Lecturer
2005 – 2007	University of Arizona Undergraduate Department of Physiology, Graduate Teaching Assistant, PSIO 201 and PSIO 202 “Human Anatomy and Physiology,” Laboratory Instructor
2007	Cortiva Institute, Tucson, AZ, ANP 223 “Anatomy and Physiology IV CORE,” Lecturer

HONORS AND AWARDS

2018	Kenneth E. and N. Jeanne Starkey Scholarship for Medical Education, Indiana University School of Medicine
2016	John G. Haddad Young Investigator Award sponsored by Advances in Mineral Metabolism (AIMM) and the American Society for Bone and Mineral Research (ASBMR)
2015	Harold M. Frost Young Investigator Award sponsored by the American Society for Bone and Mineral Research (ASBMR)
2015	National Institutes of Health (NIH) Clinical Loan Repayment Program (LRP) through the National Cancer Institute (NCI)
2014	Department of Defense (DoD) – Breast Cancer Research Program Postdoctoral Fellowship Award (BC134025)
2012	Department of Defense (DoD) – Prostate Cancer Research Program Postdoctoral Fellowship Award (PC101890)
2013	Endocrine Fellows Foundation (EFF)/ASBMR Fellows Forum on Metabolic Bone Diseases award recipient, Baltimore, MD
2013	ASBMR President’s Poster Competition award recipient, Baltimore, MD
2011	National Institutes of Health (NIH) National Graduate Student Research Conference (NGSRC) award recipient, Bethesda, MD
2011	University of California-San Francisco (UCSF), Postdoctoral Bootcamp award recipient
2011	Women in Science and Engineering (WISE) Stipend Award Recipient, University of Arizona, Tucson, AZ
2009	North American Research Conference on Complementary & Integrative Medicine Trainee Travel Award recipient, Minneapolis, MN
2009	American Society of Pharmacognosy Student Travel Award Recipient, Honolulu, HI
2008	Ruth L. Kirschstein National Research Service Award (NRSA) for Individual Predoctoral Fellowship Training (F31, NIH/NCCAM)
2008	Trainee Award Recipient for the Endocrine Society Annual Meeting, Basic Sciences

2008 Herb Society of America Inc. Research Award Recipient
2008 1st Place Award Recipient—Best Abstract, Natural Supplements: An Evidence-Based Update Conference, Scripps Institute, San Diego, CA
2008, 2010 Herbert E. Carter Travel Award recipient, Graduate Interdisciplinary Programs, University of Arizona, Tucson, AZ

RESEARCH HIGHLIGHTS

Peer-Reviewed Publications

1. **Wright LE,** Harhash AA, Kozlow WM, Waning DL, Regan JN, She Y, John SK, Murthy S, Niewolna M, Marks AR, Mohammad KS, Guise TA. Aromatase inhibitor-induced bone loss increases the progression of estrogen receptor-negative breast cancer in bone and exacerbates muscle weakness in vivo. *Oncotarget.* 2017, Jan 31;8(5):8406-8419.
2. **Wright LE**, Ottewell PD, Rucci N, Peyruchaud O, Pagnotti GM, Chiechi A, Buijs JT, Sterling JA. Murine models of breast cancer bone metastases. *Bonekey Rep*. 2016 May 11;5:804.
3. Waning DL, Mohammad KS, Reiken SR, Wenjun X, Anderssen DC, John S, Chiechi A, **Wright LE**, Umanskaya A, Niewolna M, Trivedi T, Charkhzarrin S, Khatiwada P, Wronska A, Haynes A, Benassi MS, Witzmann FA, Zhen G, Wang X, Cao Z, Roodman GD, Marks AR, Guise TA. TGFβ mediates muscle weakness associated with bone metastases. *Nature Med*. 2015, 21(11):1262-71.
4. **Wright LE**, Buijs JT, Kim HS, Coats LE, Scheidler AM, John SK, She Y, Murthy SM, Ma N, Chin-Sinex HJ, Bellido TM, Bateman TA, Mendonca MS, Mohammad KS, Guise TA. Single-limb irradiation induces local and systemic bone loss in a murine model. *J Bone Miner Res.* 2015, 30(7):1268-79.
5. **Wright LE**, Guise TA. The role of PTHrP in skeletal metastases and hypercalcemia of malignancy. *Clin Rev Bone Miner Metab*. 2014, 12(3):119-29.
6. **Wright LE**, Guise TA. The microenvironment matters: estrogen deficiency fuels cancer bone metastases. *Clin Cancer Res*. 2014, 20(11):2817-9.
7. **Wright LE**, Frye JB, Gorti B, Timmermann BN, Funk JL. Bioactivity of turmeric-derived curcuminoids and related metabolites in breast cancer. *Current Pharma Design*. 2013, 19(34):6218-25.
8. **Wright LE**, Frye JB, Timmermann BN, Mohammad KS, Guise TA, Funk JL. Curcuminoids block TGF-β signaling in human breast cancer cells and limit osteolysis in a murine model of breast cancer bone metastasis. *J Nat Prod.* 2013, 76(3):316-21.
9. Frye JB, Lukefahr AL, **Wright LE**, Marion SL, Hoyer PB, Funk JL. Modeling perimenopause in Sprague-Dawley rats by chemical manipulation of the transition to ovarian failure. *Comp Med*. 2012, 62(3):193-202.
10. Lukefahr AL, Frye JB, **Wright LE**, Marion SL, Hoyer PB, Funk JL. Decreased BMD in rats rendered follicle deplete by an ovotoxic chemical correlates with changes in follicle-simulating hormone and inhibin A. *Calcif Tissue Int*. 2012, 90(3):239-49.
11. **Wright LE**, Frye JB, Lukefahr AL, Marion SL, Hoyer PB, Besselsen DG, Funk JL. 4-vinylcyclohexene diepoxide (VCD) inhibits mammary epithelial differentiation and induces fibroadenoma formation in female Sprague Dawley rats. *Reprod Toxicol*. 2011, 32(1):26-32.
12. **Wright LE**, Frye JB, Timmermann BN, Funk JL. Protection of trabecular bone in ovariectomized rats by turmeric is dependent on extract composition. *J Agric and Food Chem*. 2010, 58(17):9498-504.
13. **Wright LE**, Christian PJ, Rivera Z, Van Alstine WG, Funk JL, Bouxsein ML, Hoyer PB. Comparison of skeletal effects of ovariectomy versus chemically-induced ovarian failure in mice. *J Bone Miner Res*. 2008, 23(8):1296-303.

Abstracts (Presented)

1. **Wright LE**, Regan JN, Mohammad KS, Guise TA. The anti-estrogen endoxifen altered bone morphology and reduced muscle function in mice. American Association for Cancer Research (AACR) Annual Meeting, Chicago, IL, April 2018.
2. **Wright LE**, Regan JN, Marks AR, Mohammad KS, Guise TA. Effects of the anti-estrogen endoxifen on the musculoskeletal system and implications for the tumor microenvironment. American Society for Bone and Mineral Research Annual Meeting, Denver, CO, September 2017.
3. Yi X, **Wright LE**, Pagnotti GM, Regan JN, Uzer G, Rubin CT, Mohammad KS, Guise TA, Thompson WR. Low magnitude signals decrease invasion and expression of osteolytic factors in MDA-MB-231 breast

cancer cells, with subsequent suppression of osteoclastogenesis. American Society for Bone and Mineral Research Annual Meeting, Denver, CO, September 2017.

4. **Wright LE**, Harhash AA, Waning DL, Mohammad KS, Marks AR, Guise TA. Bisphosphonates prevent osteolysis and muscle weakness in aromatase inhibitor-treated mice with breast cancer bone metastases. Cancer and Bone Society (CABS) Annual Meeting, Rome, Italy, May 2016.
5. **Wright LE**, Waning DL, Harhash AA, Mohammad KS, Marks AR, Guise TA. Aromatase inhibitor-induced bone loss causes muscle weakness and increased progression of ER-negative breast cancer in bone in a murine model. American Society for Bone and Mineral Research Annual Meeting, Seattle, WA, October 2015.
6. **Wright LE**, Harhash AA, Waning DL, Chiechi A, Mohammad KS, Marks AR, Guise TA. Letrozole and ovariectomy cause bone loss, muscle weakness and increased breast cancer bone metastases in mice. American Society for Bone and Mineral Research Annual Meeting, Houston, TX, September 2014.
7. **Wright LE**, Harhash AA, Waning DL, Chiechi A, Mohammad KS, Marks AR, Guise TA. Ovariectomy combined with aromatase inhibitor treatment cause bone loss, muscle weakness and increased breast cancer metastases in mice. International Bone & Mineral Society's 13th International Conference on Cancer-Induced Bone Disease, Miami, FL, November 2013.
8. **Wright LE**, Joseph D, Harhash A, Waning D, John S, Mohammad KS, Marks AR, Guise TA. Effects of sex steroid deprivation on skeletal muscle function and ryanodine receptor (RyR1) modulation. American Society for Bone and Mineral Research Annual Meeting, Baltimore, MD, October 2013.
9. **Wright LE**, Buijs JT, John S, Peng Z, Harhash A, Waning D, Mohammad KS, Mendonca M, Chua HL, Wolfe H, Marks A, Orschell C, Guise TA. Ionizing radiation induced both direct and systemic bone loss in murine models. International Bone & Mineral Society's 12th International Conference on Cancer-Induced Bone Disease, Lyon, France, November 2012.
10. **Wright LE**, Guise TA, Mohammad KS, Funk JL. Curcuminoids decrease osteolytic breast cancer bone metastases. The Endocrine Society Annual Meeting, Boston, MA, June 2011.
11. **Wright LE**, Lukefahr AL, Frye JB, Hoyer PB, Besselsen DG, Funk JL. 4-Vinylcyclohexene Diepoxide (VCD)-induced fibroadenomas: a novel rat model of mammary tumorigenesis. The Endocrine Society Annual Meeting, San Diego, CA, June 2010.
12. **Wright LE**, Beischel Frye J, Timmermann BN, Funk JL. Curcuminoid-containing turmeric protects bone mass and microarchitecture in ovariectomized rats. American Society for Bone and Mineral Research Annual Meeting, Denver, CO, September 2009.
13. **Wright LE**, Timmermann BN, Funk JL. Differential effects of medicinal Zingiberaceae on the prevention of bone loss. American Society of Pharmacognosy Annual Meeting, Honolulu, HI, June 2009.
14. **Wright LE**, Beischel Frye J, Timmermann BN, Funk JL. Effects of medicinal Zingiberaceae on bone loss in musculoskeletal disease. North American Research Conference on Complementary & Integrative Medicine, Minneapolis, MN, May 2009.
15. **Wright LE**, Beischel Frye J, Timmermann BN, Funk JL. Medicinal Zingiberaceae in the prevention of menopausal bone loss. Planta Medica. 74:1174, 2008.
16. **Wright LE**, Christian PJ, Rivera Z, Funk JL, Bouxsein ML, Hoyer PB. Skeletal deterioration in an ovary-intact mouse model of menopause. The Endocrine Society Annual Meeting, San Francisco, CA, June 2008.

Book Chapter

Wright LE. (2018 *in press*). Radiation Therapy-Induced Osteoporosis. In CJ Rosen, R Bouillon, JE Compston & V Rosen (Eds.) *Primer on the Metabolic Bone Diseases and Disorders of Mineral Metabolism, 9th Edition (pp. TBD)*. Ames, IA: Wiley-Blackwell.

RESEARCH SUPPORT

Completed Research Support

- BC134025 — Wright (PI) — 9/2014 – 9/2018
  Department of Defense (DoD) – Breast Cancer Research Program — $438,833
  Musculoskeletal complications and bone metastases in breast cancer patients undergoing estrogen deprivation therapy

The objective of this grant is to evaluate the effects of aromatase inhibitor therapy on the musculoskeletal system by determining how estrogen depletion impairs muscle function and whether estrogen deprivation-induced bone loss can prime the bone microenvironment in ways that increase the progression of breast cancer bone metastases.

- American Cancer Society (ACS), Internal Research Grant — Wright (PI) — 9/2017 – 8/2018
  Indiana University Simon Cancer Center — $40,000
  Effect of marrow adipose tissue accumulation on breast cancer bone metastases
  The objective of this project is to measure marrow adipose tissue (MAT)-induced changes in breast cancer growth and invasiveness using *in vitro* and *in vivo* models and to identify probable molecular mechanism(s) by which MAT alters breast cancer cell behavior.

- IU Health Strategic Research Initiative in Oncology — Wright & Waning (co-PI's) — 11/2013 – 10/2014
  Melvin and Bren Simon Cancer Center, Bio-Plex Core Pilot Project Grant — $17,820
  Systemic factors responsible for cancer- and cancer therapy-induced ryanodine receptor 1 remodeling and muscle weakness

  The goal of this project was to identify systemic factors and signaling molecules responsible for maladaptive biochemical modifications to a critical calcium channel in skeletal muscle (RyR1), which leads to muscle weakness during cancer therapy-induced bone loss.

- PC101890 — Wright (PI) — 6/2012 – 5/2014
  Department of Defense (DoD) – Prostate Cancer Research Program — $123,463
  Mechanisms of radiation-induced bone loss and effects on prostate cancer bone metastases

  The main objective of this study was to elucidate the mechanisms of radiation-induced bone loss and to determine how radiation exposure alters the bone microenvironment to increase the progression of prostate cancer bone metastases.

- F31 AT004875-04 — Wright (PI) — 9/2008 – 5/2012
  National Institutes of Health (NIH) — $146,588
  National Center for Complementary and Alternative Medicine (NCCAM)
  Ruth L. Kirschstein National Research Service Award (NRSA)
  Ginger extracts in the prevention of metabolic bone disease

  This was an individual fellowship training grant supporting four years of doctoral training in physiological sciences. Specifically, this grant supported my dissertation research on the bone-sparing effects of natural product-derived compounds in translational models of osteoporosis and lytic breast cancer bone metastases.

Citation: BoneKEy Reports **5**, Article number: 804 (2016) | doi:10.1038/bonekey.2016.31

www.nature.com/bonekey

LABORATORY METHODS

Murine models of breast cancer bone metastasis

Laura E Wright[1], Penelope D Ottewell[2], Nadia Rucci[3], Olivier Peyruchaud[4], Gabriel M Pagnotti[5], Antonella Chiechi[1], Jeroen T Buijs[6] and Julie A Sterling[7,8]

[1]Division of Endocrinology, Department of Medicine, Indiana University, Indianapolis, IN, USA. [2]Department of Oncology, Mellanby Center for Bone Research, University of Sheffield, Sheffield, UK. [3]Department of Biotechnological and Applied Clinical Sciences, University of L'Aquila, L'Aquila, Italy. [4]Physiopathologie, Diagnostic et Traitements des Maladies Osseuses, INSERM, UMR_S1033, Lyon, France. [5]Department of Biomedical Engineering, Stony Brook University, Stony Brook, NY, USA. [6]Department of Thrombosis & Hemostasis, Leiden University Medical Center, Leiden, The Netherlands. [7]Department of Medicine, Division of Clinical Pharmacology, Vanderbilt University, Nashville, TN, USA. [8]Department of Veterans Affairs, Tennessee Valley Healthcare System, Nashville, TN, USA.

Bone metastases cause significant morbidity and mortality in late-stage breast cancer patients and are currently considered incurable. Investigators rely on translational models to better understand the pathogenesis of skeletal complications of malignancy in order to identify therapeutic targets that may ultimately prevent and treat solid tumor metastasis to bone. Many experimental models of breast cancer bone metastases are in use today, each with its own caveats. In this methods review, we characterize the bone phenotype of commonly utilized human- and murine-derived breast cell lines that elicit osteoblastic and/or osteolytic destruction of bone in mice and report methods for optimizing tumor-take in murine models of bone metastasis. We then provide protocols for four of the most common xenograft and syngeneic inoculation routes for modeling breast cancer metastasis to the skeleton in mice, including the intra-cardiac, intra-arterial, orthotopic and intra-tibial methods of tumor cell injection. Recommendations for *in vivo* and *ex vivo* assessment of tumor progression and bone destruction are provided, followed by discussion of the strengths and limitations of the available tools and translational models that aid investigators in the study of breast cancer metastasis to bone.

BoneKEy Reports **5**, Article number: 804 (2016) | doi:10.1038/bonekey.2016.31

Introduction

Breast cancer metastasis to the skeleton and subsequent bone destruction often result in severe bone pain, fragility fractures, nerve compression syndromes and hypercalcemia of malignancy resulting in significant morbidity and mortality.[1,2] Elucidation of the molecular mechanisms that mediate breast cancer bone metastases and cancer-induced bone destruction has begun to reveal potential therapeutic targets that may lead to improved patient survival and quality of life; however, further investigation is necessary to address this currently irreversible late-stage complication of malignancy. Therefore, it is of utmost importance for investigators to establish well-characterized *in vivo* models of breast cancer bone metastasis.

Unlike the study of postmenopausal osteoporosis where the ovariectomy model is the clear FDA-mandated choice,[3] there are numerous murine models of breast cancer metastasis to bone, each with its own benefits and limitations. Because spontaneous metastasis to the skeleton from primary tumors in animals is rare,[2] and no single model reproduces all of the genetic and phenotypic changes of human breast cancer bone metastasis, researchers must select a model or a combination of models that best suits the aspect of the metastatic disease that they wish to investigate. Here we (1) identify the most commonly utilized breast cancer cell lines that elicit osteolytic, osteoblastic or mixed phenotypes in bone, (2) provide protocols for tumor cell inoculation routes that model metastatic disease in the skeleton and (3) explore methods for the post-inoculation monitoring of breast cancer progression in bone.

Modeling osteolytic breast cancer bone metastases

Inoculation of bone trophic tumor cells directly into the blood stream provides a useful tool for investigating the processes associated with breast cancer cell homing, colonization and subsequent metastatic tumor growth and osteolytic lesion

Correspondence: Dr LE Wright, Division of Endocrinology, Department of Medicine, Indiana University, 980 West Walnut Street Walther Hall R3, Room C132, Indianapolis, IN 46202, USA.
E-mail: laewrig@iu.edu

Received 21 October 2015; accepted 2 April 2016; published online 11 May 2016

formation in bone. Intra-cardiac inoculation of human triple negative MDA-MB-231 adenocarcinoma cells into immune-compromised mice (i.e., BALB/c nude, MF1 nude and NOD/SCID) results in tumor cell dissemination through the arterial vascular system and homing primarily to long bones, spine, jaw and lungs (**Figure 1a**; **Table 1**).[4,5] In syngeneic tumor models where murine-derived cell lines are inoculated into a murine host, a bone metastatic profile can be observed with varying degrees of success following intra-cardiac injection of 4T1 or PyMT MMTV mammary cancer cells into immune competent BALB/c or FVB/N mice, respectively (**Table 1**).[6,7]

Visceral metastases, particularly to the lung, can significantly shorten the life span of a mouse and thus limit the experimental time frame during which skeletal metastases can be studied *in vivo*. MDA-MB-231 and 4T1 cell lines have therefore been manipulated in the laboratory to produce bone-seeking sub-lines that favor homing to and colonization of mouse tibiae and femurs with a reduced propensity to metastasize to the lung. Bone-seeking sub-lines, often referred to in the literature as MDA-MB-231-B02, MDA-MB-231-1833, MDA-MB-231-B, MDA-IV and MDA-MB-231-bone, form tumors in the long bones of up to 90% of mice following intra-cardiac inoculation in BALB/c nude mice.[8–12] Intra-cardiac inoculation of the subline 4T1-2 cells into BALB/c mice results in bone metastases in 70–80% of animals (**Table 1**).[13]

Direct intra-tibial injection of a number of breast cancer cell lines including MDA-MB-231, MDA-MB-436 and SUM1315 into immunocompromised mice and 4T1 and PyMT MMTV cell lines into immune competent BALB/c and FVB/N mice results in the development of osteolytic mammary tumors in bone with minimal impact outside of bone marrow engraftment (**Figure 1b**; **Table 1**).[7,14,15] The intra-tibial model bypasses the early stages of metastasis including homing to the bone microenvironment and is therefore useful for a more direct assessment of tumor–bone interactions, particularly when interested in studying genetic manipulations of the host or tumor cells of interest.

Intra-cardiac, intra-arterial and intra-tibial inoculation of cancer cells provide useful tools for examining the later stages of breast cancer bone metastasis; however, these aforementioned models do not permit investigation into the stages that precede the colonization of breast cancer in bone, including primary tumor growth or the dissemination of tumor cells through intravazation. The 4T1 mouse mammary cancer cell line was derived from a BALB/c spontaneous mammary carcinoma,[16] and orthotopic inoculation of 4T1 cells into the

Figure 1 Radiographs of the distal femur and proximal tibia of mice with breast cancer bone metastases. Representative images are presented of (**a**). MDA-MB-231 breast cancer bone metastases 4 weeks post inoculation of 100 000 cells via intra-cardiac route, (**b**). ZR-75-1 breast cancer bone metastases 25 weeks post inoculation of 100 000 cells via intra-cardiac route, (**c**). 4T1 breast cancer bone metastases 4 weeks post inoculation of 10 000 cells via intra-tibial route, and (**d**). MCF-7 breast cancer bone metastases 20 weeks post inoculation of 100 000 cells via intra-tibial route.

Table 1 Human and mouse mammary cancer cell lines that form osteolytic bone lesions following inoculation into mice

Cell line	*Species*	*Origin*	*Subline*	*Mouse strain*	*Inoculation route*	*Metastatic site(s)*	*Time to lesion formation*
MDA-MB-231	Human	Human mammary adenocarcinoma isolated from a pleural effusion from a 51-year-old Caucasian female	Parental	BALB/c nude MF1 nude NOD/SCID NSG	Intra-cardiac Intra-tibial Orthotopic	Mouse long bones, spine and jaw Mouse tibiae Mouse bones	2–3 weeks 1–3 weeks 7 weeks
			MDA-MB-231-BO2	BALB/c nude	Intra-cardiac Intra-tibial Intra-arterial	Mouse long bones, spine and jaw Mouse tibiae Mouse long bones	2–3 weeks 1–3 weeks 2–3 weeks
			MDA-MB-231-IV	BALB/c nude	Intra-cardiac Intra-tibial Intra-arterial Intra-venous Orthotopic	Mouse long bones, spine and jaw Mouse tibiae Mouse long bones Mouse long bones Human bone X-plants	2–3 weeks 1–3 weeks 2–3 weeks 2–3 weeks 10–14 weeks
MDA-MB-436	Human	Human mammary adenocarcinoma isolated from a pleural effusion from a 43-year-old Caucasian female	Parental	MF1 nude BALB/c nude NOD/SCID	Intra-osseous	Mouse tibiae	2–3 weeks
SUM1315	Human	Isolated from a metastatic nodule of a Caucasian female patient with ductal carcinoma	Parental	NOD/SCID	Intra-tibial Orthotopic	Mouse tibiae Human bone X-plants	3–4 weeks 8–12 weeks
4T1	Mouse	Isolated from a stage 1 V mammary tumor from a female BALB/c cfC3H mouse	Parental	BALB/c cfC3H	Intra-cardiac Intra-tibial Orthotopic	Mouse long bones, spine, jaw and lungs Mouse tibiae Mouse long bones, jaw and lungs	2–3 weeks 1–3 weeks 3–6 weeks
			4T1-2	BALB/c cfC3H	Intra-cardiac Intra-tibial Orthotopic	Mouse long bones, spine, jaw and lungs Mouse tibiae Mouse long bones, jaw and lungs	2–3 weeks 1–3 weeks 3–4 weeks
PyMT MMTV	Mouse	Isolated from mammary tumour induced by MMTV viral oncogene in FVB/N female mouse	Parental	FVB/N	Intra-cardiac Intra-tibial	Mouse long bones, spine, jaw and lungs Mouse tibiae	2–3 weeks 1–2 weeks
KEP	Mouse	Mouse invasive lobular carcinoma derived from a Keratin14-driven E-cadherin/p53 (KEP) knock out primary mammary carcinoma	KEP/Luc KEP/Luc	$RAG^{-/-}$; $IL2R\gamma c^{-/-}$ BALB/c BALB/c nude	Orthotopic Intra-cardiac Orthotopic Intra-tibial	Spine Mouse long bones and spine Mouse long bones and spine Mouse tibiae	3–5 weeks 2–4 weeks 6–9 weeks 2–4 weeks

mammary fat pad of BALB/c mice results in spontaneous metastasis to lungs (~60% of mice) and bone (~20–30% of mice; **Table 1**).[17] Incidence of bone metastasis can be increased to 50–70% by utilizing the bone-seeking 4T1-2 subline.[18,19] This syngeneic model has the benefit of utilizing an immune competent mouse.

Recently, it was shown that orthotopic inoculation of luciferase-transduced murine invasive lobular breast carcinoma cells (KEP cells) resulted in the formation of bone metastases in the appendicular and axial skeleton within 3 weeks after resection of the orthotopic tumor with minimal lung involvement in BALBc nude mice (**Table 1**).[20] Although MDA-MB-231 do not metastasize to murine bone from the orthotopic site in BALB/c nude and NOD SCID mice, distant metastases at skeletal sites were observed when using NSG mice,[21] suggesting the importance of NK cells in regulating the metastatic process.

Spontaneous metastasis of an orthotopic human breast cancer tumor to bone can be achieved in an immune-compromised mouse using a unique model that incorporates human-derived bone X-plants. In recent studies, orthotopic inoculation of human-derived SUM-1315 or MDA-MB-231-IV cells into the mammary fat pad of NOD SCID mice 4 weeks following ectopic implantation of human bone resulted in spontaneous metastasis of human breast cancer cells specifically to the human bone grafts in 40–60% of animals (**Table 1**).[22,23]

Modeling osteoblastic breast cancer bone metastases

Although patients with breast cancer usually develop osteolytic bone metastases, as many as 25% will present with osteoblastic bone metastases.[24] The human breast cancer cell lines ZR-75-1 and MCF-7 can be utilized to establish an osteoblastic bone metastatic phenotype in mice.

ZR-75-1 cultures were initially derived from a malignant ascetic effusion in a 63-year-old Caucasian female with ductal carcinoma. ZR-75-1 cells possess receptors for all four classes of steroid hormones and are thus responsive to estradiol stimulation.[25,26] Mice inoculated via intra-cardiac route with ZR-75-1 cells develop osteoblastic bone metastases in the long bones; however, bone metastases are typically not detectable by X-ray for 12–25 weeks post inoculation (**Figure 1c**; **Table 2**).

Table 2 Human mammary cancer cell lines that form osteoblastic bone lesions following inoculation into mice

Cell line	*Species*	*Origin*	*Subline*	*Mouse strain*	*Inoculation route*	*Metastatic site(s)*	*Time to lesion formation*
MCF-7	Human	Human mammary adenocarcinoma isolated from a pleural effusion in a 69-year-old Caucasian female	Parental	BALB/c nude	Intra-cardiac Intra-tibial	Mouse long bones Mouse tibiae	20–25 weeks 1–3 weeks
			MCF-7/Neu	BALB/c nude	Intra-cardiac Intra-tibial	Mouse long bones Mouse tibiae	10–12 weeks 1–3 weeks
ZR-75-1	Human	Human ductal carcinoma derived from a malignant ascetic effusion in a 63-year-old Caucasian female	Parental	BALB/c nude	Intra-cardiac	Mouse long bones and spine	12–25 weeks

Human MCF-7 breast cancer cells were derived from a metastatic pleural effusion in a 69-year-old Caucasian female with breast carcinoma.[27] MCF-7 cells retain characteristics of differentiated mammary epithelium and possess estrogen receptors.[27,28] Intra-cardiac inoculation of MCF-7 cells in immune-compromised mice results in mixed osteolytic/osteoblastic bone metastases in the long bones after 20–25 weeks (**Table 2**). In order to speed metastatic progression, the MCF-7 cell line has been stably transfected with the oncogene Neu, and this cell line establishes mixed osteolytic and osteoblastic bone metastases in immunocompromised mice within 10–12 weeks after intra-cardiac inoculation.[29] Because ER + MCF-7 cell growth is estrogen dependent mice should be implanted subcutaneously with slow-release estradiol pellets (0.25 mg) prior to intra-cardiac tumor cell inoculation in order to more closely mimic a pre-menopausal tumor environment and speed the progression of tumor growth in bone.[30,31] MCF-7 and MCF-7/Neu cells are also commonly utilized to establish bone lesions in mice via the intra-tibial inoculation route, with lesions developing in a shorter time span of 1–3 weeks post injection (**Figure 1d**; **Table 2**). Estradiol supplementation is typically not introduced when MCF-7 cells are directly implanted into bone.

Materials and Methods

This section begins by detailing recommendations for the preparation of breast cancer cells and pre-operative care instructions for the handling of mice prior to inoculation. Four of the most commonly utilized cell inoculation routes resulting in breast cancer bone metastases are then described, including lists of necessary materials for each technique. Recommendations for the post-inoculation monitoring of animals and assessment of tumor progression in bone *in vivo* and *post mortem* are then described.

Breast cancer cell preparation

Manufacturer specifications should guide the user as to the appropriate growth conditions for the cell line of interest. As a general rule for all tumor cell inoculation routes, prepare cells from a fresh batch of low passage number. Split cells 1–2 days prior to the injections such that they reach ~80% confluence on the day of inoculation. Overcrowding of tumor cells can affect their metastatic potential *in vivo;* therefore, cell confluence prior to inoculation must be monitored judiciously. Wash flasks briefly with the appropriate cold cell culture media or phosphate-buffered saline (PBS), trypsinize (0.15% Trypsin EDTA) at 37 °C, and remove cells with ice-cold media containing 10% fetal bovine serum (FBS). Centrifuge (200 g, 5 min) and suspend the cell pellet in ice-cold PBS for quantitation. Re-suspend the cells at the desired concentration (**Table 3**) in cold PBS and keep the cell suspension for no more than 30 min on ice until the moment of inoculation. Prepare cells in small batches (enough for 1–2 cages or 5–10 animals) and keep on ice to minimize clumping and risk of embolism during the *in vivo* inoculation. Because of volumetric limitations of the mouse circulation 100 μl is the recommended injection volume using the intra-cardiac or intra-arterial routes.

Reagents for tumor cell preparation

(1) PBS (without Ca^{2+} and Mg^{2+})
(2) 0.15% Trypsin EDTA
(3) Cold Dulbecco's Modified Eagle Medium (or other media) with 10% FBS

Pre-operative management of mice

For the intra-cardiac, intra-arterial and intra-venous metastasis models, mice are inoculated between 4 and 6 weeks of age, as tumor-take is markedly reduced after 6 weeks. For the intra-tibial injection, 6- to 8-week-old mice are typically used, as tibiae of younger mice are small and difficult to inject accurately. A ketamine/xylazine cocktail (100 mg kg^{-1} and 10 mg kg^{-1}, respectively) or isoflurane (2.5% isoflurane at 2–3 l min^{-1} O_2) may be utilized for anesthesia during the inoculation of tumor cells depending on the laboratory's preference. Many groups, however, experience improved survival rates following intra-cardiac inoculation with the use of isoflurane (vs ketamine/xylazine), likely due to increased vascular tone and body temperature. If the mouse strain selected is furred, it may be important to shave the mouse at the site of inoculation for better visualization of anatomical landmarks.

Cellular inoculation routes for modeling breast cancer bone metastases in mice

Intra-cardiac inoculation of breast cancer cells. Once a mouse has been properly anesthetized and is unresponsive to pinch, place it on a sterile surface in supine position ensuring that the vertebral column is straight. Tape the forelimbs away from the torso at a slightly angled and upward position (**Figure 2a**). Prior to inoculation, clean the chest of the animal thoroughly with betadine and wipe with an alcohol pad or as per the institutional standard operating procedures. Once the chest has been sterilized, gently place one hand on the chest of the mouse to tighten the skin and mark the top of the sternum and the xyphoid process (distal sternum) with a permanent marker (**Figure 2a**). Make a third mark in the middle of these two landmarks and slightly to your right (animal's left) just over the heart in the third intercostal space (**Figure 2a**). This mark identifies the location of the left cardiac ventricle where you will insert the needle for tumor cell inoculation.

With intra-cardiac inoculation, prepare the needle by leaving a small air space in the top of the syringe before slowly drawing up the desired volume of cell suspension into the syringe (**Figure 2b**). This air space will permit a small influx of bright red oxygenated blood into the syringe hub when properly inserted into the left cardiac ventricle. Hold the skin of the mouse tight with one hand and insert the needle perpendicularly into the middle marking (**Figure 2c**). When the needle has entered the left cardiac ventricle, watch for the pulse of blood to appear in the hub of the needle. The appearance of air bubbles in the needle hub upon insertion

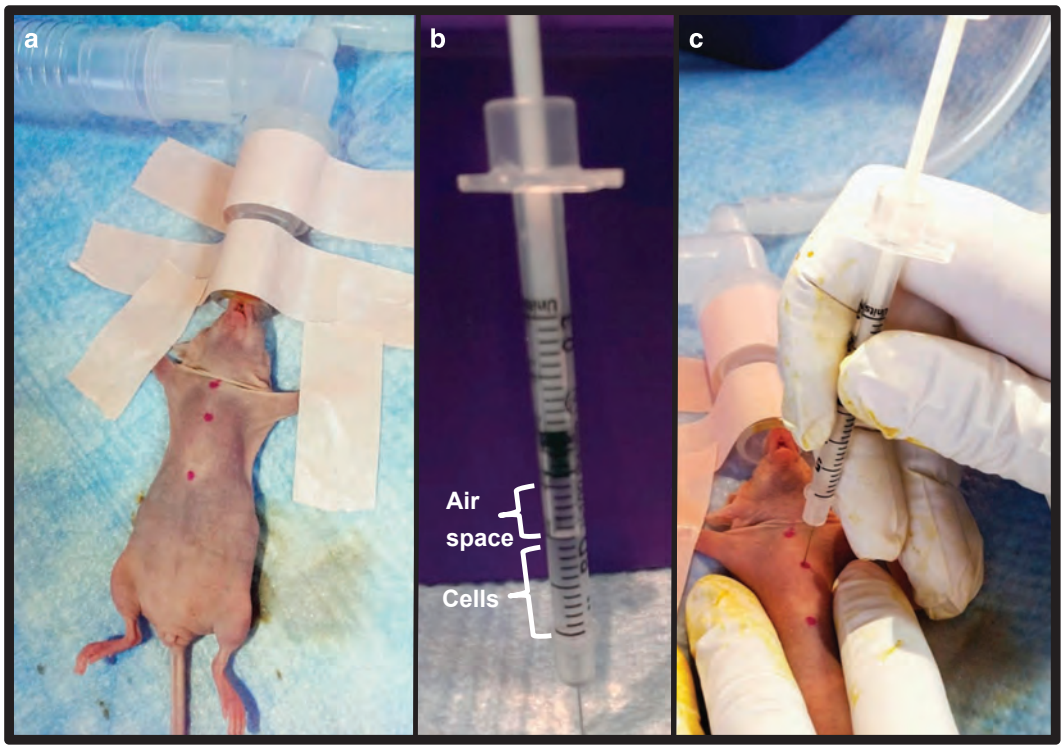

Figure 2 Inoculation of breast cancer cells in the left cardiac ventricle of a mouse. (**a**) Sterilize the chest of an anesthetized mouse and mark the top of the sternum and the xyphoid process (distal sternum) with a permanent marker. Make a 3rd mark in the middle of these two landmarks and slightly to your right (animal's left) just over the heart in the third intercostal space. (**b**) Prepare the needle by leaving a small air space in the top of the syringe before slowly drawing up the desired volume of cell suspension into the syringe. This air space will permit a small influx of bright red oxygenated blood into the syringe hub when properly inserted into the left cardiac ventricle. (**c**) Once the needle is correctly positioned in the left cardiac ventricle, inject the cell suspension slowly into the left ventricle being careful not to move the needle or press it deeper into the thoracic cavity.

indicates that it has likely entered the lungs and will need to be removed and repositioned. If you do not see a red pulse of blood in the needle hub but are confident that you are in the correct location, you can pull up slightly on the syringe plunger to verify your position in the cardiac ventricle. If there is still no visible red pulse, the needle can be slowly and slightly adjusted up or down. When small adjustments are futile, remove and reposition the insertion point completely or set the mouse aside temporarily. Extended anesthesia can cause vasoconstriction and reduce the animal's blood pressure such that the pulse of blood into the needle's hub becomes less noticeable.

Once the needle is correctly positioned in the left cardiac ventricle, inject the cell suspension slowly into the left ventricle being careful not to move the needle or press it deeper into the thoracic cavity. Keep a close eye on the cell suspension in the syringe and do not inject the air bubble at the top of the syringe (**Figure 2b**). As soon as the cells have been inoculated, quickly remove the needle, apply slight pressure at the injection site for a few seconds and place the mouse on a heating pad until fully awake. Once mice have fully recovered, monitor their behavior for 24 h and watch for potential signs of embolism or distress.

Materials for intra-cardiac inoculation

(1) Anesthetized mouse (immune compromised if using human cells)
(2) Cellular suspension
(3) 0.5–1 cc insulin syringe, 27–29G, 0.5 inch
(4) Surgical tape
(5) Betadine and alcohol swabs
(6) Permanent marker
(7) Water recirculating heating pad

Intra-arterial inoculation of breast cancer cells in the tail. Once a mouse has been anesthetized with isoflurane, place it on a sterile surface in supine position and tape the torso of the mouse to the table for

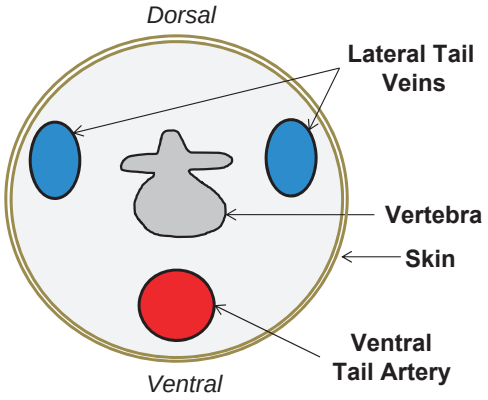

Figure 3 Schematic representation of the tail vasculature of a mouse.

stability. Use a heating pad or lamp to dilate the vessels within the tail for 2–3 min in order to facilitate greater ease of inoculation. Alternatively, the tail can be placed in warm water (30–35 °C). Using an alcohol pad, disinfect the tail vigorously, which will also help dilate the vessels within the tail and facilitate inoculation. Keep the tail clinched between the forefinger and thumb and insert the needle (beveled edge facing up) horizontally across the proximal section of the tail into the artery (**Figure 3**). Once the needle has entered the artery, the opposite hand is used to retract the syringe plunger slightly to inspect for a tight fitting within the artery and inspect the barrel of the syringe for a small amount of blood, which should appear at the needle hub. This will not occur if the needle has not breached the epithelial membrane of the artery or if the syringe has protruded through the artery. Once the syringe is properly

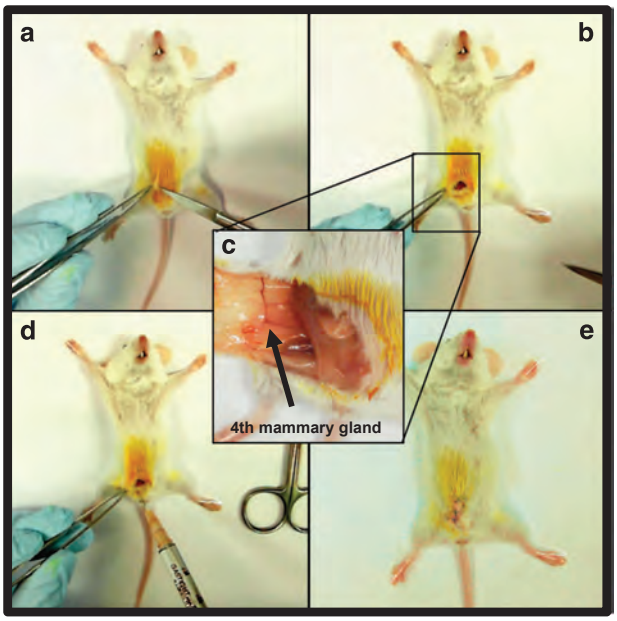

Figure 4 Inoculation of breast cancer cells in the 4th mammary fat pad of a mouse. (**a**, **b**) Place an anesthetized mouse in supine position on a sterile surface and tape the forelimbs and hind limbs away from the torso. Prior to inoculation, clean the inguinal surface of the animal thoroughly with betadine and alcohol. Using sterile surgical instruments, create a small incision in the skin adjacent to the 4th mammary fat pad. (**c**, **d**). Insert the needle into the fourth mammary gland fat pad and slowly inoculate the tumor cell suspension. The fourth mammary gland fat pad is located at the intersection of three prominent blood vessels. (**e**) After the injection of cells, close the wound with 4–6 sutures, administer an analgesic as per institutional guidelines and place the mouse on a heating pad until fully awake.

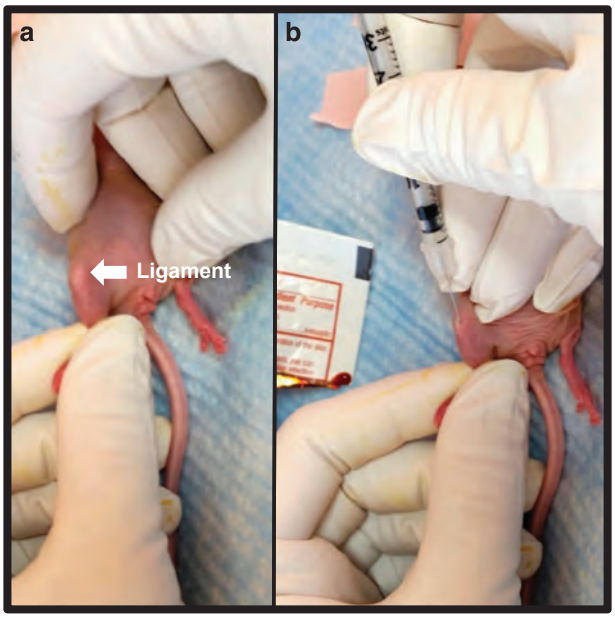

Figure 5 Inoculation of breast cancer cells in the proximal tibia of a mouse. (**a**) After sterilizing the hind limbs of an anesthetized mouse, bend the knee to nearly 90°. While holding the hind limb between the thumb and index finger, locate the patellar ligament between the knee and the tibia, which should be visible through the skin as a white longitudinal structure. (**b**) Holding the needle parallel to the tibia in the dominant hand, push the needle through the center of the patellar ligament and into the proximal end of the tibia. Resistance will be felt once the needle reaches the bone. Twist the needle slightly to drill through the growth plate until the needle can be felt giving way. Once inserted into the bone approximately 2–3 mm, inject the cell suspension slowly and then withdraw the needle using the same drilling motion used to enter the bone.

seated within the artery, depress the plunger slowly in order to minimize cell lysis resulting from fluid shear. The needle should ideally pierce the artery just once in order for the cell bolus to be delivered in its entirety. However, when small adjustments are futile, remove the needle completely and reposition the insertion point proximally to the initial site of injection. Once mice have fully recovered, monitor their behavior for 24 h and watch for potential signs of embolism, pain, or distress.

Materials for intra-arterial tail inoculation

(1) Anesthetized mouse (immune compromised if using human cells)
(2) Cellular suspension
(3) 0.5–1 cc insulin syringe, 27–29G, 0.5 inch
(4) Surgical tape
(5) Betadine and alcohol swabs
(6) Water recirculating heating pad

Orthotopic (mammary fat pad) inoculation of breast cancer cells. Place an anesthetized mouse in supine position on a sterile surface and tape the forelimbs and hind limbs away from the torso (**Figure 4a**). Prior to inoculation, clean the inguinal surface of the animal thoroughly with betadine and wipe with an alcohol pad or as per the institutional standard operating procedures. Using sterile surgical instruments, create a small incision in the skin adjacent to the fourth mammary fat pad (**Figures 4b and c**). Insert the needle into the fourth mammary gland fat pad and slowly inoculate the tumor cell suspension (**Figures 4d and e**; Supplementary Video 1). The 4th mammary gland fat pad is located at the intersection of three prominent blood vessels (**Figure 4c**). As with all techniques, it may be important for investigators to practice and familiarize themselves with the necessary anatomical landmarks prior to initiation of a multi-animal study. After the injection of cells, close the wound with 4–6 unconnected sutures, administer an analgesic as per institutional guidelines and place the mouse on a heating pad until fully awake.

In order to limit the occurrence of spontaneous tumor metastases to the lungs when using murine-derived cells (for example, 4T1), primary tumors can be surgically resected from anesthetized mice when tumors reach ~1 cm^3. Animals can then be followed for 3–4 additional weeks for the development of bone metastases.

Some laboratories have reported that orthotopic implantation of the human-derived breast cancer cell lines SUM-1315 and MDA-MB-231-IV into immune-compromised mice can elicit spontaneous metastasis to bone when preceded by engraftment of human bone plugs.[22,23] In this model, 5 mm bone biopsy cores obtained from human femoral heads (within 2–4 h of removal from the patient) can be implanted under the skin on the posterior surface of the animal prior to tumor cell inoculation in the mammary fat pad. Four weeks after bone plug implantation, the human bone grafts become vascularized and bone marrow resembles that of normal bone.[22,23] Orthotopic injection of human-derived tumor cells can then proceed as described, and the human bone plugs are then excised at the termination of the study (~8–14 weeks) and evaluated for the presence of breast cancer metastases.

Materials for orthotopic inoculation

(1) Anesthetized mouse (immune compromised if using human cells)
(2) Cellular suspension
(3) 0.1 cc Hamilton syringe, 25–27G, 0.5 inch
(4) Tape
(5) Betadine and alcohol swabs
(6) Sterile scissors and forceps
(7) Suture
(8) Water recirculating heating pad
(9) Analgesic

Intra-tibial inoculation of breast cancer cells. Prepare a syringe with the desired tumor cell suspension and set aside until ready to inject. After sterilizing the hind limbs, bend the knee to nearly 90° (**Figure 5a**). While holding the hind limb between the thumb and index finger, locate the patellar ligament between the knee and the tibia, which should be visible through the skin as a white longitudinal structure. Some laboratories choose to make a 2–3 mm incision through the skin on the knee to more easily visualize the tibia and patellar ligament; however, with practice this may not be necessary. Holding the needle parallel to the tibia in the dominant hand, push the needle through the center of the patellar ligament and into the proximal end of the tibia (**Figure 5b**). Resistance will be felt once the needle reaches the bone. Twist the needle slightly to drill through the growth plate until the needle can be felt giving way. Once inserted into the bone ~2–3 mm, attempt to move the needle slightly from side to side. When the needle is in the tibia, it will not be easily moved. If it moves freely from side to side, the needle is most likely embedded primarily in muscle and the insertion will need to be repeated. When the needle is accurately placed inside the marrow cavity of the tibia, inject the cell suspension slowly and then withdraw the needle using the same drilling motion used to enter the bone. In the event that the needle becomes clogged when penetrating or drilling through the top of the tibia, remove the original needle and re-insert a new needle, trying to follow the route created by the first needle. Once complete, use the same technique to inject the contralateral tibia with sterile PBS or desired vehicle to serve as a sham control. Bleeding rarely occurs; however, if blood does appear, apply pressure at the site. Administer an analgesic as per institutional guidelines, place the mouse on a heating pad and monitor until active.

Although cells can be inoculated into the tibia at any age, it is more difficult to penetrate the tibia in older animals once the growth plates have mineralized (>8-week old). On the other hand, very young mice can present injection difficulties due to the small size of the tibia; most laboratories therefore select 4- to 6-week-old mice for the intra-tibial inoculation route. If the mouse strain selected is furred, shave or wet the hair on the hind limb prior to the inoculation in order to better visualize the patellar ligament and other landmarks in the knee.

Materials for intra-tibial inoculation

(1) Anesthetized mouse (immune compromised if using human cells)
(2) Cellular suspension
(3) 0.1 cc Hamilton syringe, 25–27G, 0.5 inch
(4) Betadine and alcohol swabs
(5) Water recirculating heating pad
(6) Analgesic

Assessment of tumor progression in bone

Throughout a bone metastasis experiment, mice should be monitored daily for changes in activity levels, mobility and onset of cachexia, which is a paraneoplastic syndrome characterized in mice by loss of body weight, muscle atrophy and weakness, arched appearance and lethargy.[32,33] Mice should be euthanized when >10–20% body weight is lost, tumor progression impairs mobility (for example, long bone fracture, head-tilt, paraplegia) or an animal appears to be in respiratory distress. A subset of mice may require euthanasia sooner than other mice in large studies. With the exception of survival studies, it is important that mice be euthanized on the same day or as close to the same day as possible such that the experimental time frame is identical for all mice, thus permitting an accurate comparison of tumor progression between groups.

Osteolytic lesion area and abnormal bone remodeling can be visualized and assessed weekly *in vivo* using a cabinet X-ray machine (**Figure 6a**; **Table 4**). Because X-ray analysis is an assessment of overt osteolytic lesion formation and provides only indirect information on tumor cell growth, cancer cell lines are commonly transfected with bioluminescent proteins permitting *in vivo* visualization and quantitation of tumor growth at metastatic sites using bioluminescence imaging (BLI; **Table 4**).[11,20,34] BLI serves as an ideal complement to X-ray analysis of osteolysis, as it provides information on the presence of extra-skeletal metastases as well as micrometastases in bone, which precede bone destruction. Although not utilized to quantitate skeletal tumor burden, intra-vital microscopy may be useful for studying individual tumor cell motility and behavior in the bone microenvironment.[35]

At the termination of the study, mice should be subjected to necropsy and examined closely for gross evidence of metastatic foci outside of bone. For an intra-cardiac tumor inoculation study, evidence of tumor growth in the mediastinum surrounding the heart indicates that tumor cells were not accurately injected into the left cardiac ventricle, and the mouse should be excluded from the study. Fix all vital organs for future analysis. Carefully cut and scrape away skeletal muscle from the forelimbs, hind limbs and vertebral column, and fix the skeletal samples. Prior to decalcification of the bones, high-resolution *ex vivo* bone microcomputed tomography (μCT) can be performed to assess osteolytic or osteoblastic bone destruction and BV/TV at the distal femur, proximal tibia or lumbar vertebrae (**Figure 6b**).

Following decalcification, paraffin-embedded bone should be sectioned and stained with hematoxylin/eosin (H&E), and tumor burden (mm^2) should be measured in long bones and spine using image analysis software (**Figure 6c**). Osteoblast numbers may also be quantitated in H&E stained sections. Histological sections should also be stained for tartrate-resistant acid phosphatase activity in order to assess the total osteoclast number relative to the bone surface and the osteoclast number at the bone and tumor interface, all of which are known to increase with cancer-induced osteolysis (**Figure 6d**; **Table 4**).[36–37] Finally, serum can be assayed for the presence of bone turnover markers, hormones, inflammatory factors or growth factors of interest.

When applicable, quantification of spontaneous metastases to lung, liver, brain or adrenals can be performed in paraffin-embedded organs collected at necropsy. For these analyses, 5 μm sections can be cut every 200 μm through the organ and stained with H&E. The number and area of metastatic foci for each section can then be determined using image analysis software, and results can be expressed as the total metastatic foci number per organ and as total metastatic area per organ.

Discussion

When considering skeletal metastasis models with the intention of studying breast cancer osteolysis, a common choice is the intra-cardiac injection of human breast cancer cells in immune-compromised mice.[38–40] Alternatively, these human cells can be directly implanted into bone, bypassing earlier steps in the metastatic process. A benefit of the former model is that tumor cells detected in bone have themselves 'seeded the soil,' thus replicating the more natural progression of disseminated tumor cells formation of micrometastases, which progress in size over time, as occurs in humans. The necessity of using immune cell-deficient mice when inoculating human cell lines is typically seen as a limitation because it does not accurately model the immune competent human patient. It can, however, be seen as an advantage, as it eliminates possible confounding effects related to the animal's immune response and permits the study of human cells in a very permissive host environment.

The pathogenesis of breast cancer bone destruction in the intra-cardiac MDA-MB-231 model is relatively similar to the human condition. Upon inoculation, breast cancer cells circulate in the vasculature, home to the bone compartment, and micrometastases can be detected by BLI in distant skeletal sites in as early as 1 week after injection.[41] As the tumor cells proliferate in the bone microenvironment, tumor-derived

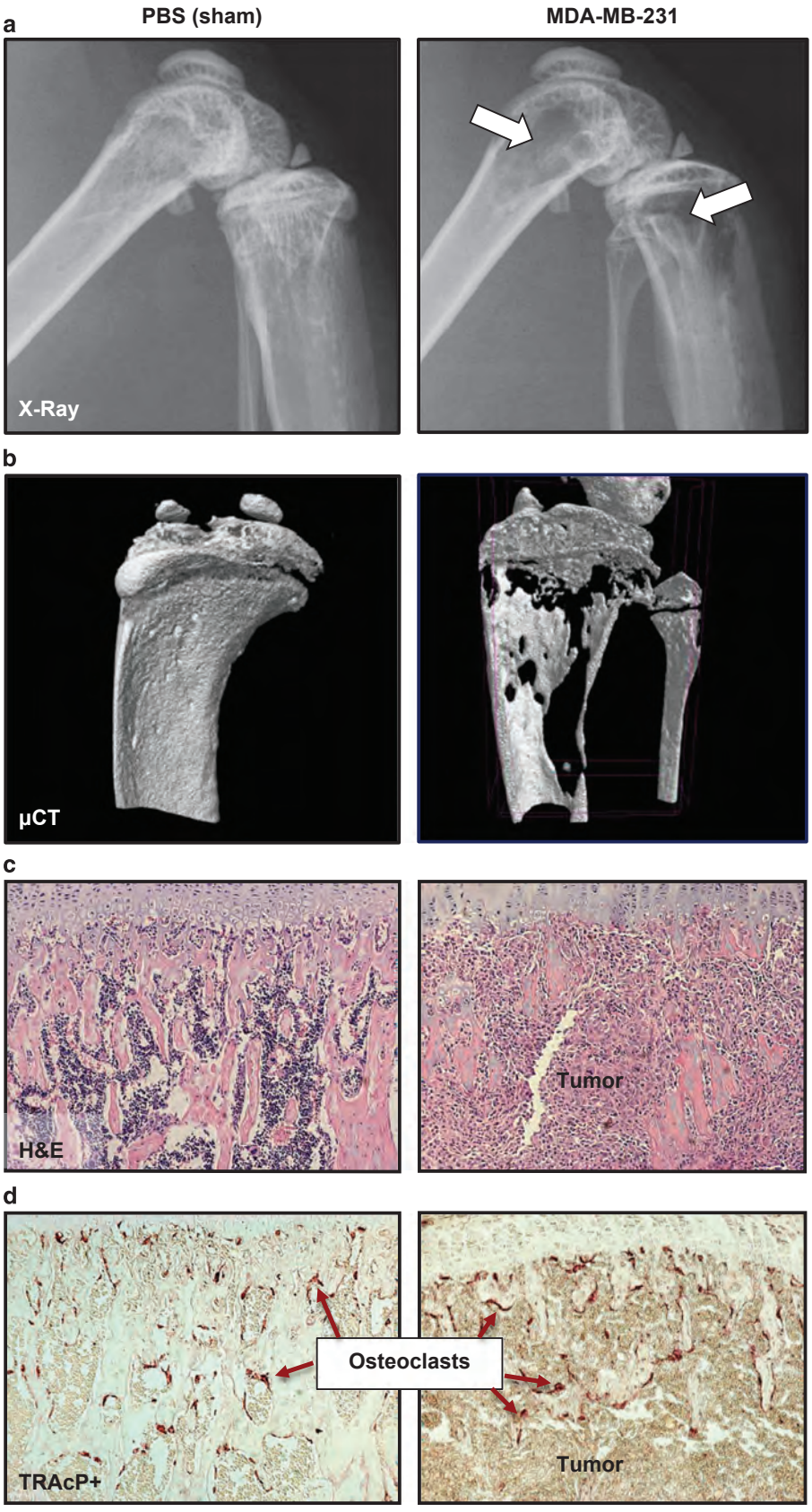

Figure 6 The assessment of tumor progression in bone can be carried out by (**a**) quantitation of osteolytic lesion area by X-Ray, (**b**) measurement of bone volume fraction (BV/TV) by bone high-resolution microcomputed tomography (μCT), (**c**) histological assessment of tumor area using hematoxylin/eosin (H&E) staining of long bones and vertebrae and (**d**) quantitation of tartrate-resistant acid phosphatase (TRAcP) + osteoclasts.

Table 3 Preparation of breast cancer tumor cells for inoculation in mice

Inoculation route	*Cell number*	*Volume (PBS)*	*Syringe/needle*
Intra-cardiac	100 000	100 μl	0.5–1 cc insulin/27–29G, 0.5 inch
Intra-arterial (tail)	100 000	100 μl	0.5–1 cc insulin/7–29G, 0.5 inch
Orthotopic	100 000–5 00 000	10–20 μl	0.1 cc Hamilton/25–27G, 0.5 inch
Intra-tibial	10 000–2 50 000	10–20 μl	0.1 cc Hamilton/25–27G, 0.5 inch

Table 4 Principal end points used to characterize the development of bone metastases in mice

Type	*Frequency*
In vivo analyses	
Activity levels and hind limb mobility	Daily
Respiratory distress	Daily
Symptoms of cachexia	Daily
X-ray analysis of osteolytic lesions	Weekly or bi-monthly
Bioluminescence imaging (BLI; if applicable)	Weekly or bi-monthly

Type	*Endpoint*
Post-mortem analyses	
Gross dissection	Inspection for visceral metastases in lung, liver, adrenals and brain tissue
Bone microcomputed tomography (μCT)	Trabecular bone volume/total volume (BV/TV) of the proximal tibia, distal femur and lumbar vertebrae
Histomorphometric analysis of bone	Tartrate-resistant acid phosphatase (TRAcP) staining of bone Osteoclast number/bone surface (OcN/BS) Osteoclast surface/bone surface (OcS/BS) Osteoclast number at the bone–tumor interface Hematoxylin/eosin (H&E) staining of bone for BV/TV and osteoblast number/bone surface (ObN/BS)
Tumor characterization	H&E staining of forelimbs, hind limbs and spine for total tumor area in bone Immunohistochemical staining for proteins of interest (e.g., cytokeratin, phospho-smads) H&E staining of visceral organs for quantitation of soft tissue metastases
Serum factors	Biomarkers, if applicable (e.g., bone turnover markers, hormones, inflammatory factors, growth factors, tumor-derived factors)

osteolytic factors stimulate osteoclastic bone resorption and the development of bone lesions, which are quantifiable by X-ray. The most substantial bone destruction tends to occur in the metaphyses of the distal femur and proximal tibia, likely due to the high vascularization and metabolic activity characteristic of these trabecular bone compartments.[42]

Estrogen receptor (ER)+ MCF-7 cells and triple negative MDA-MB-231 cells are two of the most commonly studied human breast cancer cell lines.[40] Although ER+ primary tumors have a high propensity to metastasize to bone in patients,[43] ER+ MCF-7 cells are utilized less frequently in models of breast cancer bone metastasis, as tumor-take can be limited using the intra-cardiac inoculation route, and MCF-7 cells require a longer time to develop osteolytic and osteoblastic lesions.[44,45] In contrast, ER− MDA-MB-231 cells readily metastasize to bone and develop osteolytic lesions as early as 2–3 weeks post inoculation.[39] In defense of the use of an ER− cell line, it should also be noted that there is a large discordance between the ER status of primary tumors and the ER status of the bone metastatic tumors in patients.[43]

The intra-tibial inoculation method is ideal for modeling the final stages of breast cancer bone metastasis and for studying direct interactions between tumor cells and the bone microenvironment without concerns about differential tumor-take from animal to animal. Murine-derived 4T1 cell proliferation in the tibia and subsequent development of osteolytic lesions can occur with the injection of as few as 10 000 murine-derived cells. At higher cellular concentrations (50 000–200 000 cells), our laboratories have observed 4T1 cell metastasis to contralateral tibiae, femurs, forelimbs and the lungs, often limiting the duration and utility of the model. As with all techniques presented here, it is recommended that investigators thoroughly characterize their cell line and inoculation route of choice by conducting dose–response studies in order to establish the optimal protocols prior to embarking on large animal trials.

Inoculation of cancer cells into the tail vein is a well-established bone metastasis model for multiple myeloma.[46,47] Our laboratories and others have found that the injection of breast cancer cells into the tail vein results almost exclusively in lung metastases, with limited tumor-take in bone.[22,48] When skeletal metastases are desired, we therefore recommend utilization of the tail artery as the tumor inoculation route for breast cancer models.[22,48–52]

In addition to specific limitations related to model choice discussed above, standard methodologies used by bone metastasis researchers to assess bone destruction and tumor burden have their own limitations. Osteolytic lesion area and tumor burden area in bone are typically assessed by measurement of X-Ray scan or by serial histological sectioning, respectively, and are thus merely two-dimensional approximations of three-dimensional tumors. Improvement in imaging has enhanced sensitivity of detection and yields more accurate

quantification of metastases. Typically, BLI using codon-optimized luciferase-labeled cells yields higher detection than fluorescent imaging using GFP-labeled cells.[53] Small animal imaging of bone has forged ahead with the development of high-resolution *in vivo* μCT scanners[54] in combination with BLI.[55] However, the bone metastasis research community has been slower to adopt such methodologies. One reason for this is that cumulative radiation exposure from CT scanners has been found to enhance metastases[56] and thus could confound cancer metastasis models if radiation exposure is not monitored judiciously.

Despite their limitations and caveats, the established murine models of breast cancer bone metastases have proven to be excellent tools for the study of bone and cancer cross talk and for the evaluation of potential therapeutics that prevent cancer progression and disrupt the cycle of bone destruction driven by metastasis.

Multimedia

The following article documents and visually demonstrates intra-cardiac and intra-tibial inoculation of cancer cells in mice and also demonstrates representative experimental end points of bone metastasis: http://www.jove.come/video/4260.

Conflict of Interest

The authors declare no conflict of interest.

Acknowledgements

We thank Alyssa Merkel and Kristin Kwakwa for capturing the photographs in **Figures 2 and 5** and Johnny Ribeiro and Khalid Mohammad for their technical input on the orthotopic and intra-tibial models, respectively. This work was supported by the Department of Defense Breast Cancer Research Program BC134025 (LEW) and by grants from INSERM (OP), the Comité Départemental de la Loire de la Ligue Contre le Cancer (OP), the Fondation ARC (OP), NIAMS AR43498 (GMP), The Netherlands Organization for Scientific Research NWO, VENI-Grant, 916.131.10 (JTB), the Department of Veterans Affairs 1I01BX001957 (JAS) and NCI 1R01CA163499 (JAS). Supported by the IBMS-ECTS Young Investigators.

References

1. Coleman RE. Skeletal complications of malignancy. *Cancer* 1997; **80**: 1588–1594.
2. Mundy GR. Metastasis to bone: causes, consequences and therapeutic opportunities. *Nat Rev Cancer* 2002; **2**: 584–593.
3. Thompson DD, Simmons HA, Pirie CM, Ke HZ. FDA Guidelines and animal models for osteoporosis. *Bone* 1995; **17**: S125–S133.
4. Ottewell PD, Wang N, Brown HK, Reeves KJ, Fowles CA, Croucher PI *et al.* Zoledronic acid has differential antitumor activity in the pre- and postmenopausal bone microenvironment *in vivo*. *Clin Cancer Res* 2014; **20**: 2922–2932.
5. Ottewell PD, Wang N, Brown HK, Fowles CA, Croucher PI, Eaton CL *et al.* OPG-Fc inhibits ovariectomy-induced growth of disseminated breast cancer cells in bone. *Int J Cancer* 2015; **137**: 968–977.
6. Lee JH, Kim B, Jin WJ, Kim JW, Kim HH, Ha H *et al.* Trolox inhibits osteolytic bone metastasis of breast cancer through both PGE2-dependent and independent mechanisms. *Biochem Pharmacol* 2014; **91**: 51–60.
7. Werbeck JL, Thudi NK, Martin CK, Premanandan C, Yu L, Ostrowksi MC *et al.* Tumor microenvironment regulates metastasis and metastasis genes of mouse MMTV-PymT mammary cancer cells *in vivo*. *Vet Pathol* 2014; **51**: 868–881.
8. Pécheur I, Peyruchaud O, Serre CM, Guglielmi J, Voland C, Bourre F *et al.* Integrin alpha(v)beta3 expression confers on tumor cells a greater propensity to metastasize to bone. *FASEB J* 2002; **16**: 1266–1268.
9. Ottewell PD, Deux B, Mönkkönen H, Cross S, Coleman RE, Clezardin P *et al.* Differential effect of doxorubicin and zoledronic acid on intraosseous versus extraosseous breast tumor growth *in vivo*. *Clin Cancer Res* 2008; **14**: 4658–4666.
10. Kang Y, Siegel PM, Shu W, Drobnjak M, Kakonen SM, Cordón-Cardo C *et al.* A multigenic program mediating breast cancer metastasis to bone. *Cancer Cell* 2003; **3**: 537–549.
11. Wetterwald A, van der Pluijm G, Que I, Sijmons B, Buijs J, Karperien M *et al.* Optical imaging of cancer metastasis to bone marrow: a mouse model of minimal residual disease. *Am J Pathol* 2002; **160**: 1143–1153.
12. Nutter F, Holen I, Brown HK, Cross SS, Evans CA, Walker M *et al.* Different molecular profiles are associated with breast cancer cell homing compared with colonisation of bone: evidence using a novel bone-seeking cell line. *Endocr Relat Cancer* 2014; **21**: 327–341.
13. Nasrazadani A, Van Den Berg CL. c-Jun N-terminal kinase 2 regulates multiple receptor tyrosine kinase pathways in mouse mammary tumor growth and metastasis. *Genes Cancer* 2011; **2**: 31–45.
14. Fathers KE, Bell ES, Rajadurai CV, Cory S, Zhao H, Mourskaia A *et al.* Crk adaptor proteins act as key signaling integrators for breast tumorigenesis. *Breast Cancer Res* 2012; **14**: R74.
15. Ottewell PD, Woodward JK, Lefley DV, Evans CA, Coleman RE, Holen I. Anticancer mechanisms of doxorubicin and zoledronic acid in breast cancer tumor growth in bone. *Mol Cancer Ther* 2009; **8**: 2821–2832.
16. Aslakson CJ, Miller FR. Selective events in the metastatic process defined by analysis of the sequential dissemination of subpopulations of a mouse mammary tumor. *Cancer Res* 1992; **52**: 1399–1405.
17. Abdelaziz DM, Stone LS, Komarova SV. Osteolysis and pain due to experimental bone metastases are improved by treatment with rapamycin. *Breast Cancer Res Treat* 2014; **143**: 227–237.
18. Lelekakis M, Moseley JM, Martin TJ, Hards D, Williams E, Ho P *et al.* A novel orthotopic model of breast cancer metastasis to bone. *Clin Exp Metastasis* 1999; **17**: 163–170.
19. Withana NP, Blum G, Sameni M, Slaney C, Anbalagan A, Olive MB *et al.* Cathepsin B inhibition limits bone metastasis in breast cancer. *Cancer Res* 2012; **72**: 1199–1209.
20. Buijs JT, Matula KM, Cheung H, Kruithof-de Julio M, van der Mark MH, Snoeks TJ *et al.* Spontaneous bone metastases in a preclinical orthotopic model of invasive lobular carcinoma; the effect of pharmacological targeting TGFβ receptor I kinase. *J Pathol* 2015; **235**: 745–759.
21. Iorns E, Drews-Elger K, Ward TM, Dean S, Clarke J, Berry D *et al.* A new mouse model for the study of human breast cancer metastasis. *PLoS ONE* 2012; **7**: e47995.
22. Kuperwasser C, Dessain S, Bierbaum BE, Garnet D, Sperandio K, Gauvin GP *et al.* A mouse model of human breast cancer metastasis to human bone. *Cancer Res* 2005; **65**: 6130–6138.
23. Holen I, Nutter F, Wilkinson JM, Evans CA, Avgoustou P, Ottewell PD. Human breast cancer bone metastasis *in vitro* and *in vivo*: a novel 3D model system for studies of tumour cell-bone cell interactions. *Clin Exp Metastasis* 2015; **32**: 689–702.
24. Suva LJ, Washam C, Nicholas RW, Griffin RJ. Bone metastasis: mechanisms and therapeutic opportunities. *Nat Rev Endocrinol* 2011; **7**: 208–218.
25. Engel LW, Young NA, Tralka TS, Lippman ME, O'Brien SJ, Joyce MJ. Establishment and characterization of three new continuous cell lines derived from human breast carcinomas. *Cancer Res* 1978; **38**: 3352–3364.
26. Engel LW, Young NA. Human breast carcinoma cells in continuous culture: a review. *Cancer Res* 1978; **38**: 4327–4339.
27. Soule HD, Vazguez J, Long A, Albert S, Brennan M. A human cell line from a pleural effusion derived from a breast carcinoma. *J Natl Cancer Inst* 1973; **51**: 1409–1416.
28. Levenson AS, Jordan VC. MCF-7: the first hormone-responsive breast cancer cell line. *Cancer Res* 1997; **57**: 3071–3078.
29. Yi B, Williams PJ, Niewolna M, Wang Y, Yoneda T. Tumor-derived platelet-derived growth factor-BB plays a critical role in osteosclerotic bone metastasis in an animal model of human breast cancer. *Cancer Res* 2002; **62**: 917–923.
30. Thomas RJ, Guise TA, Yin JJ, Elliott J, Horwood NJ, Martin TJ *et al.* Breast cancer cells interact with osteoblasts to support osteoclast formation. *Endocrinology* 1999; **140**: 4451–4458.
31. Canon J, Bryant R, Roudier M, Branstetter DG, Dougall WC. RANKL inhibition combined with tamoxifen treatment increases anti-tumor efficacy and prevent tumor-induced bone destruction in an estrogen receptor-positive breast cancer bone metastasis model. *Breast Cancer Res Treat* 2012; **135**: 771–780.
32. Fearon KC, Glass DJ, Guttridge DC. Cancer cachexia: mediators, signaling, and metabolic pathways. *Cell Metab* 2012; **16**: 153–166.
33. Waning DL, Mohammad KS, Reiken SR, Wenjun X, Anderssen DC, John S *et al.* TGFβ mediates muscle weakness associated with bone metastases. *Nat Med* 2015; **21**: 1262–1271.
34. Rucci N, Capulli M, Ventura L, Angelucci A, Peruzzi B, Tillgren V *et al.* Proline/arginine-rich end leucine-rich repeat protein N-terminus is a novel osteoclast antagonist that counteracts bone loss. *J Bone Miner Res* 2013; **28**: 1912–1924.
35. Ellenbroek SI, van Rheenen J. Imaging hallmarks of cancer in living mice. *Nat Rev Cancer* 2014; **14**: 406–418.
36. Guise TA. Molecular mechanisms of osteolytic bone metastases. *Cancer* 2000; **88**: 2892–2898.
37. Wright LE, Frye JB, Lukefahr AL, Timmermann BN, Mohammad KS, Guise TA *et al.* Curcuminoids block TGF-β signaling in human breast cancer cells and limit osteolysis in a murine model of breast cancer bone metastasis. *J Nat Prod* 2013; **76**: 316–321.
38. Arguello F, Baggs RB, Frantz CN. A murine model of experimental metastasis to bone and bone marrow. *Cancer Res* 1988; **48**: 6876–6881.
39. Guise TA, Yin JJ, Taylor SD, Kumagai Y, Dallas M, Boyce BF *et al.* Evidence for a causal role of parathyroid hormone-related protein in the pathogenesis of human breast cancer-mediated osteolysis. *J Clin Invest* 1996; **98**: 1544–1549.

40. Yoneda T, Sasaki A, Dunstan C, Williams PJ, Bauss F, De Clerck YA *et al.* Inhibition of osteolytic bone metastasis of breast cancer by combined treatment with the bisphosphonate ibandronate and tissue inhibitor of the matrix metalloproteinase-2. *J Clin Invest* 1997; **99**: 2509–2517.
41. Johnson LC, Johnson RW, Munoz SA, Mundy GR, Peterson TE, Sterling JA. Longitudinal live animal micro-CT allows for quantitative analysis of tumor-induced bone destruction. *Bone* 2011; **48**: 141–151.
42. Rosol TJ, Tannehill-Gregg SH, Corn S, Schneider A, McCauley LK. Animal models of bone metastasis. *Cancer Treat Res* 2004; **118**: 47–81.
43. Coleman RE, Rubens RD. The clinical course of bone metastases from breast cancer. *Br J Cancer* 1987; **55**: 61–66.
44. Rucci N, Ricevuto E, Ficorella C, Longo M, Perez M, Di Giacinto C *et al.* In vivo bone metastases, osteoclastogenic ability, and phenotypic characterization of human breast cancer cells. *Bone* 2004; **34**: 697–709.
45. Lu X, Wang Q, Hu G, Van Poznak C, Fleisher M, Reiss M *et al.* ADAMTS1 and MMP1 proteolytically engage EGF-like ligands in an osteolytic signaling cascade for bone metastasis. *Genes Dev* 2009; **23**: 1882–1894.
46. Dallas SL, Garrett IR, Oyajobi BO, Dallas MR, Boyce BF, Bauss F *et al.* Ibandronate reduces osteolytic lesions but not tumor burden in a murine model of myeloma bone disease. *Blood* 1999; **93**: 1697–1706.
47. Mitsiades CS, Mitsiades NS, Bronson RT, Chauhan D, Munshi N, Treon SP *et al.* Fluorescence imaging of multiple myeloma cells in a clinically relevant SCID/NOD in vivo model: biologic and clinical implications. *Cancer Res* 2003; **63**: 6689–6696.
48. Yang S, Zhang JJ, Huang XY. Mouse models for tumor metastasis. *Methods Mol Biol* 2012; **928**: 221–228.
49. van der Horst G, van der Pluijm G. Preclinical models that illuminate the bone metastasis cascade. In: Joerger M, Gnant M (eds). *Prevention of Bone Metastases*. Springer-Verlag: Berlin, Heidelberg, Germany, 2012, p. 1–24.
50. Buijs JT, Henriquez NV, van Overveld PG, van der Horst G, Que I, Schwaninger R *et al.* Bone morphogenetic protein 7 in the development and treatment of bone metastases from breast cancer. *Cancer Res* 2007; **67**: 8742–8751.
51. Bachelier R, Confavreux CB, Peyruchaud O, Croset M, Goehrig D, van der Pluijm G *et al.* Combination of anti-angiogenic therapies reduces osteolysis and tumor burden in experimental breast cancer bone metastasis. *Int J Cancer* 2014; **135**: 1319–1329.
52. Croset M, Goehrig D, Frackowiak A, Bonnelye E, Ansieau S, Puisieux A *et al.* TWIST1 expression in breast cancer cells facilitates bone metastasis formation. *J Bone Miner Res* 2014; **29**: 1886–1899.
53. Peyruchaud O, Winding B, Pécheur I, Serre CM, Delmas P, Clézardin P. Early detection of bone metastases in a murine model using fluorescent human breast cancer cells: application to the use of the bisphosphonate zoledronic acid in the treatment of osteolytic lesions. *J Bone Miner Res* 2001; **16**: 2027–2034.
54. Bouxsein ML, Boyd SK, Christiansen BA, Guldberg RE, Jepsen KJ, Müller R. Guidelines for assessment of bone microstructure in rodents using micro-computed tomography. *J Bone Miner Res* 2010; **25**: 1468–1486.
55. Lim E, Modi K, Christensen A, Meganck J, Oldfield S, Zhang N. Monitoring tumor metastases and osteolytic lesions with bioluminescence and micro CT imaging. *J Vis Exp* 2011; **50**: 2775.
56. Cowey S, Szafran A, Kappes J, Zinn KR, Siegal GP, Desmond RA *et al.* Breast cancer metastasis to bone: evaluation of bioluminescent imaging and microSPECT/CT for detecting bone metastasis in immunodeficient mice. *Clin Exp Metastasis* 2007; **24**: 389–401.

Supplementary Information accompanies the paper on the BoneKEy website (http://www.nature.com/bonekey)

www.impactjournals.com/oncotarget/ Oncotarget, 2017, Vol. 8, (No. 5), pp: 8406-8419

Research Paper

Aromatase inhibitor-induced bone loss increases the progression of estrogen receptor-negative breast cancer in bone and exacerbates muscle weakness *in vivo*

Laura E. Wright[1], Ahmed A. Harhash[1], Wende M. Kozlow[2], David L. Waning[3], Jenna N. Regan[1], Yun She[1], Sutha K. John[1], Sreemala Murthy[1], Maryla Niewolna[1], Andrew R. Marks[4], Khalid S. Mohammad[1], Theresa A. Guise[1]

[1]Department of Medicine, Division of Endocrinology, Indiana University, Indianapolis, IN, USA

[2]Department of Internal Medicine, Division of Endocrinology, University of Virginia, Charlottesville, VA, USA

[3]Department of Cellular and Molecular Physiology, The Pennsylvania State University College of Medicine, Hershey, PA, USA

[4]Department of Physiology, Columbia University, New York, NY, USA

Correspondence to: *Laura E. Wright,* ***email:*** *laewrig@iu.edu*

Keywords: *breast cancer, bone, metastasis, aromatase inhibitor, skeletal muscle*

Received: *October 20, 2016* ***Accepted:*** *November 23, 2016* ***Published:*** *December 25, 2016*

ABSTRACT

Aromatase inhibitors (AIs) cause muscle weakness, bone loss, and joint pain in up to half of cancer patients. Preclinical studies have demonstrated that increased osteoclastic bone resorption can impair muscle contractility and prime the bone microenvironment to accelerate metastatic growth. We hypothesized that AI-induced bone loss could increase breast cancer progression in bone and exacerbate muscle weakness associated with bone metastases. Female athymic nude mice underwent ovariectomy (OVX) or sham surgery and were treated with vehicle or AI (letrozole; Let). An OVX-Let group was then further treated with bisphosphonate (zoledronic acid; Zol). At week three, trabecular bone volume was measured and mice were inoculated with MDA-MB-231 cells into the cardiac ventricle and followed for progression of bone metastases. Five weeks after tumor cell inoculation, tumor-induced osteolytic lesion area was increased in OVX-Let mice and reduced in OVX-Let-Zol mice compared to sham-vehicle. Tumor burden in bone was increased in OVX-Let mice relative to sham-vehicle and OVX-Let-Zol mice. At the termination of the study, muscle-specific force of the extensor digitorum longus muscle was reduced in OVX-Let mice compared to sham-vehicle mice, however, the addition of Zol improved muscle function. In summary, AI treatment induced bone loss and skeletal muscle weakness, recapitulating effects observed in cancer patients. Prevention of AI-induced osteoclastic bone resorption using a bisphosphonate attenuated the development of breast cancer bone metastases and improved muscle function in mice. These findings highlight the bone microenvironment as a modulator of tumor growth locally and muscle function systemically.

INTRODUCTION

Breast cancer is the most commonly diagnosed cancer in women [1] and the majority of breast tumors are hormone-responsive [2]. Adjuvant endocrine therapies that impair the action of estrogen on breast tissue have become an important treatment strategy, reducing the risk of recurrence and death in women with estrogen receptor (ER)-positive disease [3-5]. Aromatase inhibitors, which block the rate-limiting step of estrogen biosynthesis [6], have replaced selective estrogen receptor modulators (SERMs; e.g., tamoxifen) as the standard of care in postmenopausal breast cancer patients due to improved disease-free survival [7, 8]. AI treatment regimens in the adjuvant setting are typically administered for five years and the extension of AI treatment regimens to ten years is

under study [9]. Between 25-50% of women treated with AIs report musculoskeletal toxicities, including joint pain, muscle weakness, and fragility, which result in diminished quality of life and poor compliance [10-19]. Relatively little is known about the molecular mechanism(s) of AI-induced arthralgia or muscle dysfunction. However, it is well established that AI treatment results in significant bone loss and increased fracture risk [17-19]. Our laboratory has had a longstanding interest in investigating how bone loss can impact tumor behavior in the bone microenvironment, a question that is of relevance to breast cancer patients undergoing prolonged AI therapy in the absence of a bone-protective intervention.

During a state of excessive bone resorption, matrix-derived growth factors have been shown to increase the growth of metastatic cancer cells in bone as well as stimulate their expression of osteolytic factors, which further perpetuate the destructive cycle of breast cancer in the skeleton [20]. Additionally, osteoclast-derived proteolytic enzymes have been shown to promote angiogenesis, cancer cell invasiveness, and engraftment at metastatic sites [21]. In the case of estrogen deficiency, a strong systemic increase in oxidative stress and inflammatory tone [22] could further perpetuate bone loss and, ultimately, cancer progression. Effects of bone loss resulting from AI-induced depletion of peripheral estrogen levels on the breast cancer bone metastases have not yet been tested. Our first aim was to assess the role of AI therapy-induced bone loss on the progression of disseminated breast cancer cells *in vivo*.

The impact of AI therapy on skeletal muscle function at the cellular and molecular level remains unknown despite clinical reports of muscle fatigue in AI-treated patients [10-13]. Because the bone matrix can be a source of growth factors, including members of the transforming growth factor (TGF)-β superfamily that affect both bone and muscle [23, 24], a state of high bone turnover could cause release of growth factors into circulation where they act on peripheral tissues. Previous studies in our laboratory have demonstrated that bone-derived TGFβ leads to oxidative overload in neighboring skeletal muscle and impaired muscle contractility in mice with osteolytic bone metastases [25]. The second aim of this study was to evaluate the effect of AI therapy and bone loss on skeletal muscle function in mice with bone metastases.

The overarching hypothesis driving this work is that estrogen deprivation therapy results in a high bone turnover state that increases breast cancer bone metastases and potentiates muscle weakness. It is important to note that we selected a triple negative breast cancer cell line (MDA-MB-231) in order to examine microenvironment-specific effects on tumor growth in the absence of direct effects of inhibition of ER signaling. Here we report that AI treatment causes bone loss and skeletal muscle weakness in OVX mice, and that the prevention of osteoclastic bone resorption attenuates the development of ER-negative breast cancer bone metastases and improves muscle function in AI-treated estrogen deprived mice.

RESULTS

Aromatase inhibitor treatment reduced serum 17β-estradiol and trabecular bone volume in OVX nude mice prior to tumor inoculation

Four-week female athymic nude mice underwent ovariectomy (OVX) or sham surgery and were treated via daily subcutaneous injection with vehicle (PBS, 50μL), or the aromatase inhibitor letrozole (Let, 10μg/d) (Figure 1). A sham-Let group was included as an experimental control in order to assess potential direct effects of letrozole on muscle function in the presence of ovarian estrogen production. A second OVX-Let-treated group was treated with the bisphosphonate zoledronic acid (Zol, 5μ/kg 3x/week) in order to determine the relative importance of bone loss on tumor growth and muscle function in the setting of AI therapy (Figure 1). Prior to the inoculation of tumor cells and three weeks after surgery, serum 17β-estradiol was reduced in OVX-Let and OVX-Let-Zol mice relative to sham groups (Figure 2A). A partial reduction in serum estradiol was observed in OVX-PBS-treated mice relative to sham, although this did not reach statistical significance (Figure 2A). As a terminal and surrogate measure of estrogenic activity [26], uterine weight was recorded at the end of the study (nine weeks post-surgery and five weeks after tumor inoculation). As anticipated, OVX resulted in significant uterine atrophy relative to sham groups regardless of drug treatment, and the addition of aromatase inhibitor to ovary intact mice (sham-Let) resulted in a moderate reduction in uterine weight relative to sham-PBS, though this did not reach statistical significance (Figure 2B).

In line with observed estrogenic changes, trabecular bone volume (BV/TV) assessed by bone microcomputed tomography was reduced in sham-Let and OVX-PBS mice (-29% and –52%, respectively) relative to estrogen-replete sham-PBS controls (Figure 3A). The combination of OVX and letrozole (OVX-Let) resulted in 67% reduction in trabecular bone volume relative to sham-PBS mice (Figure 3A). The anti-resorptive zoledronic acid increased trabecular bone volume in the OVX-Let-Zol mice by over three times that of sham-PBS mice and over ten times that of OVX-Let mice after three weeks of treatment (Figure 3A). Bone microarchitectural parameters, including connectivity density, structure model index, and trabecular number, separation and thickness, mirrored changes observed in trabecular bone volume for all treatment groups (Figure 3B-3G). In summary, each microarchitectural property assessed was severely compromised in OVX-Let mice relative to estrogen-replete sham-PBS mice and these maladaptive

modifications in trabecular bone were significantly improved by zoledronic acid treatment (Figure 3B-3G).

Osteolysis and tumor burden were increased in aromatase inhibitor-treated OVX mice

Having established an estrogen deficiency-driven high bone turnover state in OVX-Let mice by week three, MDA-MB-231 human breast cancer cells were inoculated into the left cardiac ventricle to generate a model of breast cancer metastatic to bone in order to determine the importance of aromatase inhibitor-induced changes to the bone microenvironment on tumor progression in the skeleton. Weekly body weight measurements were performed as a general assessment of disease progression and overall health [27]. For the duration of the study, OVX-Let-Zol mice maintained a higher average absolute body weight, achieving statistical significance relative to sham-Let and OVX-Let animals (Figure 4A). Body composition analyses by dual energy X-ray absorptiometry (DXA) revealed similar patterns of change in lean mass and fat mass percentage over time between groups, with differences observed only in fat mass percentage at week nine between OVX-Let-Zol and sham-PBS-treated mice (Figure 4B, 4A). The rapid decline in total body weight, lean mass, and fat mass observed in all treatment groups at week six (three weeks post-tumor inoculation) (Figure 4A-4C) is indicative of tumor progression in this model [27].

Changes in bone mineral density (BMD) following the inoculation of tumor cells were assessed by DXA over time. Consistent with the observed increase in trabecular bone volume three weeks after onset of Zol treatment (Figure 3A), BMD was significantly increased in the total skeleton, lumbar vertebrae, distal femur, and proximal tibia in OVX-Let-Zol mice relative to estrogen-replete (sham-PBS), partial estrogen-deprived (sham-Let, OVX-PBS), and total estrogen-deprived mice (OVX-Let) (Figure 4D-4G), confirming that the drug's anti-resorptive effect persisted throughout the study. Importantly, the OVX-Let group had a significant reduction in total skeletal BMD at the nine-week time point relative to sham-PBS (Figure 4D), indicating that AI treatment continued to cause significant bone loss over the course of the nine-week study due to estrogen deficiency and its possible role in cancer-induced osteolysis.

In order to directly assess cancer-induced destruction of bone, radiographs were acquired three and five weeks post-tumor inoculation, and X-rays were

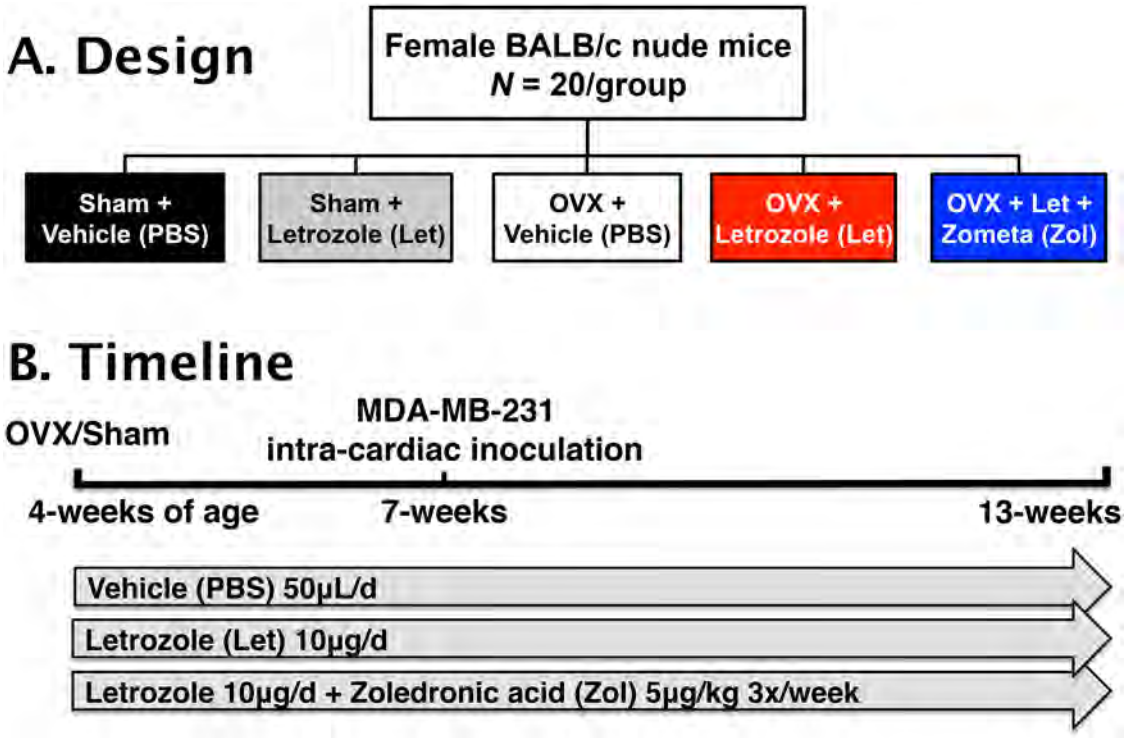

Figure 1: Study design. Panel A. Female BALB/c athymic nude (n=20/group) mice were randomized into five treatment groups 1) sham + vehicle (PBS), 2) sham + letrozole (Let), 3) ovariectomized (OVX) + vehicle, 4) OVX + letrozole, and 5) OVX + letrozole + zometa (Zol). **Panel B.** At four-weeks of age, mice underwent sham surgery or OVX, and drug treatments commenced 24 hours later. After changes in bone volume and microarchitecture were assessed by micro-computed tomography (µCT) three weeks post-surgery, groups were inoculated in the left cardiac ventricle with $1x10^5$ MDA-MB-231 human breast cancer cells. Mice were followed for six weeks for the development of bone metastases and tissues were collected following euthanasia at 13-weeks of age.

carefully examined for radiolucent regions indicative of cancer-mediated osteolysis. Osteolytic lesion area was increased in estrogen deprived OVX-Let mice relative to all treatment groups (Figure 5A, 5B). Lesions were detected in AI-treated OVX mice treated with bisphosphonate (OVX-Let-Zol) (Figure 5A); however, the anti-resorptive effects of Zol drastically reduced the total osteolytic lesion area relative to their estrogen-deprived counterparts (OVX-let) (Figure 5A, 5B). These data were corroborated at the histological level through the quantitation of multinucleated bone-resorbing osteoclasts at the bone-tumor interface in the marrow compartment [27]. Osteoclast numbers were increased in OVX-let mice relative to all groups, and Zol treatment reversed this heightened state of osteoclastogenesis (Figure 6A), in line with the drug's ability to induce osteoclast apoptosis [28].

Having confirmed effects on bone, a primary aim of the study was to evaluate how these AI- and Zol-induced changes to the bone microenvironment could influence tumor progression in the absence of direct inhibition of tumor growth through manipulation of ER signaling. Use of the MDA-MB-231 triple-negative human breast

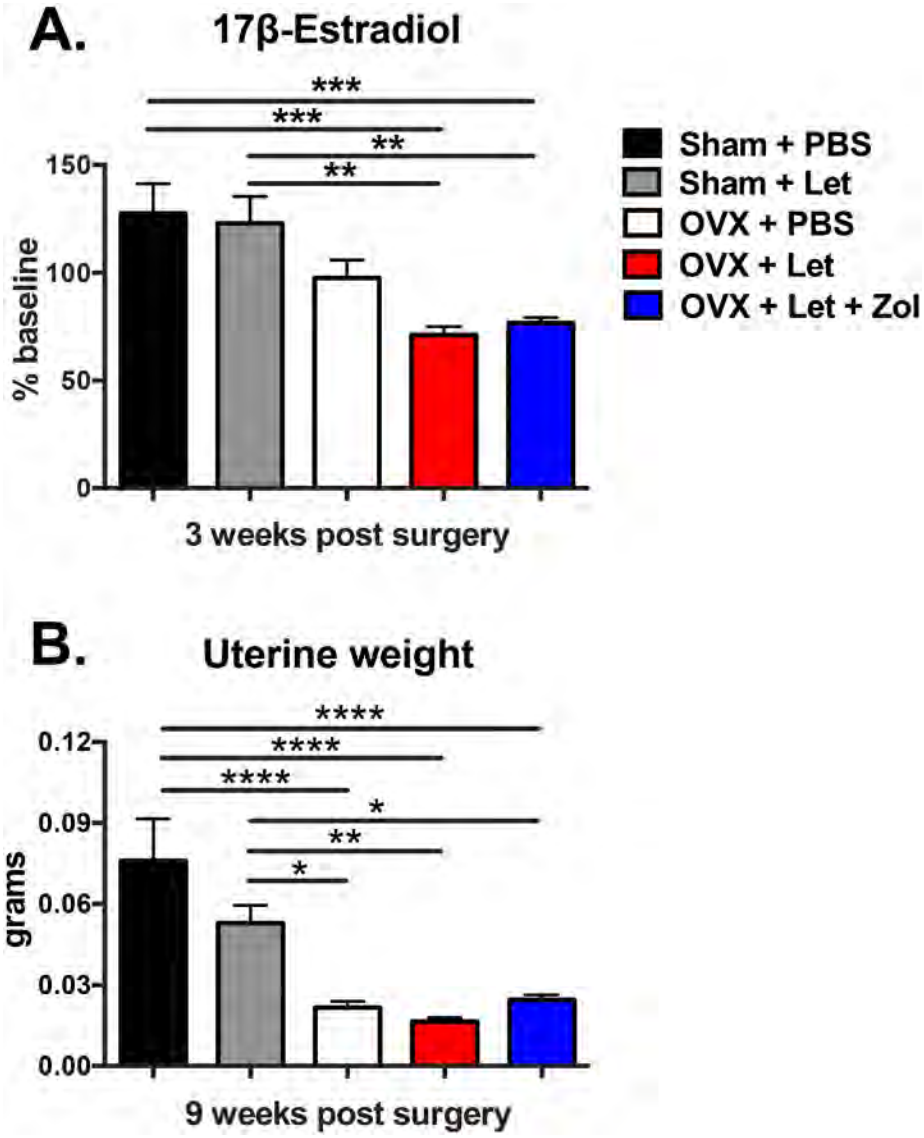

Figure 2: Impact of ovariectomy (OVX) and aromatase inhibitor (letrozole; Let) on circulating 17β-estradiol and on uterine atrophy in nude mice. Four-week female athymic nude mice underwent OVX or sham surgery and were treated with vehicle or aromatase inhibitor (letrozole, Let; 10μg/day) ±bisphosphonate (zoledronic acid, Zol; 5μg/kg 3x/week; n=20/group). **Panel A.** Serum was collected via retro-orbital puncture at baseline and three weeks after sham/OVX surgery and commencement of drug treatments. Serum 17β-estradiol was measured by immuno-assay (Calbiotech) as per manufacturer protocol, and results are expressed as % of baseline. **Panel B.** At the termination of the study nine weeks post-surgery, uteri were dissected and weighed. Results are expressed as mean ±SEM and differences were determined by one-way ANOVA with Tukey's multiple comparisons test where *p<0.05, **p<0.01, ***p<0.001, and ****p<0.0001.

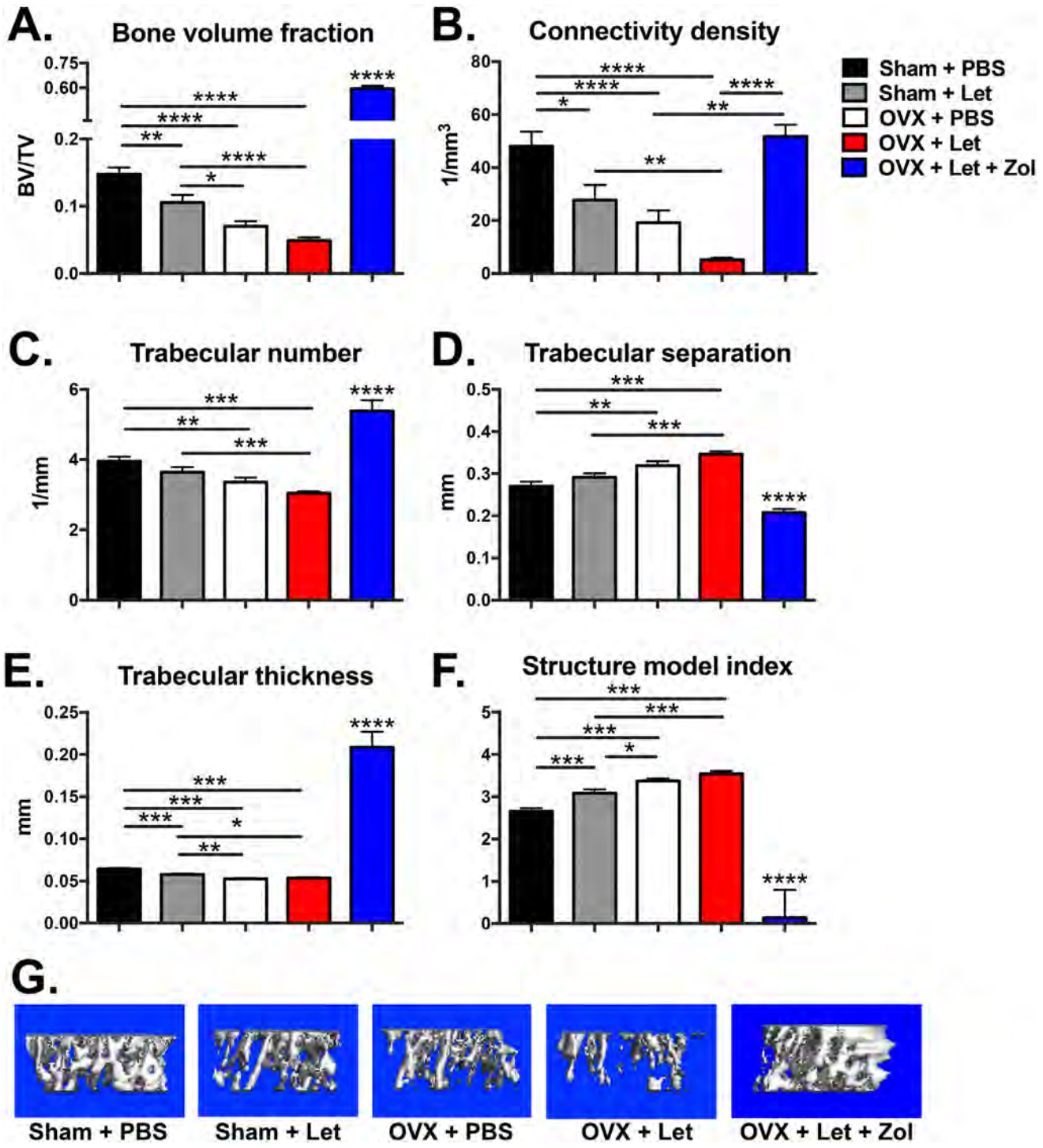

Figure 3: Bone volume and microarchitecture were compromised in nude mice after three weeks of estrogen deprivation treatment. Three weeks after OVX/sham surgery and the commencement of drug treatments, mice were anesthetized with isoflurane and bone microarchitecture was assessed in the proximal tibia by micro-computed tomography (μCT40; SCANCO Medical AG). **Panel A.** Trabecular bone volume (BV/TV), **Panel B.** connectivity density (1/mm^3), **Panel C.** trabecular number (1/mm), **Panel D.** trabecular separation (mm), **Panel E.** trabecular thickness (mm), and **Panel F.** structure model index are expressed as mean ±SEM and differences were determined by one-way ANOVA with Tukey's multiple comparisons test where *p<0.05, **p<0.01, ***p<0.001, and ****p<0.0001. **Panel G.** Representative reconstructed images of μCT scans showing trabecular bone at the proximal tibia were selected with a BV/TV % most representative of the group mean.

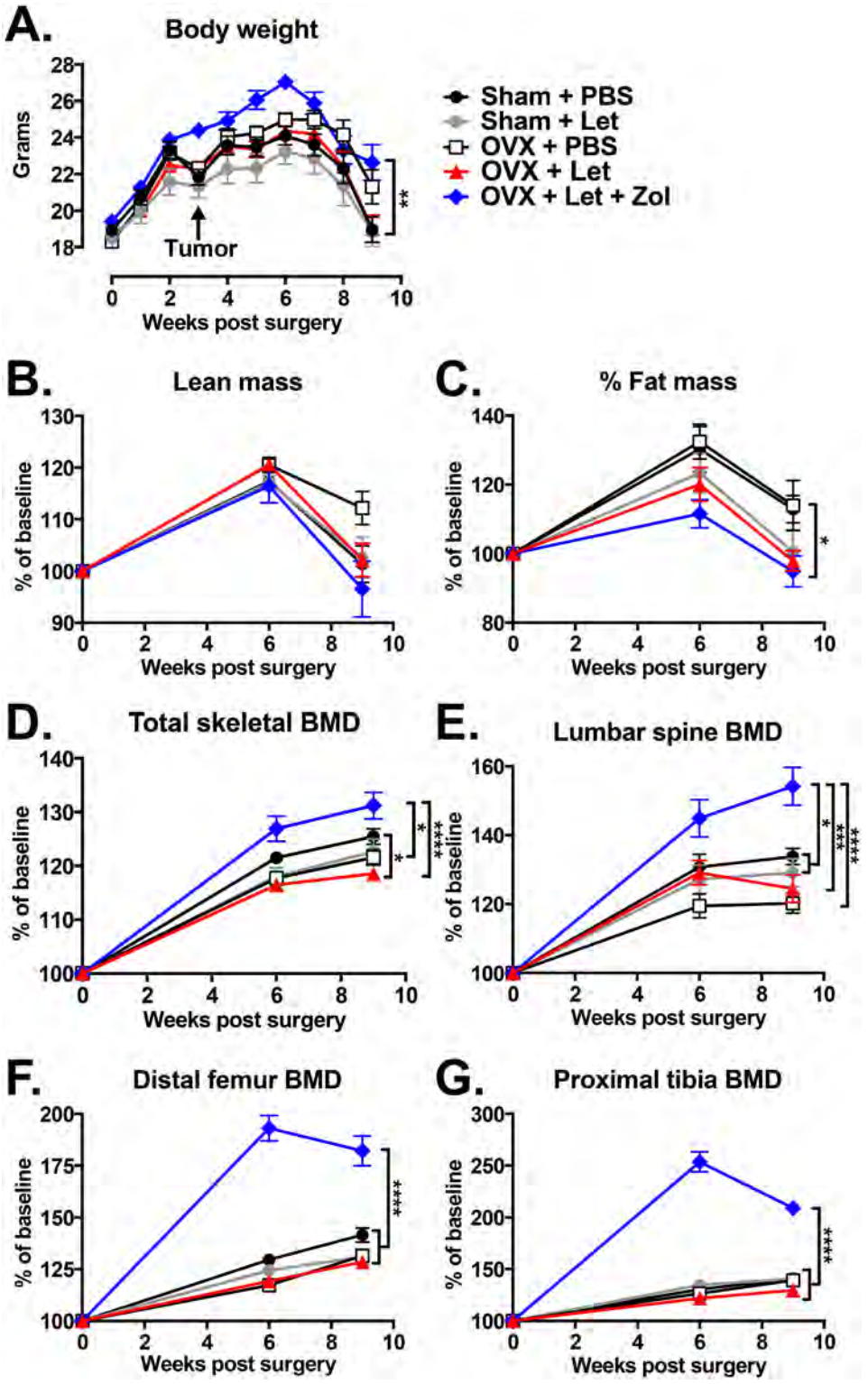

Figure 4: Changes in body composition and bone mineral density (BMD) in estrogen deficient tumor-bearing nude mice. Three weeks after the beginning of surgery and drug treatments, groups were inoculated in the left cardiac ventricle with $1x10^5$ MDA-MB-231 human breast cancer cells and followed for six weeks for the development of bone metastases. **Panel A.** Body weight was measured weekly. **Panel B.** Lean mass, **Panel C.** fat mass, **Panel D.** total body BMD, **Panel E.** BMD of the lumbar vertebrae (L4-L6), **Panel F.** distal femur BMD, and **Panel G.** proximal tibia BMD were measured at baseline, six weeks, and nine weeks after the beginning of treatments by dual energy X-ray absorptiometry (DXA). Data are expressed as mean % of baseline ±SEM, and differences were determined by two-way ANOVA with Tukey's multiple comparisons test at week nine where *p<0.05, **p<0.01, ***p<0.001, and ****p<0.0001.

cancer cell line permitted this bone-centric objective. Tumor burden in OVX-Let mice was measured at sites of skeletal metastases in histological sections, and total tumor area (mm^2) was significantly increased relative to all groups (Figure 6B-6E). Trabecular bone appeared intact in OVX-Let-Zol mice despite the presence of tumor cells (Figure 6E). The overall reduction in tumor area in Zol-treated mice relative to OVX-Let mice (Figure 6D) is likely attributed to the prevention in osteoclastic bone resorption and its feed-forward effect on osteolytic cancer metastases.

Bisphosphonates improved muscle function in AI-treated OVX mice independent of muscle mass

Whole muscle contractility of the extensor digitorum longus (EDL) was measured at the termination of the study to evaluate the potential role of bone loss on muscle dysfunction in a state of AI-induced estrogen deprivation. Estrogen-replete mice with bone metastases (sham-PBS) had a reduction in muscle specific force of the EDL relative to non-tumor age-matched controls, and this reduction reached statistical significance when mice were ovariectomized (OVX-PBS) (Figure 7A). Addition of letrozole to OVX tumor-bearing mice (OVX-Let) led to a further reduction of muscle specific force production of the EDL, reaching statistical significance relative to both tumor and non-tumor and tumor-bearing sham-PBS mice (Figure 7A). This deleterious effect on muscle function in OVX-Let mice was partially reversed by the prevention of osteoclastic bone resorption through zoledronic acid treatment (OVX-Let-Zol) (Figure 7A). Observed changes in muscle specific force production were independent of changes in EDL muscle mass because force production measurements were corrected for size and weight of the

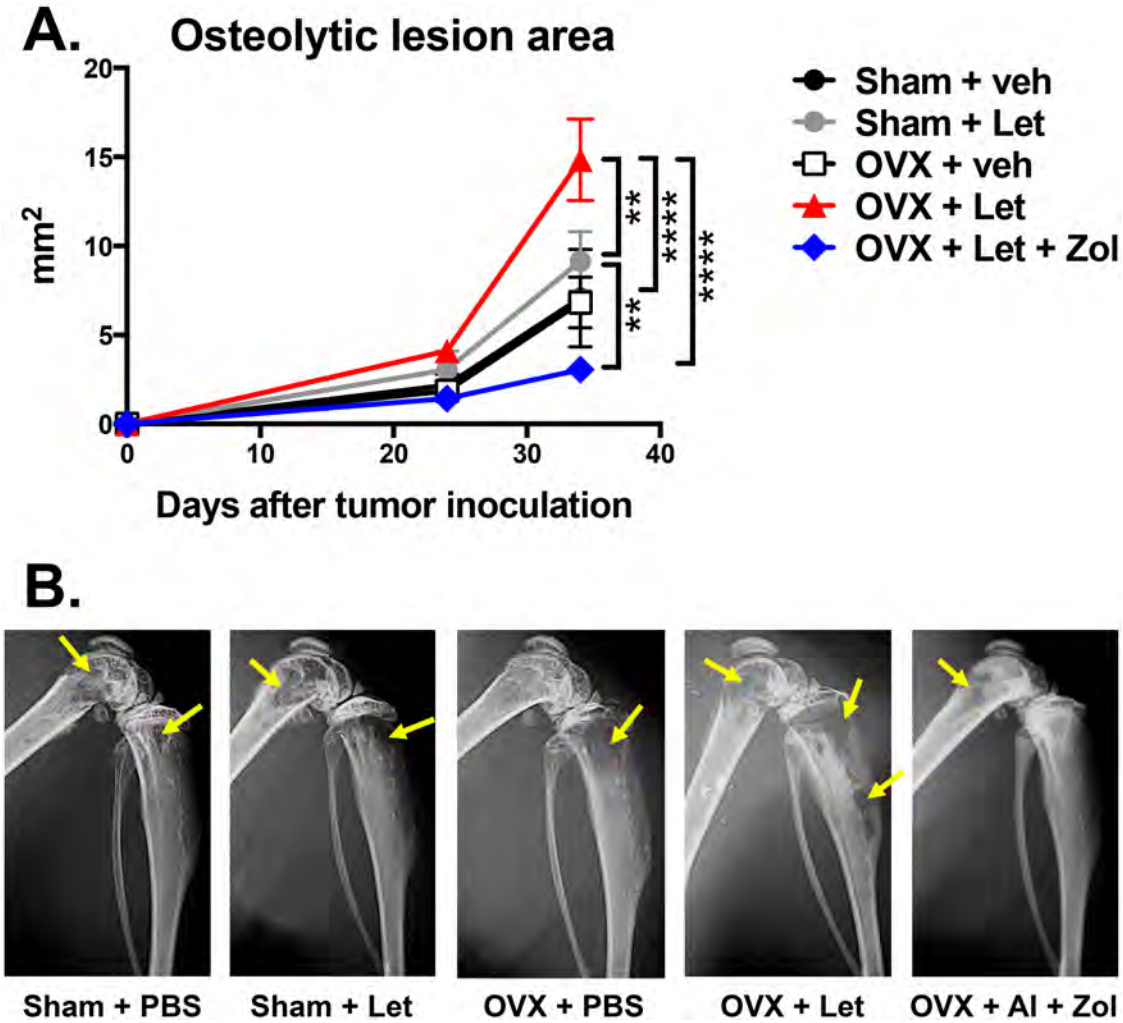

Figure 5: Osteolytic bone metastases assessed by radiography in estrogen deficient nude mice. Panel A. Osteolytic lesions were measured in anesthetized mice in prone position on d23 and d32 post tumor inoculation using a digital X-ray imager (Kubtec) at 2.7x magnification. Lytic lesion area is reported as total lesion area (mm^2) per animal in hind limb and forelimb long bones. **Panel B.** Representative X-rays showing radiolucent lytic lesions (arrows) were selected with lesion areas most representative of the group mean.

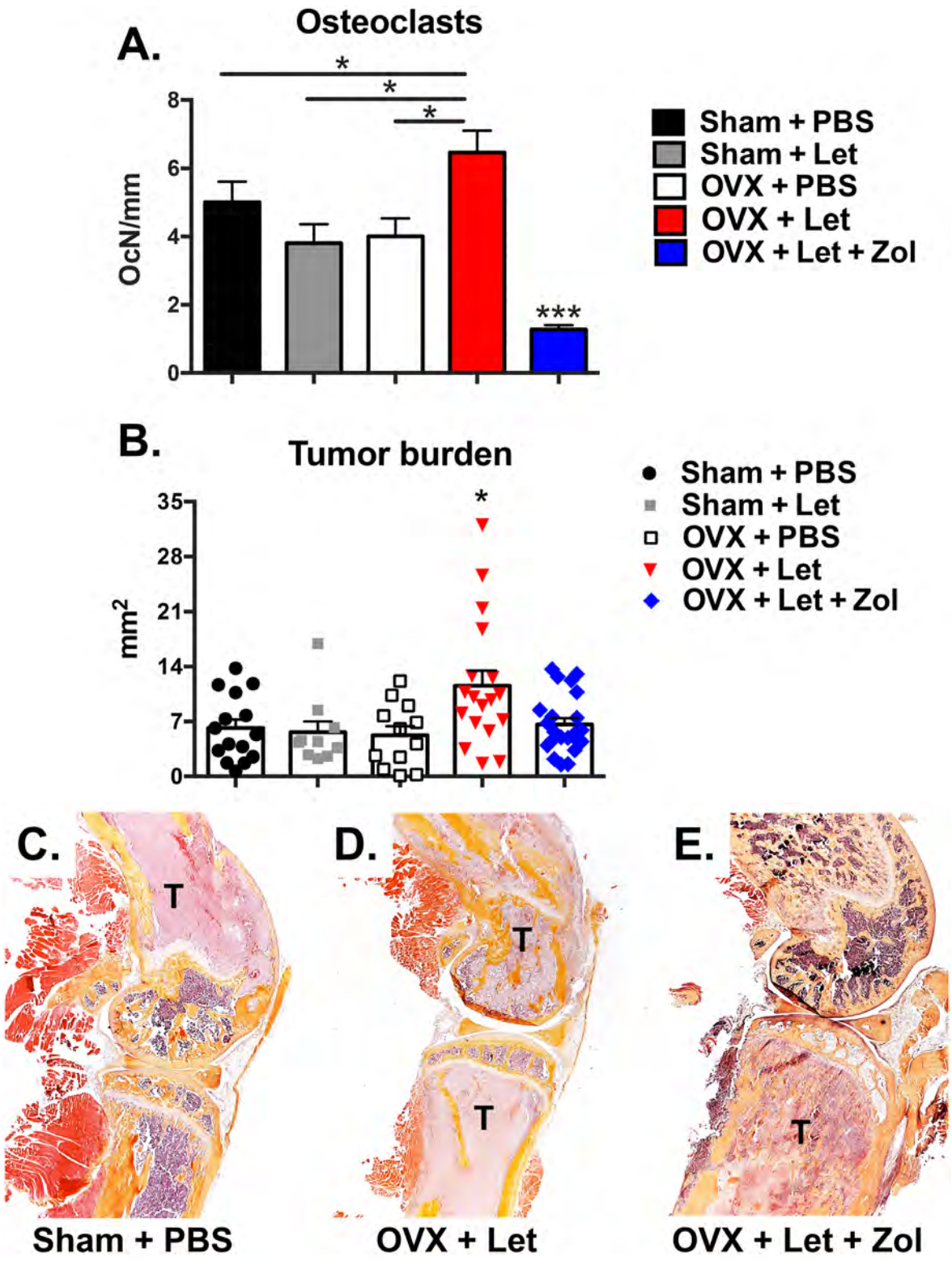

Figure 6: Histological assessment of tumor-bearing bone of estrogen deficient nude mice. Panel A. Tartrate-resistant acid phosphatase (TRAP)-positive multi-nucleated cells were quantitated at the bone-tumor interface in mid-sagittal sections of the tibia and expressed as number of osteoclasts per mm of interfacing surface (OcN/mm). **Panel B.** Mid-sagittal sections were stained with hematoxylin and eosin (H&E) and total tumor area was measured in the tibia, femur and humerus at 10x magnification. Tumor area is expressed as the combined total tumor area per animal (mm^2). **Panel C.** Representative histological images (H&E) showing tumor cells (T) in the distal femur and proximal tibia were selected with tumor areas most representative of the group mean. Differences were determined by one-way ANOVA with Tukey's multiple comparisons test where *$p<0.05$ and ***$p<0.001$.

EDL [29]. Furthermore, hind limb muscles including the EDL, tibialis anterior, gastrocnemius, and soleus collected at the termination of the study in cancer-bearing mice were similar between treatment groups (Figure 7B-7E), indicating that deficits in muscle specific force production in this study can likely be attributed to functional defects as opposed to muscle atrophy.

DISCUSSION

The estrogen-replete and estrogen-deficient bone niches differ greatly as host environments for disseminated cancer cells due to the acute sensitivity of bone and marrow cells to changes in endocrine status. Estrogen acts directly on bone cells to regulate the

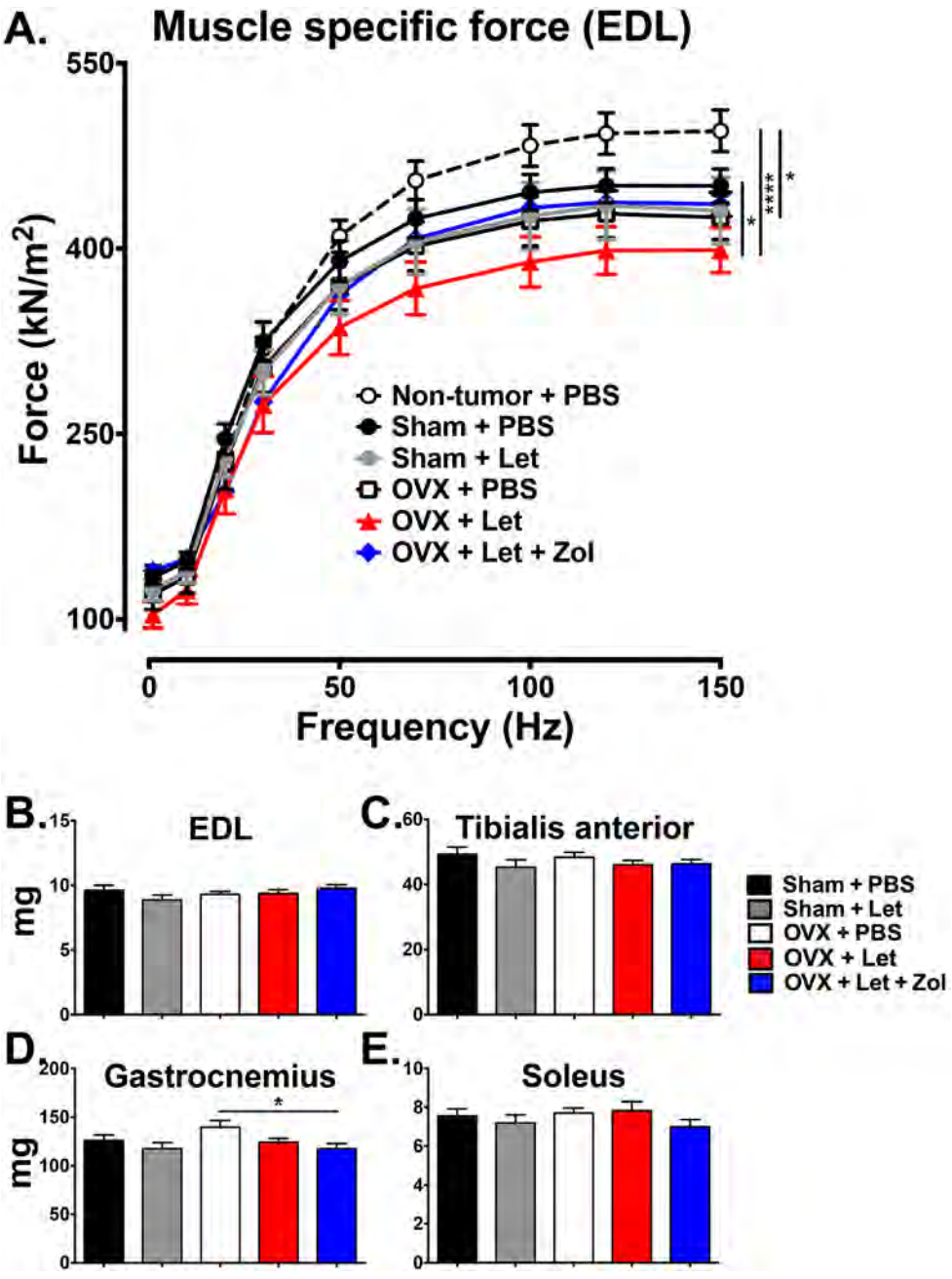

Figure 7: *Ex vivo* contractility of the EDL muscle. Panel A. *Ex vivo* muscle specific force of the extensor digitorum longus (EDL) muscle was measured in tumor and non-tumor bearing mice. Data are expressed as mean force (±SEM) normalized to muscle size, and differences were determined by two-way ANOVA with Tukey's multiple comparisons test performed at 150Hz where *p<0.05 and ****p<0.0001. **Panels B-E.** Muscles of the hind limb were dissected and weighed, including the EDL, tibialis anterior, gastrocnemius, and soleus. Differences were determined by one-way ANOVA with Tukey's multiple comparisons test where *p<0.05.

lifespan of both osteoclasts and osteoblast, and inhibits T-cell production of inflammatory cytokines, which can further drive osteoclast activation and bone resorption [22, 30]. Increased bone resorption has been demonstrated in preclinical models, including OVX, to accelerate cancer progression in bone [30-32] presumably via release of matrix-derived growth factors, (e.g., TGFβ, IGF, FGF, PDGF), which stimulate tumor growth and expression of osteolytic factors that perpetuate a feed-forward cycle of bone destruction [20]. Using an ER-negative breast cancer cell line to avoid direct tumor growth inhibitory effects, our studies support the postulate that estrogen depletion by AI treatment alters the bone microenvironment in ways that can indirectly promote cancer cell homing, growth, and/or an osteolytic phenotype in bone. The assertion that AI-induced bone loss increased metastatic tumor growth was further supported by the finding that blockade of bone resorption by zoledronic acid reduced tumor burden in bone.

Direct anti-cancer effects of bisphosphonates have been pursued with relatively little evidence that physiologically relevant doses can directly elicit cancer cell apoptosis [33, 34]. Although direct anti-tumor effects of bisphosphonates have been shown *in vitro* [34], their anti-cancer activity *in vivo* continues to be attributed to indirect effects via inhibition of osteoclastic bone resorption [30]. Recent clinical reports have demonstrated differential anti-cancer effects of bone-targeted anti-resorptives in breast cancer patients depending on menopausal status. In the AZURE, ZO-FAST, and ABCSG-12 trials, zoledronic acid consistently improved disease-free survival in breast cancer patients, however, this effect was limited to 1) postmenopausal women and 2) premenopausal women undergoing AI therapy treatment (chemical menopause) [35-37], suggesting that the anti-tumor effects of zoledronic acid were reserved for estrogen deficient populations in a high bone turnover state. In light of our studies and the clinical link between bone loss and cancer progression, it will be important to consider the skeletal health not only of cancer patients undergoing AI therapy, but of patients undergoing any therapeutic intervention known to adversely affect skeletal health (e.g., GnRH agonists, glucocorticoids, radiation therapy).

We utilized the triple-negative MDA-MB-231 human breast cancer cell line to assess the impact of the microenvironment on tumor growth in the absence of effects on ER signaling. By contrast, adjuvant AI therapy in the clinical setting is prescribed to breast cancer patients with ER-positive primary tumors [8]. Clinical reports, however, indicate that in many cases ER status at the primary tumor site does not match the ER status of disseminated tumor cells [38], making our model relevant in the setting of advanced disease where metastatic tumor cell ER expression is lost. Use of an ER-positive breast cancer model (e.g., MCF-7) would be useful in determining the relative importance of the benefit of direct tumor growth suppression versus the risk of bone resorption-induced disease progression in the context of AI therapy. Breast cancer mortality results from tumor metastases rather than primary tumor growth [20], and bone is the preferred metastatic destination for breast cancer [39]. In the case of advanced metastatic disease, the growth inhibitory effects of AIs may be overridden by tumor-promoting signals from the bone microenvironment [40]. Thus, the prevention of bone loss in early stage breast cancer patients at the very onset of AI treatment could be of importance.

AI-induced arthralgia and muscle weakness are poorly characterized, yet are often so unmanageable that patients discontinue adjuvant AI therapy [10-14]. The identification of the molecular mechanism(s) underlying AI related muscle dysfunction could be critical in the development of interventions that can restore quality of life and improve drug compliance. In our studies zoledronic acid partially improved muscle function in AI treated mice with bone metastases, suggesting that osteoclastic bone resorption played a role in reduced skeletal muscle contractility in the setting of AI therapy. Recent work reported by our group identified bone-derived TGFβ as the mediator of muscle weakness in mice with bone metastases through the up-regulation of NADPH oxidase 4 production of reactive oxygen species leading to oxidation of the ryanodine receptor (RyR1) calcium channel complex in muscle resulting in SR Ca^{2+} leak and muscle weakness [25]. Release of bone-derived TGFβ during AI therapy-induced bone loss could have downstream effects on muscle contractility via a similar mechanism, a hypothesis currently under investigation in our laboratory. We speculate that AI-induced muscle weakness is likely multi-faceted in light of the finding that bisphosphonate treatment alone did not restore muscle function to the level of non-tumor control mice. It is possible that AIs elicit direct toxic effects on myocytes, a postulate that has yet to be tested. Selective estrogen receptor modulators (SERMs; e.g., tamoxifen), which interact with the ER and inhibit its activity in breast tissue while preserving bone have also associated with muscle weakness [15], suggesting that inhibition of ER signaling in muscle impacts muscle contractility in the absence of high bone turnover. Furthermore, muscle weakness associated with declining estrogen levels during menopause in healthy women can be rescued by hormone replacement therapy [41-43], providing further proof that ER signaling blockade contributes to muscle weakness in the AI-treated patient. Relevant non-tumor models and *in vitro* studies will be useful in determining the relative role of bone loss, ER signaling blockade, and potential direct drug toxicities on muscle function following AI and SERM therapy.

In summary, the causes of AI-induced musculoskeletal complications and the consequences of AI-induced bone loss are poorly characterized. Bone-

derived factors released during an elevated state of osteoclastic bone resorption are known to have adverse effects on muscle function and can alter the bone microenvironment to favor breast cancer cell progression and perpetuate osteolysis. Our studies demonstrated that modulation of the bone microenvironment impacted tumor growth locally and muscle function systemically in AI treated mice. These findings emphasize the importance of considering the musculoskeletal health of cancer patients when selecting estrogen deprivation treatment options and the need to further investigate non-estrogenic therapeutic agents that can improve musculoskeletal outcomes in cancer patients.

MATERIALS AND METHODS

Animals

The Institutional Animal Care and Use Committee at Indiana University approved animal protocols for these studies in accordance with the National Institutes of Health Guide for the Care and Use of Laboratory Animals. Three-week female athymic nude mice were purchased from Harlan Laboratories (Indianapolis, IN) and housed in plastic cages with access to water and mouse chow *ad libitum* and maintained on a 12h light/dark schedule at 22 ±2°C. After one week of acclimation, mice were anesthetized with a ketamine/xylazine cocktail and underwent bilateral ovariectomy (OVX) or a sham surgery under sterile conditions. Aromatase inhibitor (letrozole, 10ug/d), zoledronic acid (Zometa; 5μg/kg 3x/week), and vehicle (PBS, 50μl/d) treatments were administered daily via subcutaneous injection 24h after surgery and continued for the duration of the study. Blood was collected by retro-orbital puncture three days prior to surgery (baseline) and three weeks post surgery. Serum 17β-estradiol was measured by ELISA (Calbiotech) and expressed as percent of baseline.

Bone microcomputed tomography (μCT)

Bone μCT was performed at the proximal metaphysis of the tibia using a high-resolution imaging system (μCT40; SCANCO Medical AG) on isoflurane-anesthetized mice. Bone μCT scans were acquired using a 17μm^3 isotropic voxel size, 55kVp peak X-ray tube potential, 200ms integration time, and were subjected to Gaussian filtration. Trabecular bone microarchitecture was evaluated in the proximal metaphysis of the tibia in a region that began 0.4mm distal to the growth plate and extended distally 1.0mm. A threshold of 170mg HA/cm^3 was used to segment bone from surrounding soft tissue. Trabecular bone outcomes included trabecular bone volume fraction (BV/TV; %), trabecular thickness (Tb.th; mm), trabecular number (Tb.N; mm^{-1}), trabecular separation (Tb.Sp; mm), and connectivity density (Conn.D; mm^{-3}). Scan acquisition and analyses were conducted in accordance with guidelines for use of μCT in rodents [44].

Dual energy X-ray absorptiometry (DXA)

In vivo measurement of fat mass, lean mass and bone mineral density (BMD) was performed on anesthetized mice (ketamine/xylazine) using a PIXImus II densitometer (GE Lunar, Madison, WI) calibrated with a phantom of defined density. Body composition and BMD were measured at baseline on the day of surgery, at week six post-surgery, and at the termination of the study (week nine post-surgery), and data were expressed as percent change over time.

Intra-cardiac inoculation procedure

Three weeks after OVX and sham surgeries, mice were inoculated in the left cardiac ventricle with MDA-MB-231 tumor cells, as previously described [27]. Briefly, tumor cell inoculation was performed percutaneously into the left cardiac ventricle of anesthetized mice in a supine position with a 26-gauge needle attached to a 1mL syringe containing 1×10^5 cells suspended in 0.1mL sterile PBS. Visualization of bright red blood entering the hub of the needle in pulsatile fashion was indicative of correct needle placement into the left cardiac ventricle. Mice were followed for the development of osteolytic bone lesions by radiography on days 23 and 32 of the experiment. Osteolytic lesions were visualized in anesthetized mice in prone position using a digital X-ray imager (Kubtec) at 2.7x magnification. Lytic lesion area, reported as total lesion area (mm^2) per animal in hind limb and forelimb long bones, was analyzed in a blinded fashion using ImageJ 1.48r software (National Institutes of Health).

Histology

Hind limbs were removed from mice at the time of experimental termination, fixed in 10% neutral-buffered formalin for 48h and stored in 70% ethanol. Tibiae, femora, and humeri were decalcified in 10% EDTA for two weeks, processed using an automated tissue processor (Excelsior, Thermoelectric), and embedded in paraffin. Mid-sagittal 4.5μm sections were stained with hematoxylin and eosin (H&E) with orange G and phloxine to visualize new bone, and with tartrate-resistant acid phosphatase (TRAP) to visualize osteoclasts. Total tumor area was measured in H&E-stained mid-sagittal sections of the tibiae, femora, and humeri at 10x magnification without knowledge of experimental groups. Osteoclast cells were quantified in the mid-sagittal sections of tibiae in tumor-bearing hind limbs. Briefly, TRAP-positive multinucleated cells were quantified at 40x magnification along the perimeter of the tumor where the cancer cells interfaced directly with bone surfaces. Data were expressed as number of osteoclasts

per mm of tumor-bone interface (OcN/mm), as previously described [27]. All sections were viewed on a Leica DM LB compound microscope outfitted with a Q-Imaging Micropublisher Cooled CCD color digital camera (Nuhsbaum Inc., McHenry, IL). Images were captured and analyzed using BioQuant Image Analysis Software version 13.2 (BIOQUANT Image Analysis Corporation, Nashville, TN).

Measurement of muscle specific force

Ex vivo contractility of the extensor digitorum longus (EDL) muscles was determined as previously described [25]. Briefly, EDL muscles were dissected from hind limbs and stainless steel hooks were tied to the tendons of the muscles using 4-0 silk sutures and the muscles were mounted between a force transducer (Aurora Scientific) and an adjustable hook. The muscles were immersed in a stimulation chamber containing O_2/CO_2 (95/5%) bubbled Tyrode solution (121 mM NaCl, 5.0 mM KCl, 1.8 mM $CaCl_2$, 0.5 mM $MgCl_2$, 0.4 mM NaH_2PO_4, 24 mM $NaHCO_3$, 0.1 mM EDTA, 5.5 mM glucose). The muscle was stimulated to contract using a supramaximal stimulus between two platinum electrodes. Data were collected via Dynamic Muscle Control/Data Acquisition (DMC) and Dynamic Muscle Control Data Analysis (DMA) programs (Aurora Scientific). The force–frequency relationships were determined by triggering contraction using incremental stimulation frequencies (0.5ms pulses at 1–150 Hz for 350ms at supra-maximal voltage). Between stimulations the muscle was allowed to rest for 3 min. At the end of the force measurement, the length and weight of the muscle was measured. To quantify the specific force, the absolute force was normalized to the muscle size calculated as the muscle weight divided by the length using a muscle density constant of 1.056 kg/m^{-3} [29]. The investigators were blinded to treatment of subjects.

Statistical analyses

Differences were determined by one-way or two-way ANOVA, as appropriate, with Tukey's multiple comparisons test (GraphPad, Prism 6.0f). Results are expressed as mean ±SEM and $p<0.05$ was considered significant.

CONFLICTS OF INTEREST

The authors declare no conflicts of interest.

GRANT SUPPORT

This work was supported by the Department of Defense Breast Cancer Research Program BC134025 (LEW) and BC043416 (WMK).

REFERENCES

1. Jemal A, Siegal R, Xu J, Ward E. Cancer statistics. CA Cancer J Clin. 2010; 60: 277-300.
2. Clark GM, Osborne CK, McGuire WL. Correlations between estrogen receptor, progesterone receptor, and patient characteristics in human breast cancer. J Clin Oncol. 1984; 2: 1102-1109.
3. Fisher B, Costantino J, Redmond C, Poisson R, Bowman D, Couture J, Dimitrov NV, Wolmark N, Wickerman L, Fisher ER, Margolese R, Robidoux A, Shibatga H, et al. A randomized clinical trial evaluating tamoxifen in the treatment of patients with node-negative breast cancer who have estrogen-receptor positive tumors. N Engl J Med. 1989; 320: 479-484.
4. Goss PE, Ingle JN, Martino S, Robert NJ, Muss HB, Piccart MJ, Castiglione M, Tu D, Shepherd LE, Pritchard KI, Livingston RB, Davidson NE, Norton L, et al. A randomized trial of letrozole in postmenopausal women after five years of tamoxifen therapy for early-stage breast cancer. N Engl J Med. 2003; 349: 1793-1802.
5. Early Breast Cancer Trialists' Collaborative Group (EBCTCG), Dowsett M, Forbes JF, Bradley R, Ingle J, Aihara T, Bliss J, Boccardo F, Coates A, Coombes RC, Cuzick J, Dubsky P, Gnant M, Kaufmann M, Kilburn L, Perrone F, Rea D, Thürlimann B, van de Velde C, Pan H, Peto R, Davies C, Gray R. Aromatase inhibitors versus tamoxifen in early breast cancer: patient-level meta-analysis of the randomised trials. Lancet. 2015; 386: 1341-1352.
6. Simpson ER, Davis SR. Minireview: aromatase and the regulation of estrogen biosynthesis – some new perspectives. Endocrinology. 2001; 142: 4589-4594.
7. Coates AS, Keshaviah A, Thürlimann B, Mouridsen H, Mauriac L, Forbes JF, Paridaens R, Castiglione-Gertsch M, Gelber RD, Colleoni M, Láng I, Del Mastro L, Smith I, et al. Five years of letrozole compared with tamoxifen as initial adjuvant therapy for postmenopausal women with endocrine-responsive early breast cancer: update of study BIG 1-98. J Clin Oncol. 2007; 25: 486-492.
8. Burstein HJ, Prestrud AA, Seidenfeld J, Anderson H, Buchholz TA, Davidson NE, Gelmon KE, Giordano SH, Hudis CA, Malin J, Mamounas EP, Rowden D, Solky AJ, et al. American Society of Clinical Oncology clinical practice guidelines: Update on adjuvant endocrine therapy for women with hormone receptor-positive breast cancer. J Clin Oncol 2010; 28: 3784-3796.
9. Goss PE, Ingle JN, Pritchard KI, Robert NJ, Muss H, Gralow J, Gelmon K, Whelan T, Strasser-Weippl K, Rubin S, Sturtz K, Wolff AC, Winer E, et al. Extending aromatase-inhibitor adjuvant therapy to 10 years. N Engl J Med. 2016; 375: 209-219.
10. Henry NL, Giles JT, Ang D, Mohan M, Dadabhoy D, Robarge J, Hayden J, Lemler S, Shahverdi K, Powers P, Li L, Flockhart D, Stearns V, Hayes DF, et al. Prospective characterization of musculoskeletal symptoms in early

breast cancer patients treated with aromatase inhibitors. Breast Cancer Res Treat. 2008; 111: 365-372.

11. Lintermans A, Van Calster B, Van Hoydonck M, Pans S, Verhaeghe J, Westhovens R, Henry NL, Wildiers H, Paridaens R, Dieudonné AS, Leunen K, Morales L, Verschueren K, et al. Aromatase inhibitor-induced loss of grip strength is body mass index dependent: hypothesis-generating findings for its pathogenesis. Annals Oncol. 2011; 22: 1763-1769.
12. Dent SF, Gaspo R, Kissner M, Pritchard KI. Aromatase inhibitor therapy: toxicities and management strategies in the treatment of postmenopausal women with hormone-sensitive early breast cancer. Breast Cancer Res Treat. 2011; 126: 295-310.
13. Donnellan PP, Douglas SL, Cameron DA, Leonard RC. Aromatase inhibitors and arthralgia. J Clin Oncol. 2001; 19: 2767.
14. Henry NL, Azzouz F, Desta Z, Li L, Nguyen AT, Lemler S, Hayden J, Tarpinian K, Yakim E, Flockhart DA, Stearns V, Hayes DF, Storniolo AM. Predictors of aromatase inhibitor discontinuation as a result of treatment-emergent symptoms in early-stage breast cancer. J Clin Oncol. 2012; 30: 936-942.
15. Buzdar AU. Clinical features of joint symptoms observed in the 'Arimedex,' Tamoxifen, Alone or in Combination (ATAC) trial. J Clin Oncol 2006; 24: 551.
16. Gross PE, Ingle JN, Ales-Martinez JE, Cheung AM, Chlebowski RT, Wactawski-Wende J, McTieran A, Robbins J, Johnson KC, Martin LW, Winquist E, Sarto GE, Garber JE, et al. Exemestane for breast-cancer prevention in post-menopausal women. N Engl J Med. 2010; 364: 2381-91.
17. Henry NL, Giles JT, Stearns V. Aromatase inhibitors-associated musculoskeletal symptoms: etiology and strategies for management. Oncology 2008; 22: 1401-1408.
18. Brown SA, Guise TA. Cancer treatment-related bone disease. Crit Rev Eukaryot Gene Expr. 2009; 19: 47-60.
19. Saad F, Adachi JD, Brown JP, Canning LA, Gelmon KA, Josse RG, Pritchard KI. Cancer treatment-induced bone loss in breast and prostate cancer. J Clin Oncol. 2008; 26: 5466-5476.
20. Weilbaecher KN, Guise TA. Cancer to bone: a fatal attraction. Nature Rev Cancer. 2011; 11: 411-425.
21. Bonfil RD, Cher ML. Proteolytic enzymes in metastatic bone disease. IBMS BoneKEy. 2011; 8: 16-36.
22. Frenkel B, Hong A, Baniwal SK, Coetzee GA, Ohlsson C, Khalid O, Gabet Y. Regulation of adult bone turnover by sex steroids. J Cell Physiol. 2010; 224: 305-310.
23. Mendias CL, Gumucio JP, Davis ME, Bromley CW, Davis CS, Brooks SV. Transforming growth factor-beta induces skeletal muscle atrophy and fibrosis through the induction of atrogin-1 and scleraxis. Muscle Nerve. 2012; 45: 55-59.
24. Regan JN, Waning DL, Guise TA. Skeletal muscle Ca(2+) mishandling: Another effect of bone-to-muscle signaling. Semin Cell Dev Biol. 2016; 49: 24-29.
25. Waning DL, Mohammad KS, Reiken SR, Wenjun X, Anderssen DC, John S, Chiechi A, Wright LE, Umanskaya A, Niewolna M, Trivedi T, Charkhzarrin S, Khatiwada P, et al. TGFβ mediates muscle weakness associated with bone metastases. Nature Med. 2015; 21: 1262-1271.
26. Evans JS, Varney RF, Koch FC. The mouse uterine weight method for the assay of estrogens. Endocrinology. 1941; 28: 747-752.
27. Wright LE, Ottewell PD, Rucci N, Peyruchaud O, Pagnotti GM, Chiechi A, Buijs JT, Sterling JA. Murine models of breast cancer bone metastases. BoneKEy Rep. 2016; 5: 804.
28. Rodan GA, Fleisch HA. Bisphosphonates: mechanism of action. J Clin Invest. 1996; 97: 2692–2696.
29. Yamada T, Place N, Kosterina N, Ostberg T, Zhang SJ, Grundtman C, Erlandsson-Harris H, Lundberg IE, Glenmark B, Bruton JD, Westerblad H. Impaired myofibrillar function in the soleus muscle of mice with collagen-induced arthritis. Arthritis Rheum. 2009; 60: 3280-3289.
30. Wright LE, Guise TA. The microenvironment matters: estrogen deficiency fuels cancer bone metastases. Clin Cancer Res. 2014; 20: 2817-2819.
31. Ottewell PD, Wang N, Brown HK, Reeves KJ, Fowles CA, Croucher PI, Eaton Cl, Holen I. Zoledronic acid has differential antitumor activity in pre- and postmenopausal bone microenvironment *in vivo*. Clin Cancer Res. 2014; 20: 2922-2932.
32. Schneider A, Kalikin LM, Mattos AC, Keller ET, Allen MJ, Pienta KJ, McCauley LK. Bone turnover mediates preferential localization of prostate cancer in the skeleton. Endocrinology. 2005; 146: 1727-1736.
33. Ottewell PD, Monkkonen J, Jones M, Lefley DV, Coleman RE, Holen I. Antitumor effects of doxorubicin followed by zoledronic acid in a mouse model of breast cancer. J Natl Cancer Inst. 2008; 100: 1167-1178.
34. Jagdev SP, Coleman RE, Shipman CM, Rostami-H A, Croucher PI. The bisphosphonate, zoledronic acid, induces apoptosis of breast cancer cells: evidence for synergy with paclitaxel. Br J Cancer. 2001; 84: 1126-1134.
35. Coleman RE, Marshall H, Cameron D, Dodwell D, Burkinshaw R, Keane M, Gil M, Houston SJ, Grieve RJ, Barrett-Lee PJ, Ritchie D, Pugh J, Gaunt C, et al. Breast-cancer adjuvant therapy with zoledronic acid. N Engl J Med. 2011; 365: 1396-1405.
36. Coleman R, de Boer R, Eidtmann H, Llombart A, Davidson N, Neven P, von Minckwitz G, Sleeboom HP, Forbes J, Barrios C, Frassoldati A, Campbell I, Paija O, et al. Zoledronic acid (zoledronate) for postmenopausal women with early breast cancer receiving adjuvant letrozole (ZO-FAST study): final 60-month results. Ann Oncol. 2013; 24: 398-405.
37. Gnant M, Mlineritsch B, Stoeger H, Luschin-Ebengreuth G, Heck D, Menzel C, Jakesz R, Seifert M, Hubalek M, Pristauz G, Bauernhofer T, Eidtmann H, Eiermann W, et al. Adjuvant endocrine therapy plus zoledronic acid in

premenopausal women with early-stage breast cancer: 62-month follow-up from the ABCSG-12 randomized trial. Lancet Oncol. 2011; 12: 631–641.

38. Fehm T, Hoffmann O, Aktas B, Becker S, Solomayer EF, Wallwiener D, Kimmig R, Kasimir-Bauer S. Detection and characterization of circulating tumor cells in blood of primary breast cancer patients by RT-PCR and comparison to status of bone marrow disseminated cells. Breast Cancer Res. 2009; 11: R59.
39. Tubiana-Hulin M. Incidence, prevalence and distribution of bone metastases. Bone. 1991; 12: S9-10.
40. Gradishar WJ. Safety considerations of adjuvant therapy in early breast cancer in postmenopausal women. Oncology. 2005; 69: 1-9.
41. Maltais ML, Desroches J, Dionne IJ. Changes in muscle mass and strength after menopause. J Musculoskelet Neuronal Interact. 2009; 9: 186-197.
42. Phillips SK, Rook KM, Siddle NC, Bruce SA, Woledge RC. Muscle weakness in women occurs at an earlier age than in men, but strength is preserved by hormone replacement therapy. Clin Sci (Lond). 1993; 84: 95-8.
43. Skelton DA, Phillips SK, Bruce SA, Naylor CH, Woledge RC. Hormone replacement therapy increases isometric muscle strength of adductor pollicis in post-menopausal women. Clin Sci (Lond). 1999; 96: 357-364.
44. Bouxsein ML, Boyd SK, Christiansen BA, Guldberg RE, Jepsen KJ, Müller R. Guidelines for assessment of bone microstructure in rodents using micro-computed tomography. J Bone Miner Res. 2010; 25: 1468-1486.